

UNIVERSITY OF GAZİANTEP
GRADUATE SCHOOL OF
NATURAL & APPLIED SCIENCES

NUMERICAL SIMULATION AND OPTIMIZATION OF
CROSS WEDGE ROLLING PARAMETERS

M.SC. THESIS
IN
MECHANICAL ENGINEERING

BY
ALİ İHSAN ÇELİK

AUGUST 2012

**Numerical Simulation and Optimization of Cross Wedge
Rolling Parameters**

M.Sc. Thesis

In

Mechanical Engineering

University of Gaziantep

Supervisor

Assist.Prof.Dr. Necip Fazıl YILMAZ

by

Ali İhsan ÇELİK

August 2012

©2012 [Ali İhsan ÇELİK].

T.C.
UNIVERSITY OF GAZIANTEP
GRADUATE SCHOOL OF
NATURAL & APPLIED SCIENCES
MECHANICAL ENGINEERING DEPARTMENT

Name of the thesis: Numerical Simulation and Optimization of Cross Wedge Rolling Parameters

Name of the student: Ali İhsan ÇELİK

Exam date: 09.08.2012

Approval of the Graduate School of Natural and Applied Sciences


Prof. Dr. Ramazan KOÇ
Director

I certify that this thesis satisfies all the requirements as a thesis for the degree of Master of Science.


Prof. Dr. L. Canan DÜLGER
Chairman of the Department

This is to certify that we have read this thesis and that in our opinion it is fully adequate, in scope and quality, as a thesis for the degree of Master of Science.


Assist. Prof. Dr. Necip Fazıl YILMAZ
Supervisor

Examining Committee Members

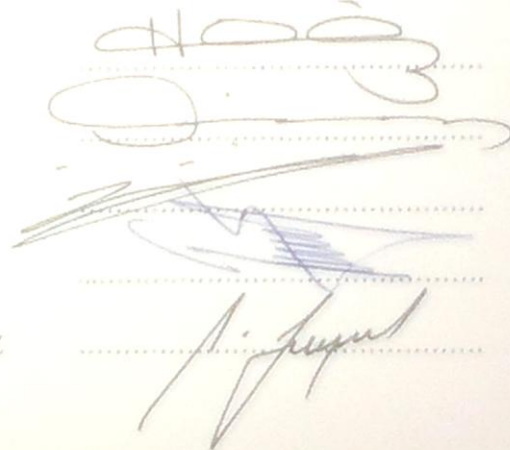
Prof. Dr. İ. Hüseyin FILİZ

Prof. Dr. Ömer EYERCIOĞLU

Prof. Dr. İbrahim Halil GÜZELBEY

Prof. Dr. Türkay DERELİ

Assist. Prof. Dr. Necip Fazıl YILMAZ



I declare that the related thesis is written properly according to academic and ethical rules and using all literature information referenced in the related thesis.

Ali İhsan ÇELİK

ABSTRACT

NUMERICAL SIMULATION AND OPTIMIZATION OF CROSS WEDGE ROLLING PARAMETERS

ÇELİK, Ali İhsan

M. Sc. In Mechanical Engineering

Supervisor: Assist. Prof. Dr. Necip Fazıl YILMAZ

August 2012, 115 pages

Cross wedge rolling (CWR) is a metal forming process for the production of rotational parts. In this process, a cylindrical billet is plastically deformed to an axisymmetric part by two wedge tools assembled in rolls or plates. Cross wedge rolling has been used in many applications in industrial production in elongated pieces, stepped shafts and axles. These kinds of parts are mainly applied in the automotive machine and aircraft industries. CWR technology has many advantages in comparison to other metal forming methods such as high productivity, high precise product, saving in material and energy cost. In addition to the positive aspects of CWR, this method has not been widely used in industry due to the difficulties of die design. This can mainly be attributed to complexities involved in CWR tool design. The design of CWR tooling is difficult because of the many parameter alternatives that can be encountered during the CWR process.

In this thesis, extensive investigation on numerical simulation have been performed to analyze the interactions of CWR parameters by using DEFORM 3D package program. Main effect plots, interactions and the contribution of the parameters were presented by the power of ANOVA and TAGUCHI methods. Prediction of the forming loads and the optimization of the parameters were also searched by ANN.

Keywords: Cross Wedge Rolling, Numerical Simulation, ANOVA, TAGUCHI

ÖZET

ÇAPRAZ KAMALI HADDELEME PARAMETRELERİNİN SAYISAL SİMÜLASYONU VE OPTİMİZASYONU

ÇELİK, Ali İhsan

Yüksek Lisans Tezi, Makine Mühendisliği Bölümü

Tez Yöneticisi: Yrd. Doç. Dr. Necip Fazıl YILMAZ

Ağustos 2012, 115 Sayfa

Çapraz kamalı haddeleme (ÇKH) silindirik iş parçalarını üretmek için kullanılan metal şekillendirme işlemidir. Bu yöntem, silindirik iş parçalarının merdaneler üzerine veya düz plakalar üzerine monte edilmiş çapraz iki kama arasında deforme edilerek eksenel simetrik şekil verme işlemidir. Çapraz kamalı haddeleme yöntemi endüstrideki birçok uzun iş parçası, kademeli şaft ve mil üretiminde kullanılmaktadır. Bu yöntem ile üretilen parçalar ağırlıklı olarak otomotiv ve havacılık sektöründe kullanılmaktadır. ÇKH yöntemin diğer metal şekillendirme yöntemlerine göre yüksek verimlilik, hassas ürün, düşük malzeme ve enerji sarfiyatı gibi birçok avantajı bulunmaktadır. Bu avantajlarının yanı sıra ÇKH'nin kalıp tasarımındaki zorluklar nedeni ile endüstride kullanımı yaygınlaşmamıştır. Bu zorluklar, işlem sırasında karşılaşılan birçok alternatif parametreden kaynaklanmaktadır.

Bu tezde sayısal simülasyon üzerine kapsamlı bir araştırma yapılmış ve ÇKH parametrelerinin etkileşimini analiz etmek için DEFORM 3D paket programı kullanılmıştır. ANOVA ve TAGUCHI istatistik yöntemi ile ana etki ve etkileşim grafikleri elde edilerek parametrelerin etkileşimi ve katkısı sunulmuştur. Ayrıca yapay sinir ağı yöntemi ile işlem sırasında ihtiyaç duyulan kuvvet tahminleri yapılmış ve parametrelerin optimizasyonu araştırılmıştır.

Anahtar Kelime: Çapraz Kamalı Haddeleme, Sayısal Simülasyon, ANOVA, TAGUCHI

ACKNOWLEDGEMENT

I would like to express my deepest respect and most sincere gratitude to my supervisor, Assist. Prof. Dr. Necip Fazıl YILMAZ, for his guidance and encouragement at all stages of my work. His constructive criticism and comments from the initial conception to the end of this work is highly appreciated.

I would like to express my special thanks to Prof. Dr. Hüseyin FİLİZ for his encouragement and endless support to my academic life.

I also wish many thanks to Prof. Dr. Ömer EYERCİOĞLU for his interprets about the results of DEFORM 3D.

I also would like to thanks to researcher Sadik OLGUNER, for his support during the studies.

I am also very thankful to my wife for her great helps and motivations during my all education life.

CONTENTS

ABSTRACT.....	III
NUMERICAL SIMULATION AND OPTIMIZATION OF CROSS WEDGE ROLLING PARAMETERS	III
ACKNOWLEDGEMENT	VII
CONTENTS.....	VIII
LIST OF FIGURES	X
LIST OF TABLES.....	XII
CHAPTER 1	1
INTRODUCTION	1
1.1 INTRODUCTION.....	1
1.2 PLACE of CROSS WEDGE ROLLING PROCESS in METAL FORMING.....	1
1.3 THE REASON FOR ANALYZING THE CROSS WEDGE ROLLING PARAMETERS	2
1.4 ORGANIZATION OF THE THESIS	3
CHAPTER 2	5
LITERATURE SURVEY	5
2.1 INTRODUCTION.....	5
2.2 LITERATURE RELATED WITH THE WORK.....	5
2.3 PLACE OF THIS WORK IN THE LITERATURE	9
CHAPTER 3	10
THEORY OF CROSS WEDGE ROLLING.....	10
3.1 INTRODUCTION.....	10
3.2 CROSS WEDGE ROLLING PROCESS.....	10
3.2.1 Flat Wedge Type	11
3.2.2 The Concave Type	12
3.2.3 One Roll Type	12
3.2.4 Two Roll Type	13
3.2.5 Three Roll Type	13
3.3 TOOL GEOMETRY OF FLAT TYPE CWR.....	14
3.4 LOAD CALCULATION OF CWR	15

CHAPTER 4	20
NUMERICAL SIMULATIONS of CWR PARAMETERS	20
4.1 INTRODUCTION.....	20
4.2 DESCRIPTION OF THE PROCESS.....	20
4.3 SETTING UP PROCEDURES ON DEFORM 3D.....	21
4.4 MESH GENERATION	32
4.5 ANALYSIS of NUMERICAL RESULTS.....	38
4.5.1 The Effect of Stretching Angle (β) on Rolling Loads.....	38
4.5.2 The Effect Forming Angle (α) on Rolling Loads.....	41
4.5.3 The Effect of Reduction Ratio (δ) on Rolling Loads	44
4.5.4 The Effect Tool Velocity (V) on Rolling Loads	47
CHAPTER 5	51
MODELING AND ANALYSIS OF CROSS WEDGE ROLLING PROCESS	51
5.1 INTRODUCTION	51
5.3 PREDICTION OF CWR LOADS USING NEURAL NETWORK	55
5.4 DESIGN OF EXPERIMENTS	59
5.4.1 Analysis of Working Conditions Using ANOVA.....	60
5.4.2 Main Effects Plots.....	64
5.4.3 Interaction Plots for Knifing and Stretching Zones	67
5.5 CONTRIBUTION OF PROCESS PARAMETERS USING TAGUCHI.....	70
CHAPTER 6	76
DISCUSSION AND CONCLUSIONS	76
6.1 INTRODUCTION.....	76
6.2 DISCUSSION AND CONCLUSIONS.....	76
RECOMMENDATION FOR FUTURE STUDIES.....	79
REFERENCES.....	80
APPENDICES	84

LIST OF FIGURES

Figure 3.1 A CWR Process	10
Figure 3.2 Flat Wedge Type Cross Wedge Rolling	12
Figure 3.3 Concave Wedge Type Cross Wedge Rolling	12
Figure 3.4 One roll type Cross Wedge Rolling.....	13
Figure 3.5 Two Roll Type Cross Wedge Rolling	13
Figure 3.6 Three Roll Type Cross Wedge Rolling	14
Figure 3.7 Some Items Produced With CWR Processes	14
Figure 3.8 Tool Geometry of CWR and Deformation Zones	15
Figure 3.9 Rolling Force Components on CWR Die.....	16
Figure 3.10 Force Diagram of the CWR.....	17
Figure 3.11 Radial and Tangential Load-Stroke Diagrams	19
Figure 4.1 Setup a New Problem	21
Figure 4.2 Simulation Control Panel	22
Figure 4.3 Definition of Workpiece.....	22
Figure 4.4 Workpiece Geometry Generation.....	23
Figure 4.5 Definition of Mesh Geometry.....	24
Figure 4.6 Generation of Mesh	24
Figure 4.7 Add of Top and Bottom dies	25
Figure 4.8 Added of Top and Bottom Dies.....	26
Figure 4.9 Definition of Dies Movement.....	26
Figure 4.10 Selection of the Material from the Material Library	27
Figure 4.11 Definition of the Material Temperature.....	28
Figure 4.12 Simulation Control Options.....	29
Figure 4. 13 Define the Relationship of Between Objects.....	29
Figure 4. 14 Define Friction Coefficient of Between Workpiece and Dies.....	30
Figure 4. 15 Generate Database	31
Figure 4.16 Run Simulator.....	31
Figure 4. 17 Effect of Reduction Ratio (δ)	32

Figure 4.18 Three dimensional model of a wedge die.....	37
Figure 4.19 Final Geometry of Workpiece	38
Figure 4.20 Wedge Geometry	38
Figure 4.21 Tangential Loads According to Stretching Angle	39
Figure 4.22 Radial Loads According to Stretching Angle (β)	40
Figure 4.23 Tangential Loads According to Forming Angle (α)	41
Figure 4.24 Radial Loads According to Forming Angle (α).....	43
Figure 4.25 Tangential Loads According to Reduction Ratio (δ).....	45
Figure 4.26 Radial Loads According to Reduction Ratio (δ)	46
Figure 4.27 Tangential Loads According to Die Velocity (V)	48
Figure 4.28 Radial Loads According to Die Velocity (V).....	49
Figure 5.1 Illustration of A Biological Neuron.....	52
Figure 5.2 Biological Neuron and Artificial Neural Network	53
Figure 5.3 A Simplified Schematic Diagram for a (FFANN) Model	54
Figure 5.4 Type of Networks and Functions	54
Figure 5.5 Selected Structure for the FF-ANN Model.....	56
Figure 5.6 Established of the FF-ANN Model.....	56
Figure 5.7 Training of the FF-ANN Model	57
Figure 5.8 Validation Performance	58
Figure 5.9 Regrassion Plots	58
Figure 5.10 Tangential Load Comparison for FEM and ANN Results	59
Figure 5.11 Radial Load Comparison for FEM and ANN Results.....	59
Figure 5.12 Parameter Alternatives of Numerical Simulations	60
Figure 5.13 Tangential Loads MEP Charts for Knifing Zone	65
Figure 5.14 Radial Loads MEP Charts for Stretching Zone	65
Figure 5.15 Tangential Loads MEP Charts for Knifing Zone	66
Figure 5.16 Tangential Loads MEP Charts for Stretching Zone	66
Figure 5.17 Tangential Loads Interaction Plots for Knifing Zone.....	67
Figure 5.18 Radial Loads Interaction Plots for Knifing Zone	68
Figure 5.19 Tangential Loads Interaction Plots for Stretching Zone.....	69
Figure 5.20 Radial Loads Interaction Plots for Stretching Zone	69

LIST OF TABLES

Table 4.1 Results of Numerical Simulations	33
Table 5.1 CWR Process Parameters and Their Levels	55
Table 5.2 Tangential Load Analysis	62
Table 5.3 Tangential Load Analysis	63
Table 5.4 Radial Load Analysis	63
Table 5.5 Radial Load Analysis	63
Table 5.6 Comparison of ANOVA and R^2	64
Table 5.7 Experiment Factors Level Using Taguchi Method	71
Table 5.8 Orthogonal Array(19) Selected Table	72
Table 5.9 Orthogonal Array(l_9) of Taguchi Method	72
Table 5.10 Result Data	73
Table 5.11 S/N ratio, sum of squares Values and SS_i	74
Table 5.12 Contribution of process parameters (%)	75

CHAPTER 1

INTRODUCTION

1.1 INTRODUCTION

In this chapter, the place of cross wedge rolling process in metal forming process is briefly identified and the importance of the analysis of cross wedge rolling parameters is presented. The aim and organization of thesis are also outlined in this chapter.

1.2 PLACE of CROSS WEDGE ROLLING PROCESS in METAL FORMING

In metal processing industry, it is important to improve traditional manufacturing processes and find new technologies so that higher quality and competitive products are generated. In traditional metal forming methods, chip formation and chipless formation forms the main headings. Main chipless manufacturing methods are forging, rolling, extrusion and wire drawing. In forging process, metal is plastically deformed and assumes the shape of the dies by the subjected high compressive force. Rolling is the process of plastically deforming metal by passing it between rollers. Cross Wedge Rolling (CWR) method occupies an overwhelming popularity and offers new trends in the chipless manufacturing method since it is relatively new commercial method other than traditional metal forming processes. CWR can be defined as the combination of forging and rolling processes [1]. In this process, two identical wedge shaped forming dies are mounted on the top and bottom plates that move in the opposite directions perpendicular to the billet axis and the workpiece plastically deformed between the dies during the rolling process. Within this process one or more axisymmetric parts, ball studs, pins and other components are being produced by using a single wedge tool.

Cross wedge rolling has attracted attention in modern technology. It has acquired great popularity in the metal forming industries. Especially, in Europe and China, CWR has replaced many conventional machining, forging and rolling in the manufacturing of rotational part. It has been reported that hundreds of product with diameter ranging 3-25 mm diameter and length from 3-2000 mm are currently being manufacture by CWR [2].

The CWR method has got many positive advantages such as high efficiency, low material cost, low energy requirement and environmental effect than many traditional manufacturing methods. Nevertheless, CWR method has not been widely used throughout the manufacturing environment due to the difficulties in die design and uncertainties in the process parameters. In that, intensive development of process, CWR method has not been completely modeled theoretically. Cross wedge rolling process has been studied for the past thirty years. However, despite all effort that has been expended, there are still no formalized systematic methods for designing rolling tools for practical applications. These are because of the unreliable geometrical changes occurring in cross wedge rolling of complex parts [3, 4].

In CWR, similar to other metal forming process, the quality of products are determined by tool design, material formability, and forming conditions. These are generally referred as process parameters. CWR process parameters have been investigated by researches ever since the CWR technique was developed.

1.3 THE REASON FOR ANALYZING THE CROSS WEDGE ROLLING PARAMETERS

CWR Parameters are divided into two manly groups, geometric parameters and forming parameters. Geometric parameters are considered as wedge length (zone) and angle. Length parameters are knifing, guiding, stretching and sizing zones while the angular parameters are forming, stretching and ramping angles. Material type, forming load, reduction ratio and the die speed forms the forming parameters.

When setting up the cross wedge rolling process, the most important task is to design the wedge tools that were used. Although there are three angles, wedge die is characterized by two very important angular parameters forming angle (α) and

stretching angle (β). Relative reduction ($\delta=d_0/d$) is also the other main CWR process parameter. In the shaping process, knifing stage of the tool reduces the workpiece diameter from d_0 to d and forms a V-shaped depth into material. In the guiding zone, die profile does not change and a V-shaped uniform slot is achieved around the workpiece surface. In some industrial conditions, it is possible to remove guiding zone of CWR tool because of no additional deformation is carried out at this stage. In the stretching zone, material is forced to flow to the ends and V-shaped slot is stretched by means of the side walls of the wedge. Then in the sizing zone, any undesired curvatures formed in previous stages are removed and dimensional tolerances and surface quality of the product is generated.

It is very important to analyze rolling parameter characteristics of cross wedge rolling processes to calculating power requirement, determining rigidity of the wedges and selecting the tools. To obtain accurate products, the analysis of parameters and forces which are effective in die design has wide importance.

In recent years, Finite Element Method (FEM) has commonly been used for numerical modeling techniques. The finite element method has advantages in solving general problems with complex shapes of the formed parts. FEM displacement representation has been used to establish simulation model for the flat cross wedge rolling process by using DEFORM 3D package program. The spontaneous remeshing technique in DEFORM 3D can relieve mesh singularity during the simulation process

Three analyzing methods have been used to analyze the CWR parameters such as analysis of variance (ANOVA), TAGUCHI and artificial neural network (ANN). Magnitudes of the main effect plots are visualized by ANOVA. Contribution of the process parameters are proposed by TAGUCHI. Prediction and the optimization of the parameters are presented by ANN.

1.4 ORGANIZATION OF THE THESIS

In this thesis, load requirement for cross wedge rolling is criticized in respect of forming parameters. Forming angle, stretching angle, reduction ratio and the die velocity determined as the affecting parameters on rolling load.

This thesis organized in six chapters.

The following chapter, Chapter 2, denotes the most related works on cross wedge rolling process. The related literature search describing previous investigations on the numerical simulation and optimization of CWR are also summarized in Chapter 2. It is noticed that there are serious gaps in the literature concerning the numerical simulation and optimization of CWR.

In Chapter 3, the general theory of CWR is presented. General knowledge and application areas of CWR are also given in this chapter.

In Chapter 4, the FEM based DEFORM 3D software package was used to attain all numerical calculations and simulation models belong to load analysis of cross wedge rolling operations. Effect of parameters on rolling load is analyzed in detail.

In Chapter 5, a feed-forward artificial neural network (FF-ANN), analysis of variance (ANOVA) and TAGUCHI method are implemented to find the influence of parameters.

Discussion and conclusion are given in Chapter 6. Recommendations for future works are also provided at the end of thesis.

CHAPTER 2

LITERATURE SURVEY

2.1 INTRODUCTION

In this chapter, previous studies related with the Cross Wedge Rolling (CWR) process are outlined. All the literature presented herein is classified according to the working areas on CWR.

2.2 LITERATURE RELATED WITH THE WORK

Cross wedge rolling has been used in many applications in industrial production in elongated pieces, stepped shafts, ball studs, pins and axles. These kinds of parts are mainly applied in the automotive machine and aircraft industries. Comparison with other metal forming method, CWR is relatively new commercial term. This technology has many advantages in comparison to other metal forming methods such as high productivity, saving in material and energy cost, high precise product, and good working conditions [5-7]. In addition to the positive aspects of CWR, this method has not been widely used in industry due to the difficulties of die design. Due to these reasons, optimization of cross wedge rolling parameters and the interaction between them is important.

In addition so far, no theoretical solution to be implemented due to the complex structure of cross-wedge rolling parameters. There are some attempts to discuss the application of numerical simulation methods. Compared to other numerical simulation methods, the finite element method (FEM) has some advantages in solving general problems with complex shapes of the formed parts [8]. This model can be used to analyze the influence of several process parameters on forming by means of cross wedge rolling process [9].

Some researchers concentrated on the simulation techniques in order for analyzing the metal deformation characteristics. Generally, numerical simulation includes all methods that can reproduce the processes of a system.

Pater [10] proposed an upper bound method to analyze the rolling parameters. Within the study, author presented for the numerical simulation of the cross wedge rolling process. The results of calculations depended upon the upper bound method enabled distribution diagrams to be obtained for: the rolling forces; the contact surface between the material and the tool; and the rolling radius within the total range of the forming process. Pater also presented a numerical analysis of cross-wedge rolling (CWR) process of ball pins in another work [11]. In this work, by dealing with the simulation of CWR processes, where a single necking of billet was formed on a shaft, were analyzed. These calculations were made assuming a number of simplifications in tool geometry and the material.

Fang et al [12] simulated and analyzed the 3-D rigid-plastic finite element method. Considering characteristics of CWR, the static implicit FEM program of DEFORM was selected. To simulate all forming stages in the CWR process, dynamic adaptive remeshing technology for tetrahedral solid elements was applied. They mentioned the stress distributions in the cross section of the forming workpiece are analyzed to interpret failure of rarefaction at the center of workpiece and the loads changing.

An experimental works of the CWR process of a hollow shaft was modeled by Bartnicki and Pater [13, 14]. The results were used for the verification of numerical simulations. The authors presented the phenomena that reduced the field of stability of CWR process parameters for hollow shaft. The wall thicknesses of the simulations were compared with the experiments. It was realized that the greater the initial wall thickness of workpiece, the more intensive material flow was present. Authors mentioned failure in CWR, how to fix them and benefit of FEM method that could be seen in the aspect of strain in 3D.

The effects of the important CWR parameters were carried out by Dong, et al [15]. In this study namely the forming angle, the area reduction and the friction coefficient, on the field of variables were investigated. A total of 14 rolling conditions were

analyzed for the billet material aluminum alloy 1100. After initially verifying the numerical results, several tendencies for the CWR process, as related to failure, were ascertained and discussed.

Wang et al [16] presented on a parameterized die design system for CWR. It was developed based on the expertise experiences, in which the optimized selection of the key factors of dies could be achieved automatically. Some empirical equations for recrystallization evolutions and transformation used in the simulation were obtained using the thermo mechanical simulator. Using the die design system, a three-dimensional (3D) solid model was generated and imported into the finite element analysis software.

They also presented the whole forming process of CWR, including knifing zone, guiding zone, stretching zone, and sizing zone. They simulated it by using the model in which dynamic adaptive remeshing technology for tetrahedral solid elements used to fix element distortion. The rigid-plastic FEM was used to build the simulation model for the two-roll CWR process. And a simulation process was carried out, which involved knifing, guiding, stretching, step shaping, and sizing of deformed part.

Pater [17, 18] presented numerical simulation for strain distributions, strain rate, mean stress and rolling load components guessing of phenomena limiting forming stability, uncontrolled slipping and core necking was capable. The rolling of reel forging was presented as more advanced thermo-mechanical model of cross wedge rolling process. He showed equivalent strain distribution simulated by using FEM for advance phase of CWR process at determined parameters.

The resource and implementation of works completed in the framework of new thread technology developed by Pater et al [18]. They described thread rolling method consists in thread forming by means of two flat wedges provided with special grooves designed for thread forming. The results obtained from numerical simulation thread rolling process were presented. The calculations were completed using finite volumes method (FVM) and finite element method (FEM). Furthermore experimental tests consisting in thread forming on the bars made of commercial lead

in laboratory conditions and results of industrial tests with simultaneous thread forming on two screws were described.

Lovell [19] developed a numerical model for cross wedge rolling which determine the critical interfacial friction in a two roll CWR machines. Function of the tool geometry and area reduction for the critical rolling condition CWR machines are expressed. The morphology of the void generation and growth in CWR ascertained and discussed.

Optimization is a mathematical discipline that concerns the finding of minimum and maximum of functions, subject to so-called constraints. Today, optimization comprises a wide variety of techniques from operations research, artificial intelligence and computer science, and is used to improve business processes in practically all industries. Many scientists have used this method of working in the field of Mechanical Engineering.

Pater [17] presented the possibilities of the application of optimization methods for the designing of the tools to be used in cross-wedge rolling processes. A detailed description of the selection procedure for the forming angle, the spreading angle and the side wedge surface designing method was presented. He also mentioned the detailed discussion of problems associated with the selection of basic wedges parameters (i.e. forming angle α , and spreading angle β) as well as in the designing of the shape of the wedge side profile was included [3]. Nongradient optimization techniques and a layer modeling method for CWR processes modeling were used. The optimization procedures were introduced into a Wedge Roll computer system aiding the designing of CWR processes.

Lee et al [20] searched the effects of the forming angle and the friction coefficient. The initiation of the Mannesmann hole defect was analyzed by using a response surface method. Integrals of four different ductile fracture models were compared with a history of the effective plastic strain at the central point. Optimization of design parameters for prevention of the Mannesmann hole defect initiation was carried out using a response surface method.

2.3 PLACE OF THIS WORK IN THE LITERATURE

In this research, an effort has been made to utilize the parameterized CWR die design and the function of approximation capabilities of analysis of variance (ANOVA) in the modeling of cross wedge rolling parameters. Main effect and interaction plots were tried to put the relations between the forming angle, stretching angle, reduction ratio and velocity of the dies to predict the rolling force. This process is characterized by the series of process parameters which govern it and the lack of adequate mathematical models to relate these parameters with the controlled variables. Rolling force may be predicted by finite element simulations or by experimentation. The great number of experiments is required but, experimentation is very difficult, time consuming and expensive due to die making costs. Finite element modeling has also several limitations. Within this work, 144 different combinations of input conditions were executed. Pre-processing and execution of each simulation took 5 days to 10 days without any interruption of dual core computer. Also any change in one process parameter requires a new pre-processing and execution to observe its effect on cross wedge rolling force. Due to these reasons, it is needed to develop much more generalized models, which can predict a wide variety of process parameters to enable the process decisions on rolling force. Therefore, in this thesis, many simulations were executed by using design of experiment (DOE) methodology and relations between the all relevant parameters were investigated. During the studies, DEFORM 3D, MINITAB and MATLAB were used to utilize the parameterized CWR die design.

CHAPTER 3

THEORY OF CROSS WEDGE ROLLING

3.1 INTRODUCTION

The aim of this chapter is to present general knowledge on Cross Wedge Rolling (CWR) method. The working principle tooling types of this manufacturing method are explained.

3.2 CROSS WEDGE ROLLING PROCESS

Cross Wedge Rolling (CWR) is a deforming process of metals, in which a cylindrical workpiece (billet) is plastically deformed to stepped rotational axisymmetric parts between wedge type tools moving tangentially relative to the workpiece. Figure 3.1 shows the schematic illustration of cross wedge rolling process. The CWR is widely applied process for the production of stepped shafts or axes being the axisymmetric parts. It has attracted great interest especially in China, Europa and USA as a respectively new production method.



Figure 3.1 A Typical CWR Machine [21]

The CWR process offers several innovative features over traditional machining operations such as; high equipment production capacity, favorable structure of material fibers, ease of maintenance, high accuracy and maximum proximity to required dimensions of finished products, minimum waste, opportunities to produce a wide product range using the same equipment and environmental effect.

Despite well-known advantages, the CWR process has not been widely used by the metal forming industry. This is partly due to lack of the adequate technical knowledge on the workpiece deformation, friction and the failure mechanisms in the process as well as the complexity of the tool design. Since the interactions between the tool and the workpiece are not predicted accurately and reliably, the automation of the CWR process is difficult. Several trial products are required in order to produce a single product design. These design techniques are based on the experience and trial-and-error method, which are often unreliable, time consuming and expensive [22].

Shafts with tapers, steps, shoulders and walls with almost no draft angles can be made by the CWR. The CWR machine is typically composed of on which wedge shaped tooling are mounted.

3.2.1 Flat Wedge Type

In a flat wedge type the tools move in the opposite directions in a back forth fashion as shown in Figure 3.2. One direction is rolling, the other is relatively faster return stroke. The best feature of this type of CWR machine is that it is cheaper to fabricate compared to the other type. Due to the “empty” return stroke, the productivity is the lowest among all available CWR configurations. Hydraulic cylinders are preferred to drive the dies compared to mechanical system that would be very complicated when converting rotary motion linear motion.

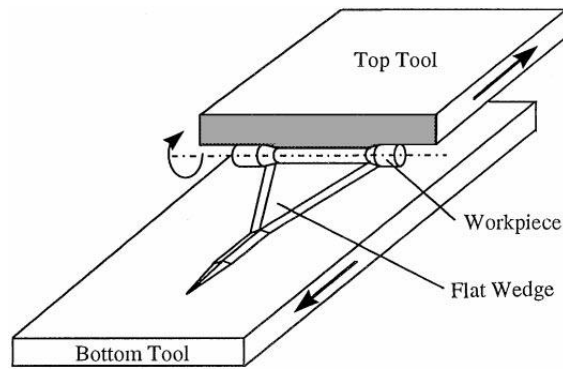


Figure 3.2 Flat Wedge Type Cross Wedge Rolling [23].

3.2.2 The Concave Type

This is the most expensive type of CWR machine to make, and is rarely used in production. The wedge shaped forming tools and the base plate has concave geometry, as shown in Figure 3.3. During the rolling process, the tools have to have a combination of linear and eccentric rotary motions. The merit of the type of CWR machines is that they have the envelope contact between the tools and workpiece to avoid workpiece internal cracks [24].

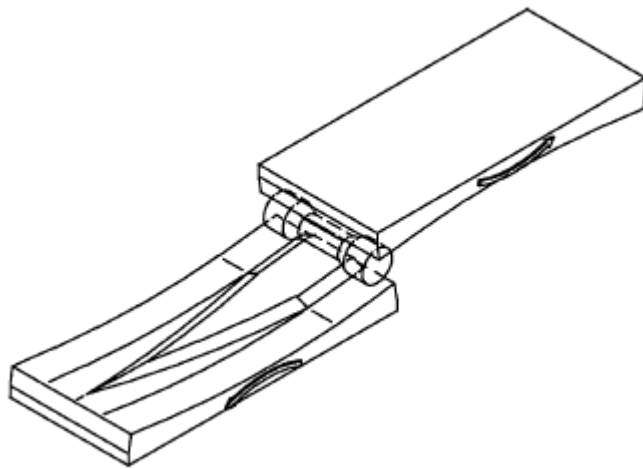


Figure 3.3 Concave Wedge Type Cross Wedge Rolling [25].

3.2.3 One Roll Type

As it shown in Figure 3.4 this type of configuration consists of a roll with the forming wedge mounted on its surface and concave wedge base. The workpiece is deformed between the rotating roll and the stationary concave wedge. In this type of tooling, there are some difficulties in die making and therefore it is not widely used in industry.

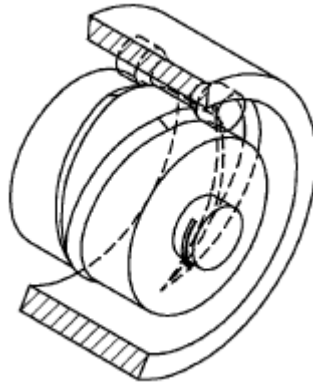


Figure 3.4 One Roll Type Cross Wedge Rolling [25]

3.2.4 Two Roll Type

All the axes of the rolls are parallel and they rotate in the same direction. With two roll tooling, the stock can be inserted from either the outside or the side of the rolls with its axis parallel to the roll axes. Two roll cross wedge rolling is shown in Figure 3.5

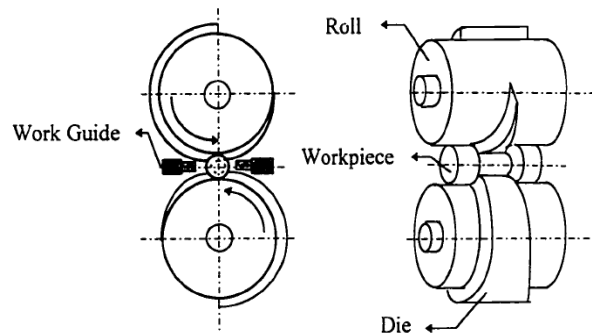


Figure 3.5 Two Roll Type Cross Wedge Rolling [25]

3.2.5 Three Roll Type

The three roll tooling configuration allows the stock to be fed into rolls from only the side. Cut billets or long bars can be used in two-roll and three roll tooling. Owing to geometrical constraints on three roll tooling, the length of deforming wedges on roll surfaces and the smallest diameter of a product restricted compared to two roll tooling [26]. At typical three roll cross wedge rolling is shown in Figure 3.6.

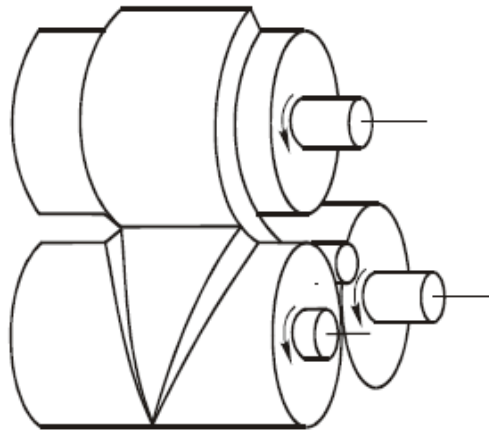


Figure 3.6 Three Roll Type Cross Wedge Rolling [25]

In order to get high quality final products the tool configurations and workpiece dimensions should be confirmed carefully. Moving of the designed wedge tools in a good harmony is another important consideration for producing high quality end products. In Figure 3.7 some of the products which are possible to produce by CWR process are shown. Axisymmetric circular parts which have a diameter of 3-125 mm and length of 3-2000 mm can be produced [27].

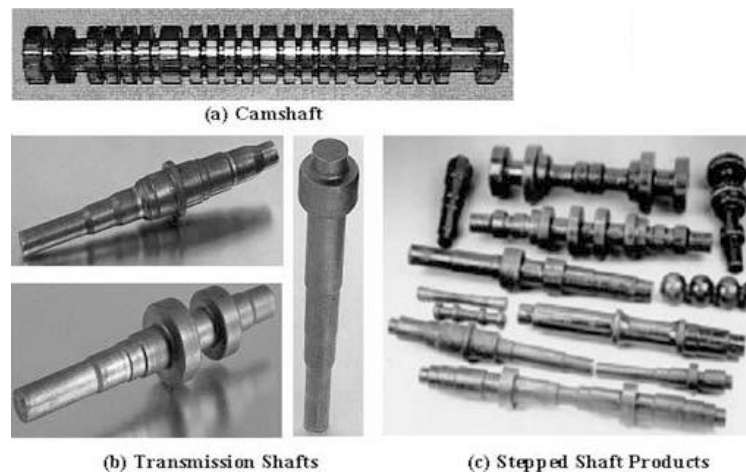


Figure 3.7 Some Items Produced With CWR Process [7]

3.3 TOOL GEOMETRY OF FLAT TYPE CWR

In flat CWR type, there are four stages of the wedge tool geometry. In addition, forming angle (α), spreading angle (β), ramp angle (γ), rolling depth (Δr) and rolling length $2L$ are the other parameters which effect the material deformation. These parameters and CWR zones are shown in Figure 3.8.

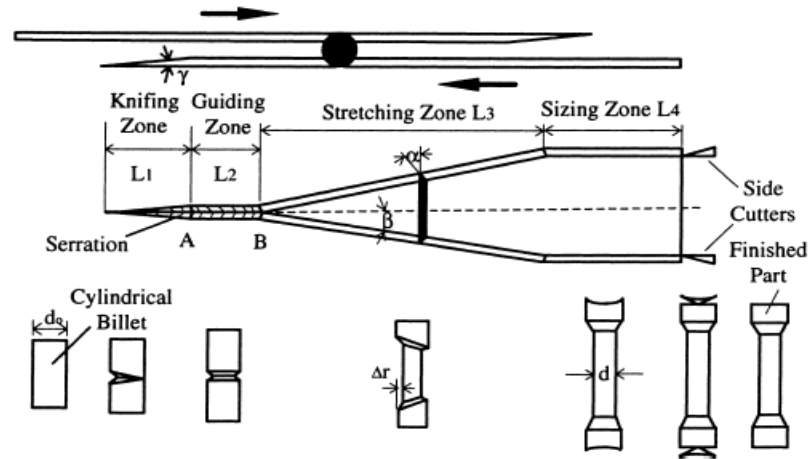


Figure 3.8 Tool Geometry of CWR and Deformation Zones[15]

1. **Knifing zone:** This is the initial zone, which is (γ) starting at zero and increase to the total reduction of height for the workpiece. The cylindrical workpiece is driven in this zone and a V-shaped groove is formed into its circumference.
2. **Guiding zone:** This is the second zone in which a uniform V-Shaped groove is formed around the workpiece surface. The wedge profile does not change in this zone. The area reduction is constant starting from this zone to the end of.
3. **Stretching zone:** In this zone, the workpiece is deformed (stretched) by increasing the width of the wedge because of stretching angle. The workpiece is forced to enlarge through the both ends by the tool wedge.
4. **Sizing zone:** The workpiece is formed into its final geometry, dimensions and surface quality in this finishing zone. In this zone, β is zero and the wedge is uniform. At the end of the sizing zone, the side cutters cut the scrapped ends of the workpiece.

3.4 LOAD CALCULATION OF CWR

In order to facilitate numerical simulations, the wedged dies were considered as rigid material models due to their negligible elastic deformation. Cylindrical workpiece

was regarded as an elastoplastic body and divided by tetrahedral meshes by adopting the three dimensional solid elements.

The rolling force in cross wedge rolling processes can be determined when its components axial, radial and tangential forces shown in Figure 3.9 are known. Axial force makes workpiece in deformation zone extend in axial direction. According to the relationship between the force and reaction, the axial force of rolled part acting on the unilateral die is F_a . This axial force stretches the workpiece in longitudinal direction. Material flow of the workpiece in longitudinal direction and steady rolling are affected by the axial force. But, axial force is not detailed here since it is not the scope of this work. The tangential force of rolled part acting on the unilateral die is important to prevent the slippage and avoid from the internal cracks and cavities. Rotational compression of the workpiece external surface by the mounting dies is caused by radial load. Since the work focuses on the tooling design and the factors acting on the die, only tangential and radial loads were taken into consideration.

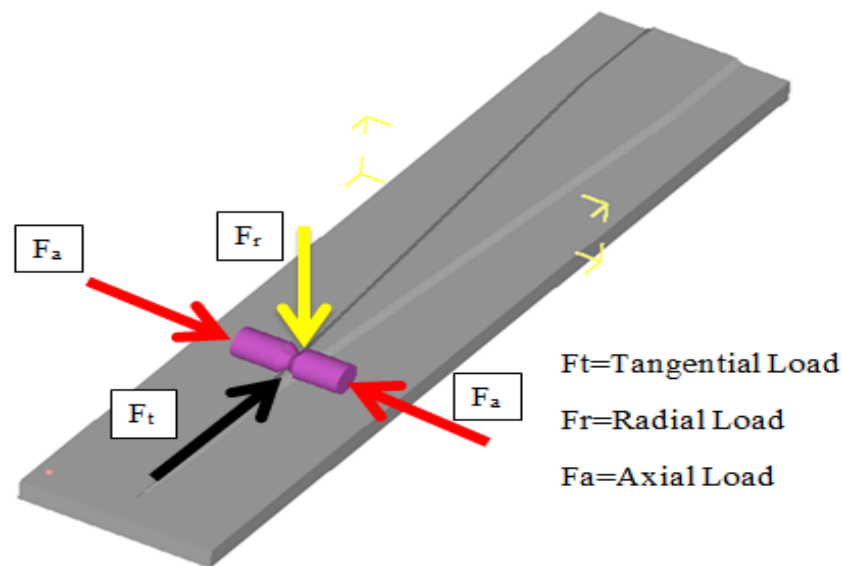


Figure 3.9 Rolling Force Components on CWR Die

Because of the complexity of the deformation zone geometry and the deformation mechanism, the theoretical analysis of the CWR process is difficult. That is why most publications which determine the rolling forces concentrate on mean unit pressure on the workpiece die contact area. Among the references, some researchers

have studied on the theoretical calculation of rolling load characteristic of CWR operations. These solutions apply the upper bound method to determine the unit pressure by assuming that main directions of the metal flow are radial and tangential. Since the mid 1980's, some contributions were made to the understanding of load calculation for CWR. Hayama [28] analyzed the rotational compression of a cylindrical bar, using the upper bound method. Na and Cho [29] developed a simple kinematically admissible velocity field for the analysis of the plane strain rotational compression of a cylindrical workpiece in CWR, by considering the tangential and radial components of a wedge shaped tool. Fu and Dean [30] determined the tangential and radial forces by minimizing the total power consumption. Pater [31] analyzed the combination of the tooling parameters to calculate radial component of rolling force by using Upper Bound Element Technique. Calculations were also carried out by Bozgeyik [32] for industrial application using the following equations. This method can be used for the prediction of the rolling force components in plain strain rotational compression. CWR workpiece forming diagram is shown in Figure 3.10.

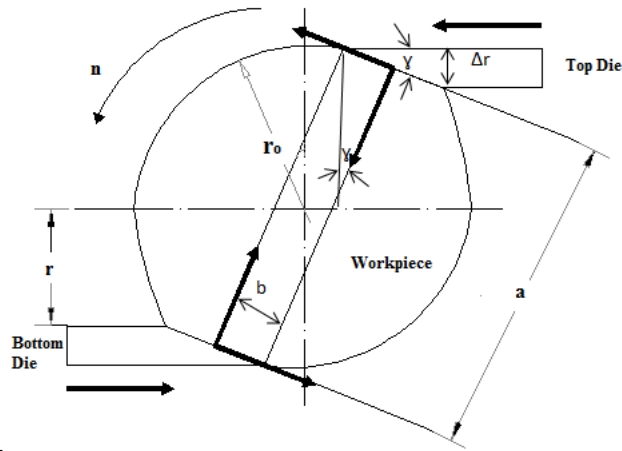


Figure 3.10 Forming Diagram of the CWR

Calculations can be done $\delta = \frac{D_0}{D}$ by the following equations using Upper Bound Element Technique (UBET).

$$f(\alpha) = \frac{1}{2} \left[\sqrt{12} - \cos \alpha * \sqrt{1 + 11 * \cos^2 \alpha} + \frac{1}{\sqrt{11}} * \ln \left(\frac{\sqrt{11} + \sqrt{12}}{\sqrt{11} * \cos \alpha + \sqrt{1 + 11 * \cos^2 \alpha}} \right) \right] \quad (1)$$

$$\frac{q_m}{\sigma_0} = \frac{1}{\delta^2 - 1} * \frac{2}{\sqrt{3}} \left[\left(\frac{f(\alpha)}{\sin^2 \alpha} + m * \frac{1}{\tan \alpha} \right) * \ln \delta z + \frac{2\alpha - \sin 2\alpha}{2 \sin^2 \alpha} + 2 * m * Lz/d \right] \quad (2)$$

$$\text{and} \quad \delta_Z = \frac{\delta+1}{2} \quad (3)$$

where q_m is the mean contact pressure; m is the friction coefficient; σ_0 is the yield strength of material; and L_Z is the substitute width of a sizing zone.

$$L_Z = \pi * r_0 * \lambda * \frac{(\tan \beta)}{2} * \delta \quad (4)$$

$$\lambda = (2.587 - 1.557 * \delta^{0.3528}) * (0.00355 * \alpha + 0.927) * \beta^{0.0568} \quad (5)$$

where λ is the rolling coefficient.

$$C = \frac{\pi * \tan \beta * \tan \alpha * \lambda * \delta}{\delta - 1} \quad (6)$$

where C is the relative rolling pitch.

If $C \leq 1$

$$A_{xy} = 1 + \frac{2}{3} * r_0^2 * \frac{\cos \beta}{\tan \alpha} * \sqrt{\frac{3}{1 + \frac{r_0}{r}} * \frac{\delta - 1}{\delta}} * \left[1 + c * \frac{\delta - 1}{\delta} \left(1 + \sqrt{\frac{2 + c * \delta - c}{2 * \delta}} \right) - \sqrt{\left(\frac{1 + c * \delta - c}{\delta} \right)^3} \right] \quad (7)$$

$$A_{xz} = \frac{2}{3} \cos \beta * r_0^2 * \sqrt{\frac{3}{1 + \frac{r_0}{r}} * c * \frac{\delta - 1}{\delta}} \left[1 - \sqrt{\left(\frac{1 + c * \delta - c}{\delta} \right)^3} + c \frac{\delta - 1}{\delta} \right] \quad (8)$$

If $C > 1$

$$A_{xy} = \frac{2}{3} \cos \beta * r_0^2 * \frac{\cos \beta}{\tan \alpha} * \frac{\delta - 1}{\delta} * \sqrt{\frac{3}{1 + \frac{r_0}{r}}} \left[1 + \frac{3}{2} (c - 1) + \sqrt{\frac{\delta - 1}{\delta}} \right] \quad (9)$$

$$A_{xz} = \frac{2}{3} * \cos \beta * r_0^2 * \frac{\delta - 1}{\delta} * \sqrt{\frac{3}{1 + \frac{r_0}{r}} + \frac{\delta - 1}{\delta}} \quad (10)$$

where A_{xy} and A_{xz} are the projected contact areas in radial and axial directions.

$$\tau = m * \frac{\sigma_0}{\sqrt{3}} \quad (11)$$

where τ is the shear stress.

$$Q_Z = 2 * (q_m * A_{xy} - \tau * \sin \beta * A_{xz}) \quad (12)$$

where Q_Z is the radial component of rolling force.

FEM displacement representation was used to establish simulation model for the CWR process by using DEFORM 3D software package. The spontaneous remeshing technique in DEFORM can relieve mesh singularity during the simulation process. Simulations showed that the radial force acting on the dies is the maximum force and greater than tangential force. Figure 3.11 illustrates the radial and tangential forces in all stages.

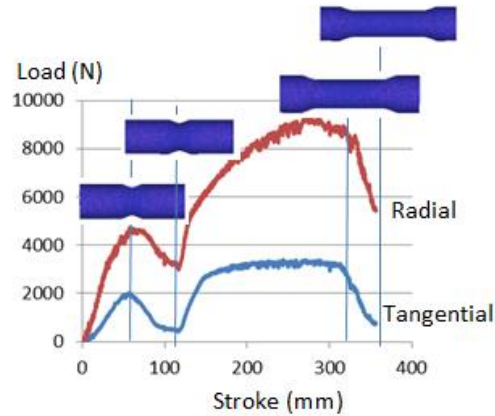


Figure 3.11 Radial and Tangential Load-Stroke Diagrams

As it is shown from Figure 3.11 during the knifing stage of the CWR process the wedges cut into the material to the desired depth and reaches to the first highest load value. In the guiding stage, V-shaped uniform slot is achieved around the workpiece surface and therefore minimum amount of metal deformation causes the lowest radial load. After reaching the proper radial load, gradual metal deformation occurs and continues until the end of stretching zone is reached. By considering the all stages, the maximum rolling force is required at this stage. In stretching zone, radial load gradually increases whilst the tangential load almost remains constant. Final stage is the sizing zone which the dimensional tolerances and surface quality of the product is generated. Rolling force in sizing zone is almost the same with the guiding stage.

As it is revealed that, maximum loads are generated in the knifing and stretching zones. Therefore, effect of influencing factors namely, forming angle (α), stretching angle (β), reduction ratio (δ) and die velocity (v) on knifing zone (first stage) and stretching zone (third stage) will be discussed in the following chapters.

CHAPTER 4

NUMERICAL SIMULATIONS of CWR PARAMETERS

4.1 INTRODUCTION

In the present chapter, CWR tools and initial billet model were generated by using CAD software named SolidWorks. FEM based DEFORM 3D software package was used to attain all simulation models belong to force analysis of flat type cross wedge rolling operations.

4.2 DESCRIPTION OF THE PROCESS

Finite Element Method (FEM) has wide acceptance on metal deformation analysis. Although cross wedge rolling is a new trend technology, there are some attempts to discuss the application of numerical simulation methods by using FEM since it has some advantages in solving general problems with complex shapes of the formed parts [8].

It is very important to analyze rolling parameter characteristics of cross wedge rolling processes to be able for calculating power requirement, determining rigidity of the wedges and selecting tools. Difficulties to reach the dimensionally accurate products, analysis of parameters and forces which are effective in die design have wide importance. In order to solve the problem, the most important process parameters influencing the forming loads such as forming angle, stretching angle, reduction ratio and die velocity are determined as effecting variables. On the grounds of three dimensional elastoplastic model, lots of cross wedge rolling conditions were simulated and analyzed by DEFORM 3D. In the following section sequence of setting processes are outlined.

4.3 SETTING UP PROCEDURES ON DEFORM 3D

Setting-up process is composed of three consecutive steps named as pre-processor, execution and post-processor. First step begins with the definition of the file name as shown in Figure 4.1, After the Problem Setup window appeared, “CWR” is written as a problem name in the box and then the “Finish” button is clicked to activate the DEFORM-3D Pre-processor.

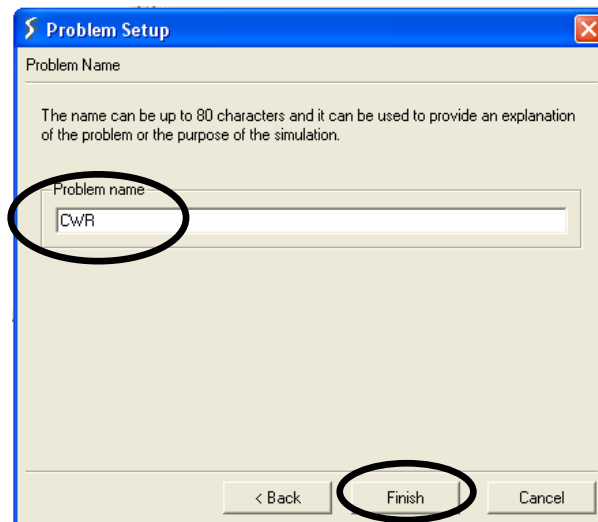


Figure 4.1 Setup a New Problem

Pre-processor starts with the definition of simulation properties. This step is executed by the simulation control panel. After checking the deformation mode option, heat transfer box is activated in order to heat transfer calculations are taken into consideration. This dialog box is shown in Figure 4.2

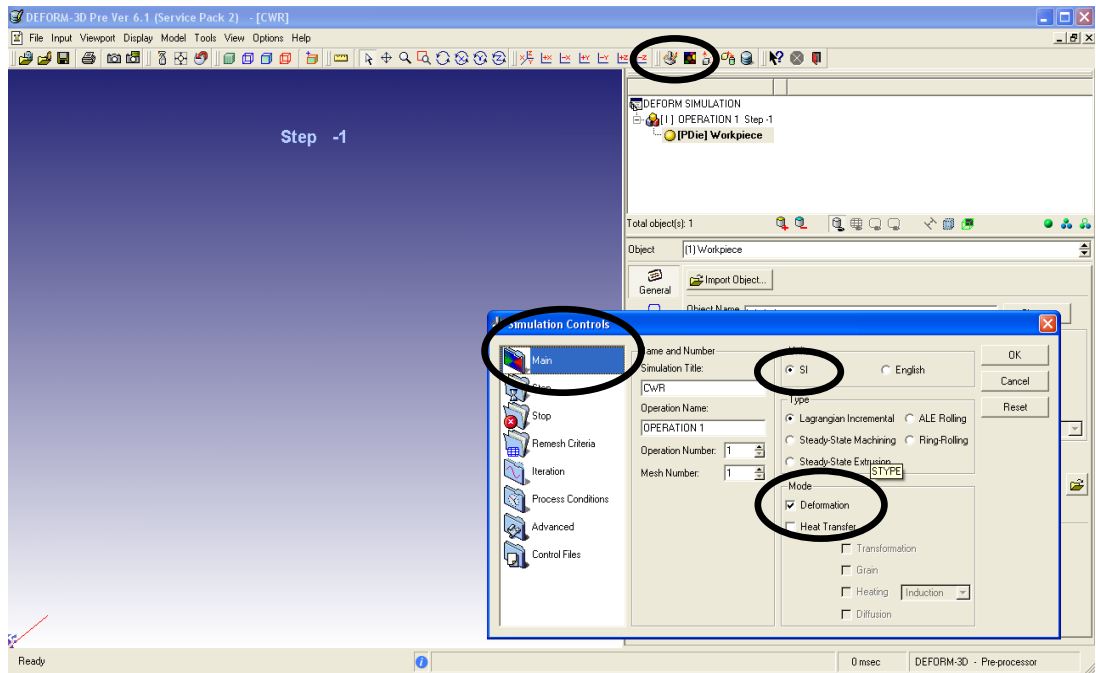


Figure 4.2 Simulation Control Panel

As shown in Figure in 4.3, workpiece geometry should be introduced to the problem by clicking the “Insert Object” button at the bottom of the object tree. Object type is set to elastoplastic.

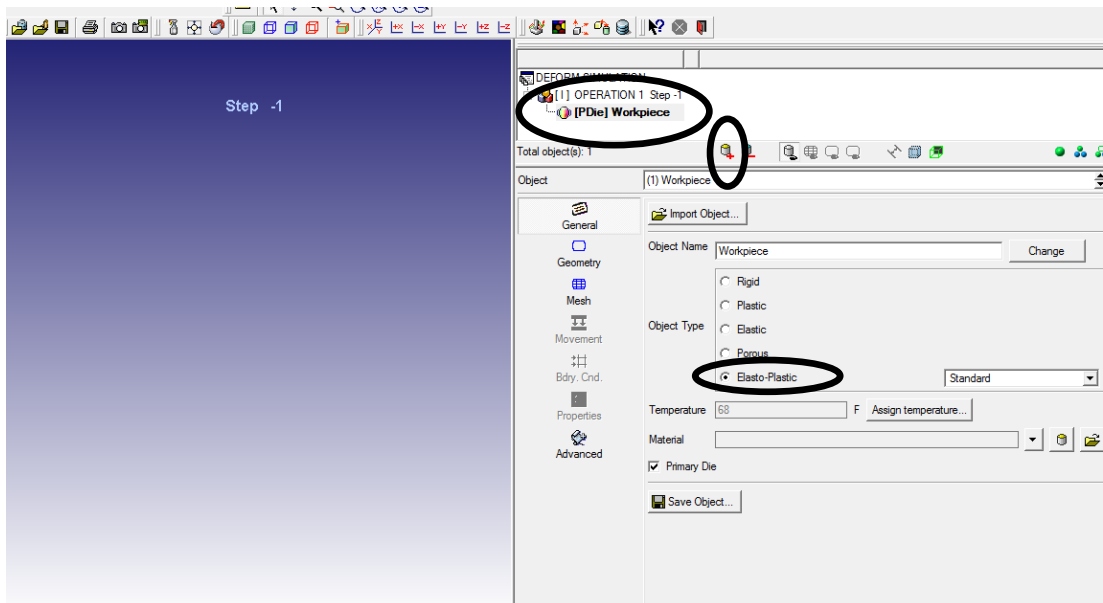


Figure 4.3 Definition of Workpiece

In order to import the object's geometry, "Geo Primitive" buttons need to be clicked. Workpiece cylinder is created by determining the radius and height of the billet as shown in Figure 4.4. Geometry of a cylindrical block appears in the display window.

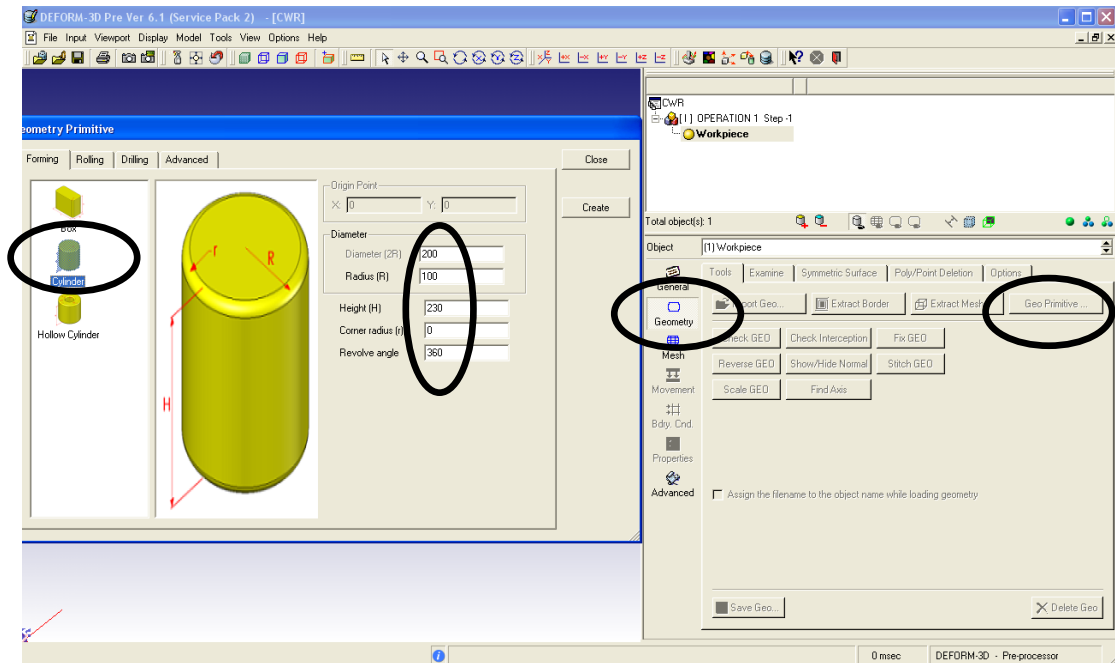


Figure 4.4 Workpiece Geometry Generation

Surface geometry is defined for the CWR and a finite element mesh is generated for the object. "Mesh" button is clicked to bring up the meshing controls. Definition of mesh geometry is shown in Figure 4.5.

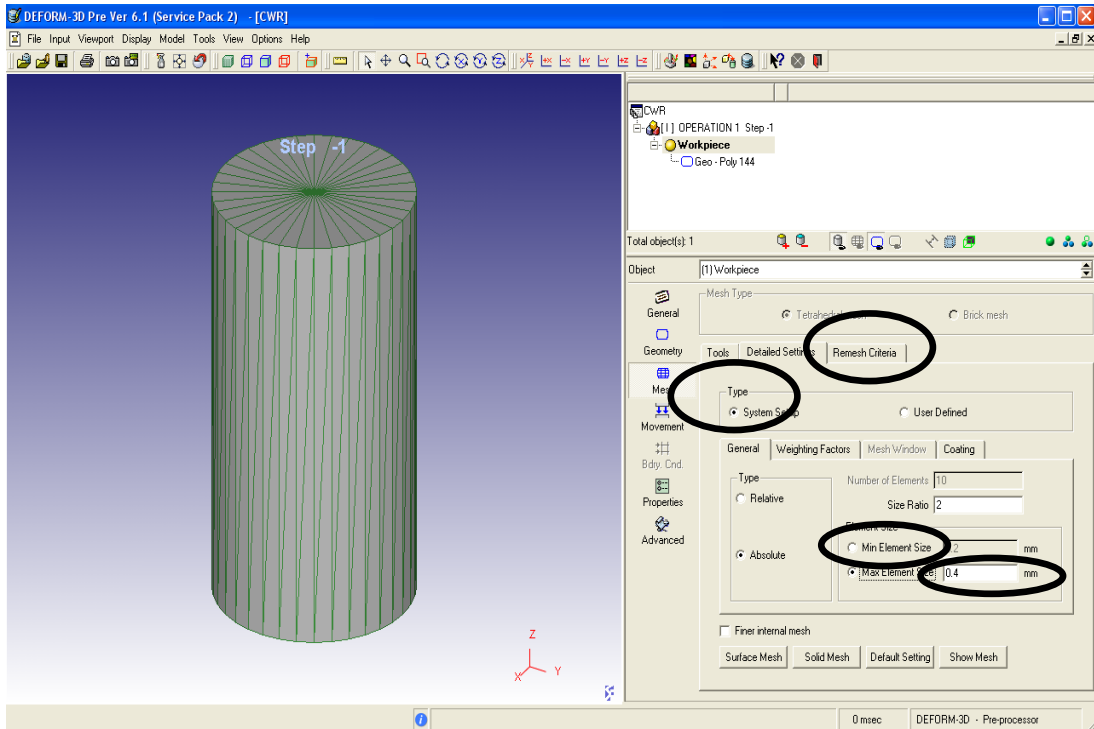


Figure 4.5 Definition of Mesh Geometry

“Absolute Type” meshing should be used under the “Detailed Settings” options. Maximum element size should be written as shown in Figure 4.6. Mesh will be generated by the program automatically after clicking the “Generate Mesh” button.

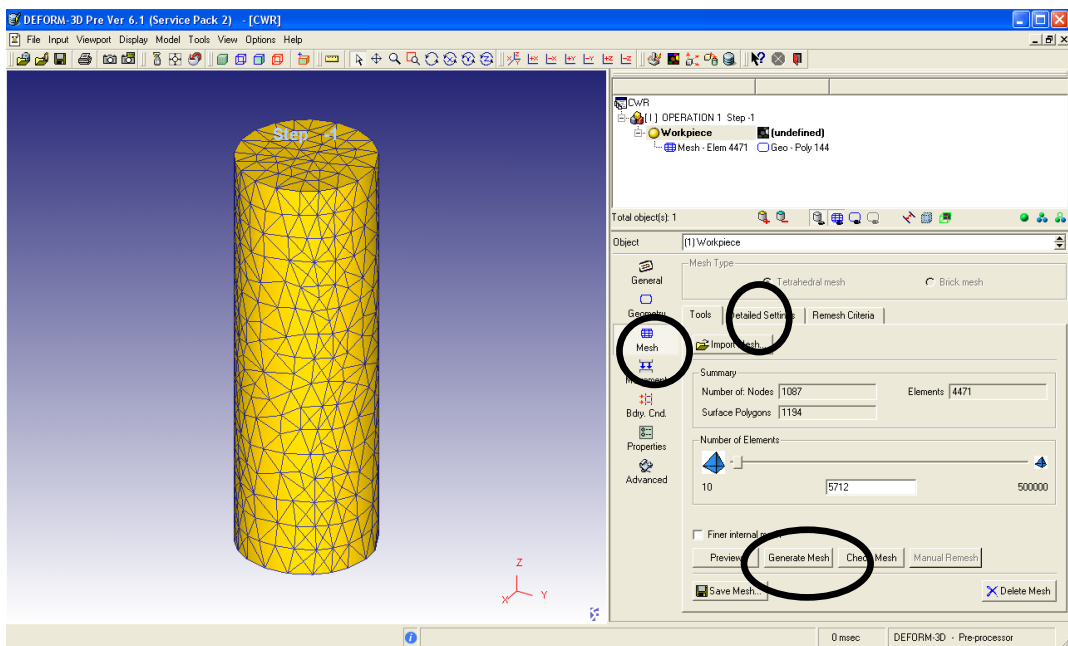


Figure 4.6 Generation of Mesh

At the bottom of the object tree, “Insert Object” icon is clicked twice. Top and Bottom dies will be added to object tree spontaneously. To define the geometry of the top die, geometry and import geometry buttons should be clicked, respectively. In order to upload the file, “.stl” format is obligatory. After loading the file, geometry of the top die appears on the display window. In order to import bottom die geometry, same procedure is followed. All settings mentioned about top and bottom dies are shown in Figure 4.7.

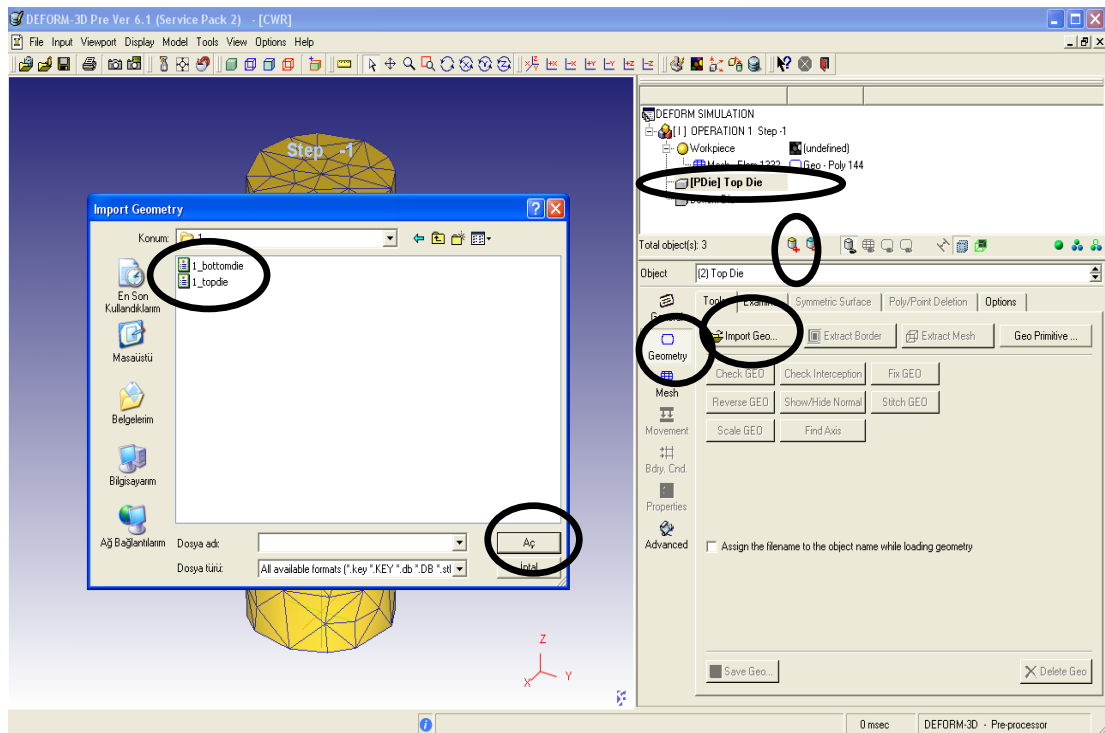


Figure 4.7 Add of Top and Bottom dies

As shown in Figure 4.8 positioning of the dies and workpiece could be adjusted by clicking “Object Positioning” icon. Several methods in order to position objects are available in the options. Apply and OK buttons should be clicked after positioning objects to new location.

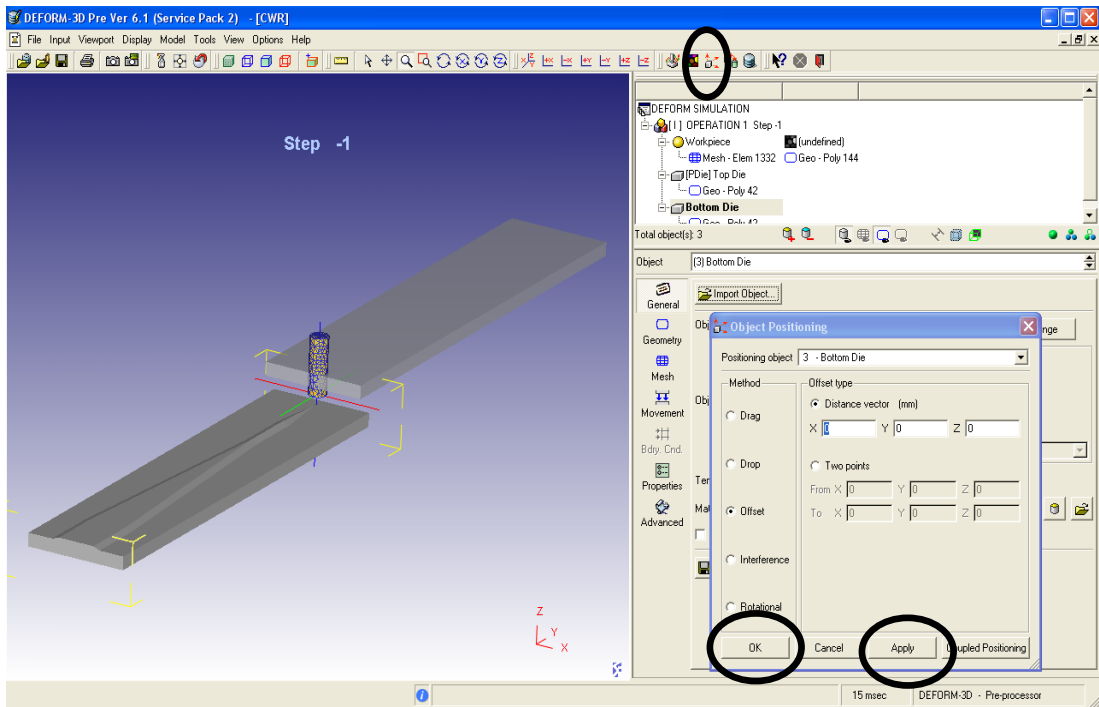


Figure 4.8 Added of Top and Bottom Dies

Movement of wedge dies, need to be defined. In our simulation, both of the dies are moving reciprocally to perform cross wedge rolling operation. To define the top die movement, as shown in Figure 4.9, direction of the motion and velocity of the die is determined by clicking the “Movement” button. Bottom die movement could be defined by applying the same top die procedure.

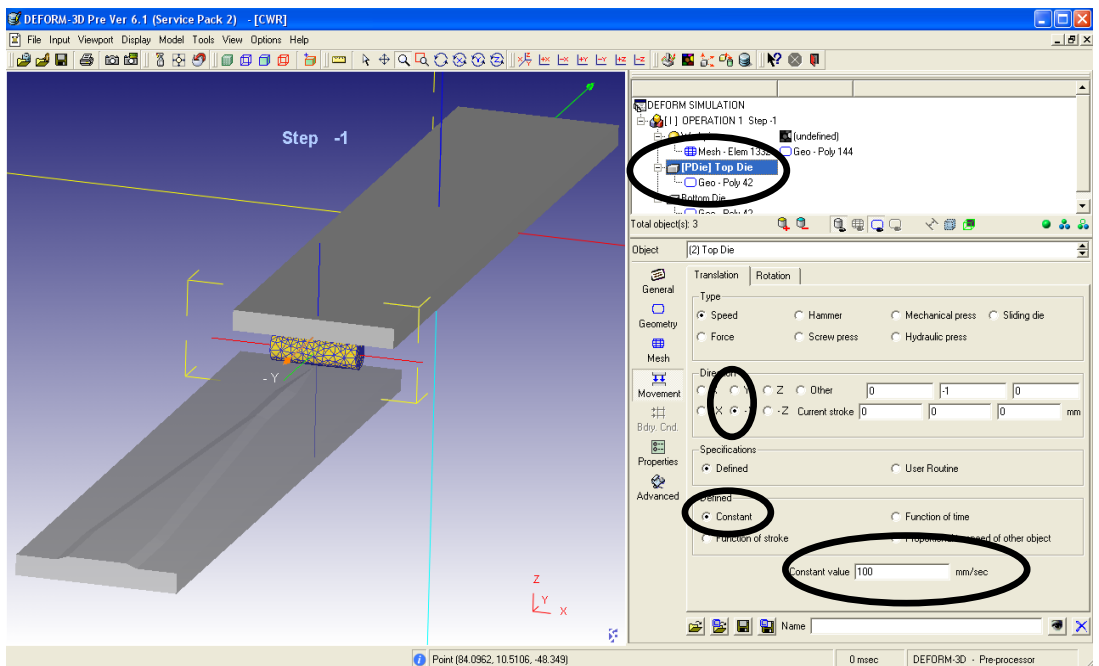


Figure 4.9 Definition of Dies Movement

Material properties of the billet should be selected from material database application. Under “General Properties” option, “Load Material From Library” icon is clicked to allow the material selection process from library. After selection of the material type, “Load” button is clicked to load the material properties of workpiece. Material selection process is shown in Figure 4.10.

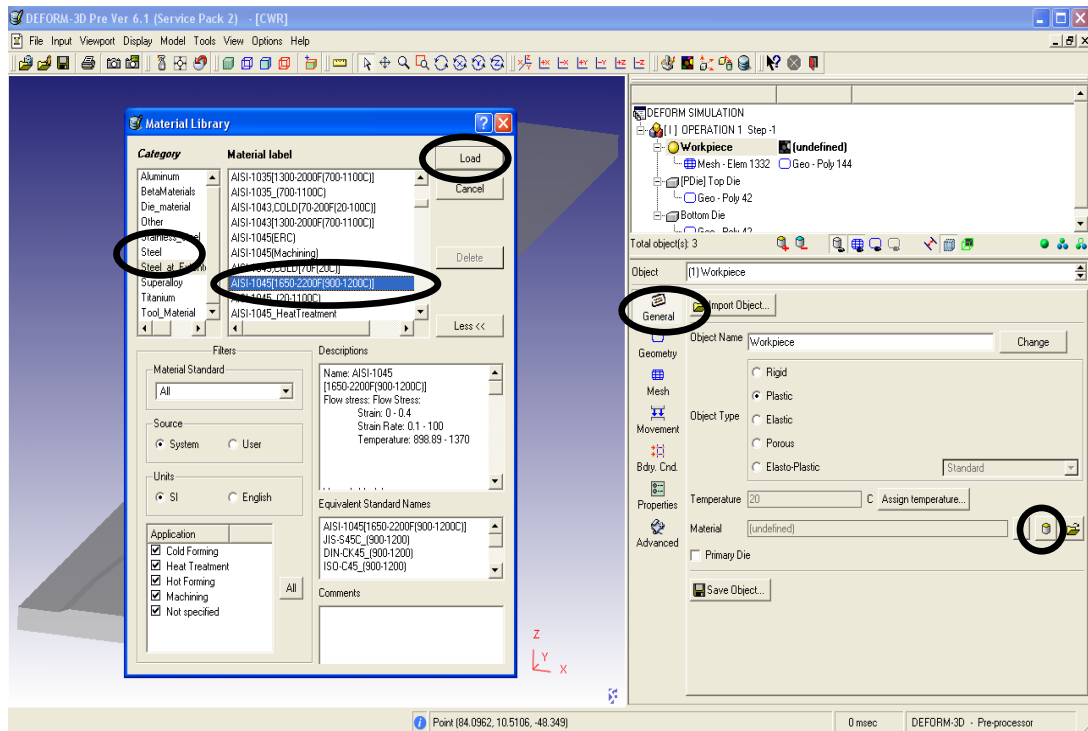


Figure 4.10 Selection of the Material from the Material Library

Owing to material properties temperature of the billet can be defined under the “General Properties” option with the “Assign Temperature” icon. Die temperature is defined with the same procedure. Definition of material temperature is shown in Figure 4.11.

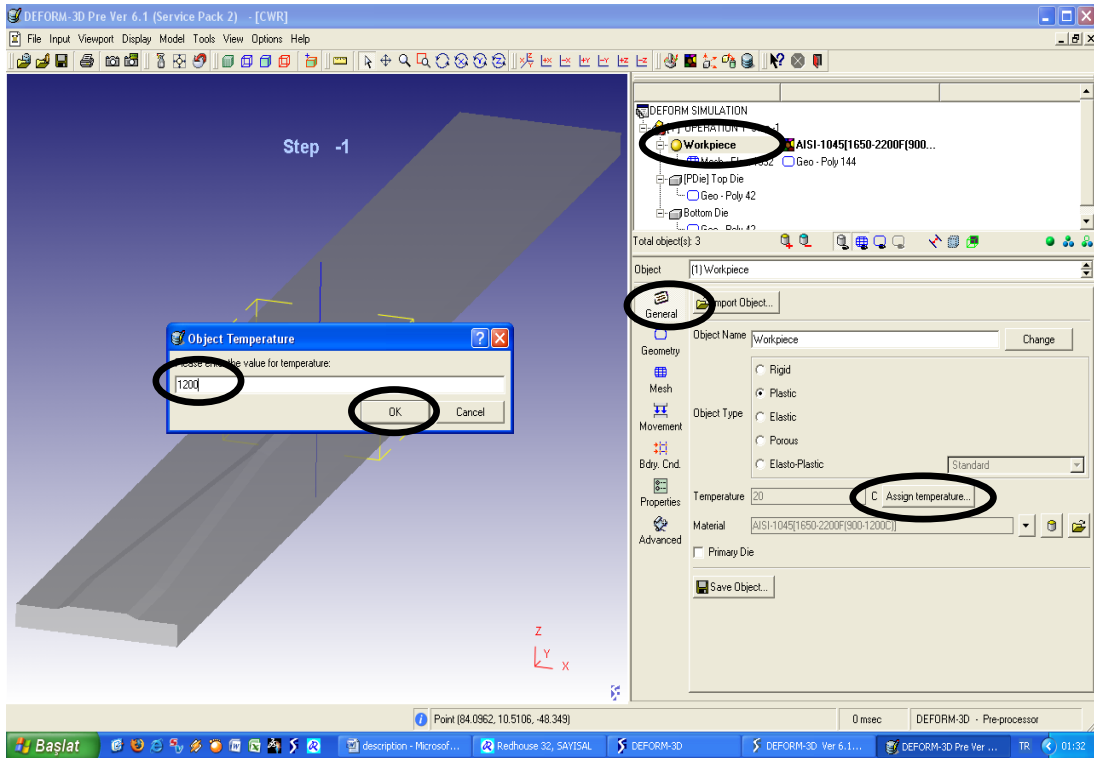


Figure 4.11 Definition of the Material Temperature

To define the interval of the simulation steps, as shown in Figure 4.12, “Simulation Control” option is used. The “Step” icon is clicked to view the time step controls. Die displacement alternative should be activated and approximately one-third of any edge of the elements that was determined with meshing should be calculated and written in the box. Also, total number of simulation steps and step increment must be defined by considering the total length of the tools.

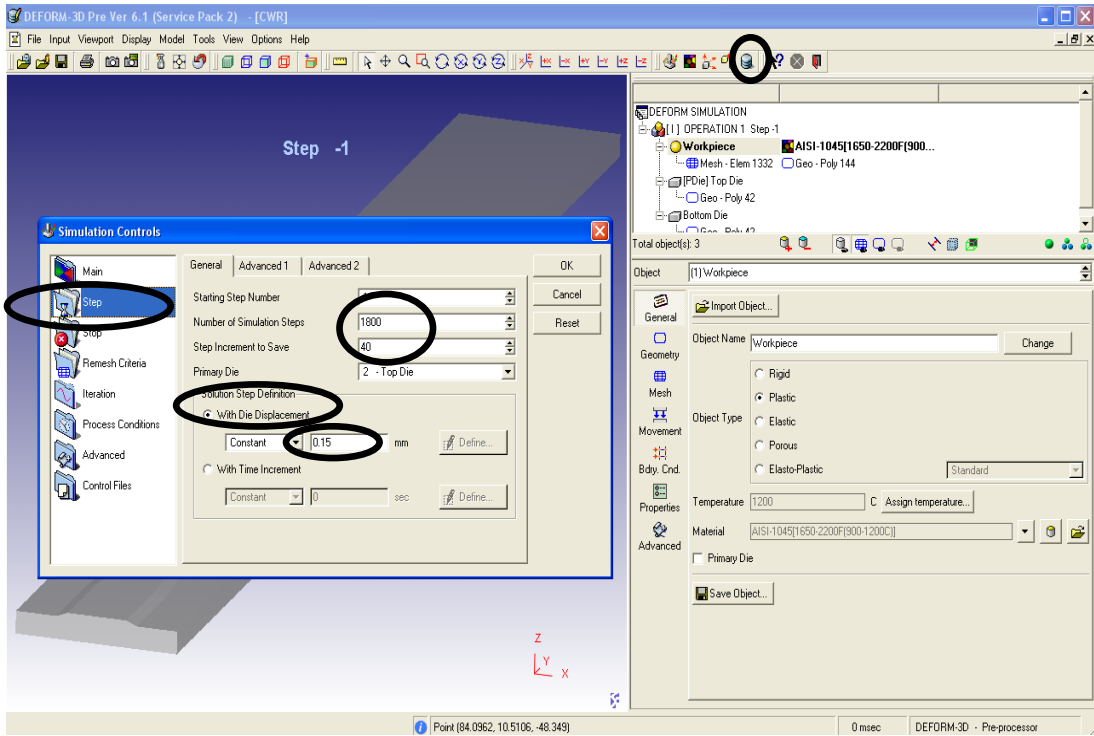


Figure 4.12 Simulation Control Options

Interaction of the objects should be defined for all FEM applications. As shown in Figure 4.13, the “Inter-Object” icon is clicked to define the relationship between the objects. Since there is no relationship currently defined, a pop-up menu will appear asking whether the system is required to add the default relationships or not.

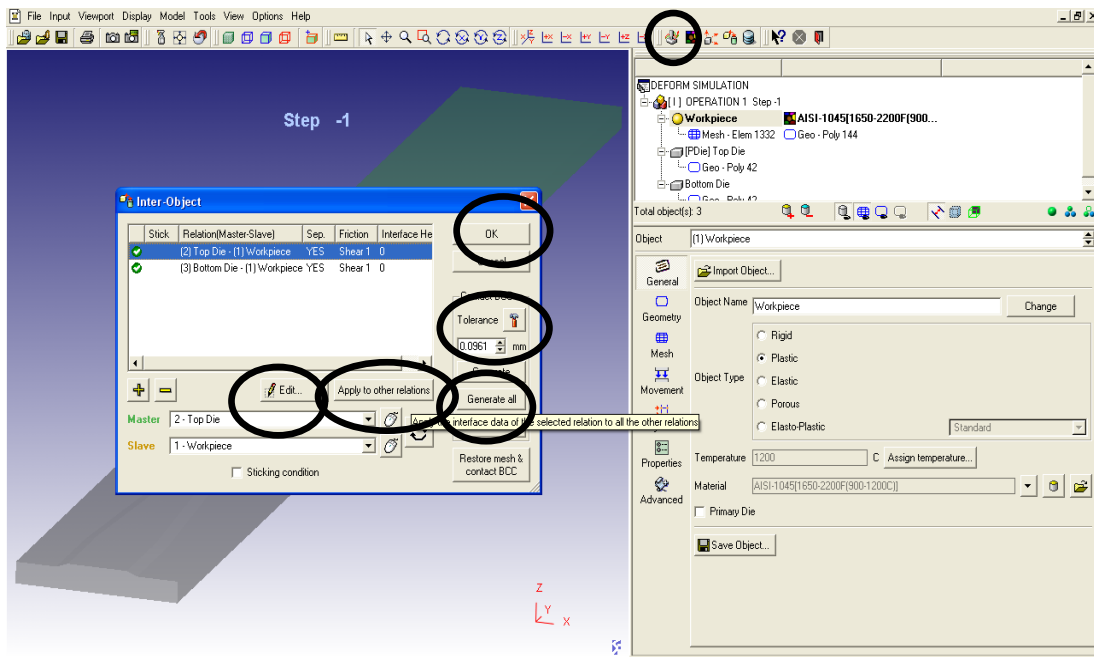


Figure 4.13 Define the Relationship of Between Objects

To define the friction between the tools and workpiece “Edit” button is clicked. “Apply to Other Relation” option can be used for the other tool interactions. Tolerance value will be defined by the system by clicking the “Tolerance” button. After all designations are completed, “Generate All Button” should be clicked to define inter-object data as shown in Figure 4.14.

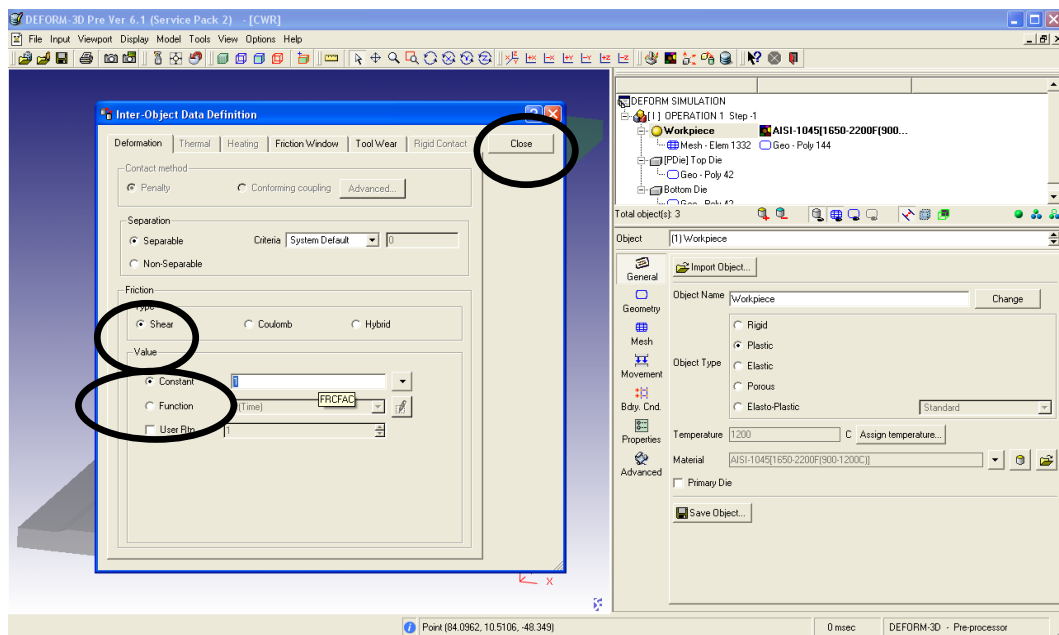


Figure 4.14 Definition of Friction Coefficient

When the problem set up has been completed, the last step is to generation of a database file. The finite element engine uses this database file to store the finite element solutions for the problem. After pressing “Database Generation”, program is checked to see if anything was missed in the problem setup or not. If there is no error for generation, “Database Generated” note appears at the end of the page. Finally as shown in Figure 4.15, “Generate” button is clicked to generate the database.

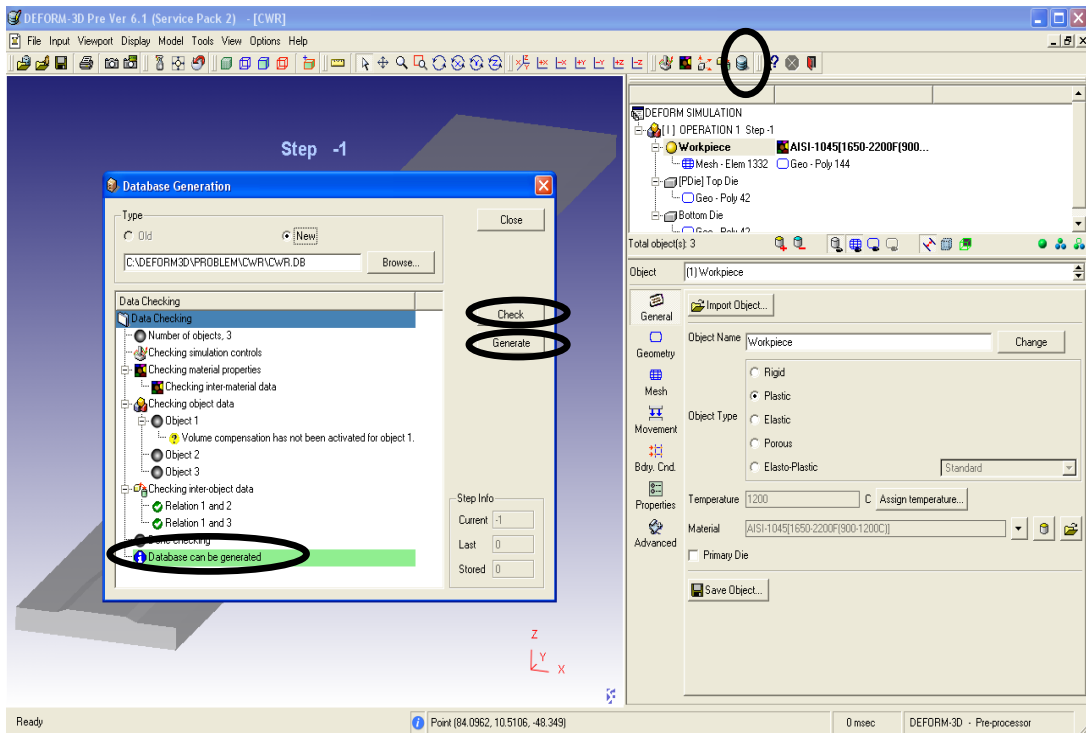


Figure 4.15 Generate Database

After database generation, Pre-processor window of DEFORM is closed. When the main window opens, database file in the problem folder in the directory list is selected and the simulation is started by clicking the “Run” in the Simulator list. “Run simulator” is shown in Figure 4.16.

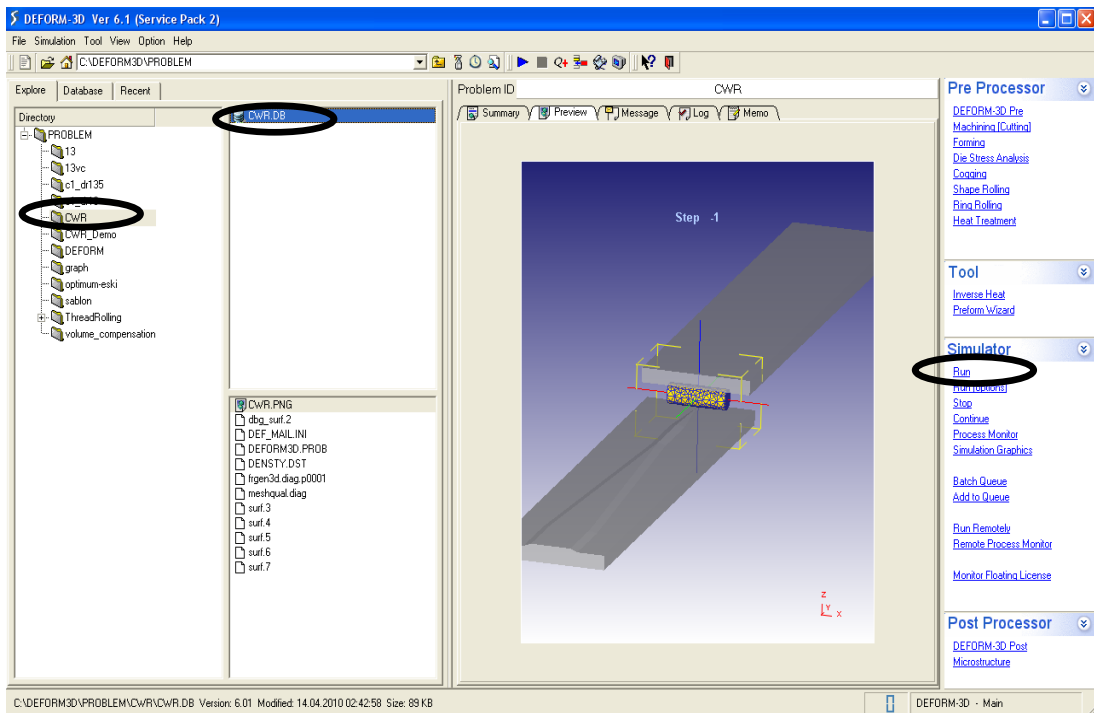


Figure 4.16 Run Simulator

4.4 MESH GENERATION

Mesh generation and determining the number of elements have vital importance in order to simulate the rotational cylindrical workpiece for Cross Wedge Rolling operations. Rolling process requires the rotational movement of the workpiece and thus, each mesh deforms continuously. In the case of less amount of element number is defined, workpiece cannot revolve it's around and final geometry may not be obtained. It also obstructs the obtaining accurate results such as load, torque and energy.

For an optimum CWR process, any edge of each element which constitutes whole shape of material should be smaller than 20% of wedge thickness. Total number of element is directly related with the size of each mesh. Following Figure 4.17 demonstrates the number of element that is going to be used according to reduction ratio.

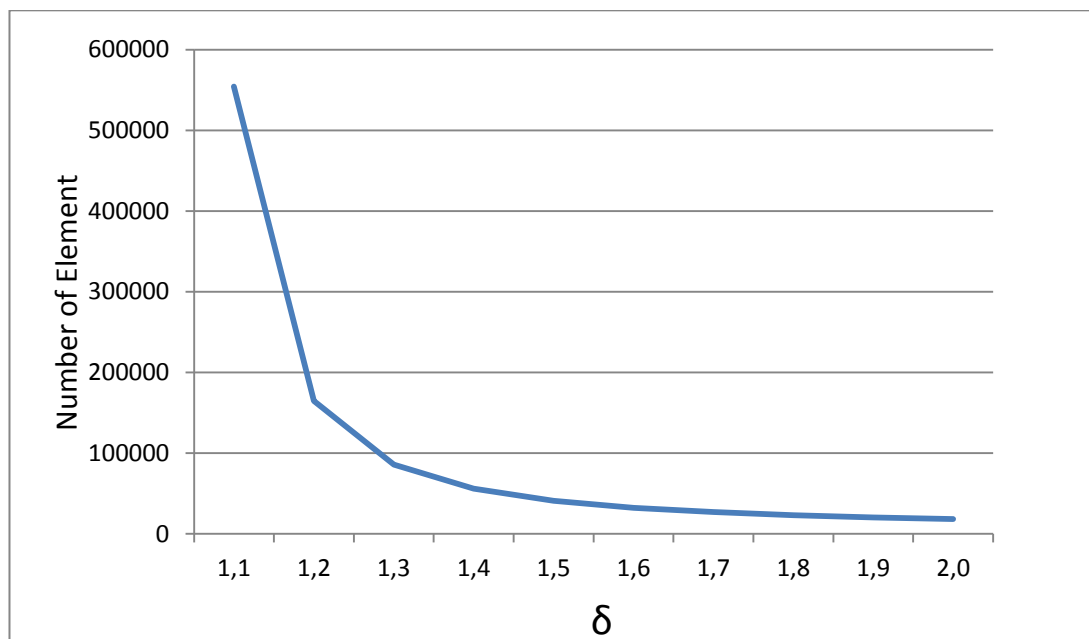


Figure 4.17 Effect of Reduction Ratio (δ)

This process is characterized by the series of process parameters which govern it and the lack of adequate mathematical models to relate these parameters with the controlled variables. The only way to predict the rolling force is to consider finite element simulations or experimentation. The great number of experiments is required but, experimentation is very difficult, time consuming and expensive due to die making costs. Finite element modeling has also several limitations. Within this work,

144 different combinations of input conditions were executed by considering the relevant parameters. Pre-processing and execution of each simulation took 5 days to 10 days without any interruption of dual core computer.

The relevant parameters: Stretching angles (β) are 4° , 6° , 8° , 10° , forming angles (α) are 20° , 30° , 40° , the reduction ratios (δ) are 1.3, 1.4, 1.5 and the die speeds (V) are 50, 75, 100, 125 mm/s. By changing the parameters, simulations were performed and the minimum tangential and radial rolling loads were recorded for knifing and stretching zones accordingly. Table 4.1 shows the alteration of these parameters and presents the rolling loads obtained from numerical simulations.

Table 4.1 Results of Numerical Simulations

NO	β	α	δ	V	Knifing Zone		Stretching Zone	
					Ft(N)	Fr(N)	Ft(N)	Fr(N)
1	4	20	1,4	100	1817,18	5351,83	1804,78	7717,42
2	4	30	1,4	100	1339,50	4224,93	1714,99	6049,49
3	4	40	1,4	100	1069,10	4119,24	1741,02	6318,94
4	6	20	1,4	100	1648,90	5266,03	2205,36	8275,32
5	6	30	1,4	100	1378,98	4639,65	2166,51	7173,99
6	6	40	1,4	100	1032,73	3972,27	2104,67	6680,09
7	8	20	1,4	100	1726,49	5447,03	2649,99	9116,26
8	8	30	1,4	100	1346,78	4479,94	2541,12	7671,40
9	8	40	1,4	100	1068,40	4129,78	2715,00	7548,16
10	10	20	1,4	100	1827,40	5388,63	3240,24	10142,62
11	10	30	1,4	100	1365,94	4465,31	3038,40	8211,91
12	10	40	1,4	100	1018,36	4165,77	3008,40	9156,05
13	4	20	1,5	100	2199,78	5929,67	1776,81	7167,91
14	4	30	1,5	100	1605,38	5218,83	1751,87	6000,36
15	4	40	1,5	100	1345,84	4490,47	1666,70	5614,31
16	6	20	1,5	100	1501,40	4691,49	1808,79	6215,47
17	6	30	1,5	100	1601,40	4991,49	2108,79	6915,47
18	6	40	1,5	100	1246,55	4283,13	2308,24	7329,89
19	8	20	1,5	100	2198,30	6005,71	2608,24	8229,89
20	8	30	1,5	100	1722,63	5138,31	2510,70	7154,07
21	8	40	1,5	100	1211,17	4442,77	2688,37	6497,84
22	10	20	1,5	100	2231,87	5832,69	3258,97	9019,23
23	10	30	1,5	100	1627,44	4940,35	3458,97	7828,08
24	10	40	1,5	100	1229,23	4581,85	3658,97	8596,66
25	4	20	1,3	100	1341,04	4503,68	1867,37	8148,78
26	4	30	1,3	100	1036,24	4119,51	1792,90	7113,68
27	4	40	1,3	100	741,38	3761,79	1848,79	6077,44

Table 4.1 Results of Numerical Simulations (Continue)

NO	β	α	δ	ν	Knifing Zone		Stretching Zone	
					Ft(N)	Fr(N)	Ft(N)	Fr(N)
28	6	20	1,3	100	1414,87	4798,86	2241,99	9007,65
29	6	30	1,3	100	1003,77	4128,77	2196,57	7949,25
30	6	40	1,3	100	864,74	3806,51	2271,87	7133,44
31	8	20	1,3	100	1403,82	4912,50	2702,46	10056,84
32	8	30	1,3	100	937,20	4085,56	2589,21	8830,69
33	8	40	1,3	100	849,33	3759,92	2877,18	8704,66
34	10	20	1,3	100	1386,97	4820,27	3317,23	11875,19
35	10	30	1,3	100	1021,15	4094,59	2999,29	9927,94
36	10	40	1,3	100	871,49	3813,81	3215,89	10536,99
37	4	20	1,4	50	1730,10	5046,37	1722,31	7452,88
38	4	30	1,4	50	1173,16	4070,67	1674,80	6158,44
39	4	40	1,4	50	937,74	3467,00	1666,45	5565,64
40	6	20	1,4	50	1687,28	5494,63	2143,98	7919,89
41	6	30	1,4	50	1270,76	4364,90	2045,77	6159,14
42	6	40	1,4	50	1035,14	4126,93	2097,29	6117,73
43	8	20	1,4	50	1648,47	5122,38	2603,82	8588,17
44	8	30	1,4	50	1302,59	4287,36	2505,94	6742,31
45	8	40	1,4	50	1016,66	3903,51	2491,09	6743,30
46	10	20	1,4	50	1285,29	4279,39	3157,77	8315,73
47	10	30	1,4	50	1285,29	4279,39	3159,80	8095,64
48	10	40	1,4	50	1033,77	4121,55	3359,80	7681,02
49	4	20	1,5	50	2110,55	5655,47	1701,46	7053,32
50	4	30	1,5	50	1540,98	4623,70	1574,34	5848,24
51	4	40	1,5	50	1259,76	4332,69	1615,74	5287,02
52	6	20	1,5	50	1359,76	4232,69	1815,74	5487,02
53	6	30	1,5	50	1510,00	5100,10	2006,16	6240,02
54	6	40	1,5	50	1173,17	4159,88	1995,49	5226,06
55	8	20	1,5	50	2065,67	5734,94	2606,47	8965,68
56	8	30	1,5	50	1565,13	4541,64	2532,30	6612,41
57	8	40	1,5	50	1246,04	4142,39	2432,30	5758,90
58	10	20	1,5	50	2105,86	5654,76	3280,30	9088,22
59	10	30	1,5	50	1605,89	4641,64	3180,30	8111,48
60	10	40	1,5	50	1222,66	4186,66	3080,30	7584,24
61	4	20	1,3	50	1316,19	4559,14	1756,83	8132,47
62	4	30	1,3	50	879,03	3226,64	1680,60	7128,53
63	4	40	1,3	50	667,02	3182,20	1556,55	6374,03
64	6	20	1,3	50	1298,05	4571,57	2085,04	8849,18
65	6	30	1,3	50	957,19	3997,41	2209,71	7283,04
66	6	40	1,3	50	766,55	3635,32	2189,97	6452,45
67	8	20	1,3	50	1292,67	4699,88	2605,43	9792,56
68	8	30	1,3	50	992,75	4088,68	2405,43	9392,56
69	8	40	1,3	50	794,27	3674,35	2654,77	8023,88
70	10	20	1,3	50	1303,04	4569,02	3119,81	11402,62

Table 4.1 Results of Numerical Simulations (Continue)

NO	β	α	δ	v	Knifing Zone		Stretching Zone	
					Ft(N)	Fr(N)	Ft(N)	Fr(N)
71	10	30	1,3	50	852,25	4018,56	3056,69	9826,68
72	10	40	1,3	50	754,48	3699,88	2956,69	9111,52
73	4	20	1,4	75	1748,57	5198,77	1783,09	7622,15
74	4	30	1,4	75	1333,90	4144,16	1696,38	6301,61
75	4	40	1,4	75	1014,44	4167,32	1711,11	6109,54
76	6	20	1,4	75	1701,41	5243,91	2212,88	8199,98
77	6	30	1,4	75	1342,35	4459,20	2090,57	7823,19
78	6	40	1,4	75	1024,34	4069,50	2171,35	6215,71
79	8	20	1,4	75	1611,48	5365,30	2598,10	8853,32
80	8	30	1,4	75	1287,38	4393,96	2534,90	7221,90
81	8	40	1,4	75	1187,38	4205,63	2434,90	7867,64
82	10	20	1,4	75	1699,23	5262,43	3067,39	9898,79
83	10	30	1,4	75	1202,24	4177,28	2367,39	9628,57
84	10	40	1,4	75	1077,98	4214,72	2067,39	9681,65
85	4	20	1,5	75	2194,90	5772,20	1769,40	7128,60
86	4	30	1,5	75	1592,38	4765,55	1607,13	5937,76
87	4	40	1,5	75	1220,93	4542,58	1624,78	5408,77
88	6	20	1,5	75	1120,93	4342,58	1590,78	5208,77
89	6	30	1,5	75	1567,36	4862,54	2049,54	6768,00
90	6	40	1,5	75	1198,23	4678,63	1992,88	5848,70
91	8	20	1,5	75	2188,30	5858,26	2567,09	8129,10
92	8	30	1,5	75	1637,79	4655,57	2581,25	6793,48
93	8	40	1,5	75	1437,79	4540,44	2581,25	6385,16
94	10	20	1,5	75	2139,48	5674,87	2381,25	9148,97
95	10	30	1,5	75	1716,37	4658,09	2481,25	9118,97
96	10	40	1,5	75	1168,90	4250,93	2281,25	9137,77
97	4	20	1,3	75	1344,59	4677,58	1801,89	8410,63
98	4	30	1,3	75	1001,10	4063,83	1755,73	7365,18
99	4	40	1,3	75	811,62	3849,73	1826,90	7228,95
100	6	20	1,3	75	1377,50	4739,14	2244,10	9245,49
101	6	30	1,3	75	1013,54	4034,20	2174,79	7936,65
102	6	40	1,3	75	905,82	3787,93	2388,35	7430,73
103	8	20	1,3	75	1312,75	4389,98	2601,75	10123,76
104	8	30	1,3	75	1512,75	3989,98	2401,75	9023,76
105	8	40	1,3	75	778,50	3705,76	2201,75	8563,76
106	10	20	1,3	75	1327,80	4454,74	3055,48	11014,53
107	10	30	1,3	75	9027,80	4104,67	3040,48	9578,43
108	10	40	1,3	75	804,01	3698,12	3127,77	9955,07
109	4	20	1,4	125	1833,92	5488,12	1833,74	7820,12
110	4	30	1,4	125	1365,24	4776,06	1746,33	6510,11
111	4	40	1,4	125	1044,37	4228,73	1772,58	6394,77
112	6	20	1,4	125	1808,20	5220,19	2287,83	8439,72
113	6	30	1,4	125	1344,77	4566,57	2210,01	6884,61
114	6	40	1,4	125	1061,33	4263,50	2104,87	6687,25

Table 4.1 Results of Numerical Simulations (Continue)

NO	β	α	δ	V	Knifing Zone		Stretching Zone	
					Ft(N)	Fr(N)	Ft(N)	Fr(N)
115	8	20	1,4	125	1700,70	5259,85	2712,29	9123,75
116	8	30	1,4	125	1306,23	5066,04	2702,67	7710,57
117	8	40	1,4	125	1071,27	4129,25	2732,67	7847,21
118	10	20	1,4	125	1805,23	5394,02	3286,90	10796,79
119	10	30	1,4	125	1334,24	4374,68	3489,69	8260,37
120	10	40	1,4	125	1062,99	4229,30	3841,13	9007,69
121	4	20	1,5	125	2200,04	6069,68	1833,18	7227,11
122	4	30	1,5	125	1672,58	4845,77	1683,88	6106,49
123	4	40	1,5	125	1261,33	4206,00	1565,89	5567,81
124	6	20	1,5	125	1261,33	4206,00	1565,89	5567,81
125	6	30	1,5	125	1602,77	4756,84	2127,21	6445,73
126	6	40	1,5	125	1259,91	4691,43	2065,66	6223,93
127	8	20	1,5	125	2334,10	6025,54	2709,45	8406,25
128	8	30	1,5	125	1691,98	5242,64	2628,88	7482,55
129	8	40	1,5	125	1391,87	4449,79	2528,88	7042,06
130	10	20	1,5	125	2256,35	5961,36	3249,85	9565,19
131	10	30	1,5	125	1680,54	5026,71	3049,85	7619,99
132	10	40	1,5	125	1298,24	4819,59	3855,30	8807,61
133	4	20	1,3	125	1396,25	4777,30	1741,06	8359,38
134	4	30	1,3	125	1056,11	4408,37	1807,65	7598,25
135	4	40	1,3	125	802,97	3738,44	1869,87	7318,62
136	6	20	1,3	125	1385,31	4886,45	2289,72	9143,86
137	6	30	1,3	125	1043,77	4290,49	2255,19	8040,54
138	6	40	1,3	125	788,98	3774,07	2211,54	7412,75
139	8	20	1,3	125	1398,28	4839,31	2781,24	10471,01
140	8	30	1,3	125	1029,28	4301,45	2718,33	8650,48
141	8	40	1,3	125	766,84	3816,92	2765,17	8781,65
142	10	20	1,3	125	1390,11	4775,97	3211,88	11449,61
143	10	30	1,3	125	1017,66	4331,52	3147,77	10558,08
144	10	40	1,3	125	801,77	3770,72	3277,90	10354,14

Because of the complexity of the process, some assumptions were made. These assumptions are:

- 1) Die material is selected as rigid and workpiece is selected as elastoplastic material.
- 2) Friction between tools and workpiece was simplified as shear friction and assumed as constant.

3) Workpiece material is AISI 1045 steel.

In addition to geometric parameters, initial length and diameter of the billet have been defined as $L_0=42.6$ mm and $d_0=14$ mm respectively. All numerical simulations have been performed for AISI-1045 steel hot forming process and tetrahedral mesh elements have been used for the billet material. Mechanical and thermal properties of the billet material such as, coefficient of thermal expansion, specific heat, thermal conductivity and Young's modulus have been assumed according to DEFORM material database. Three dimensional CWR model is shown in Figure 4.18.

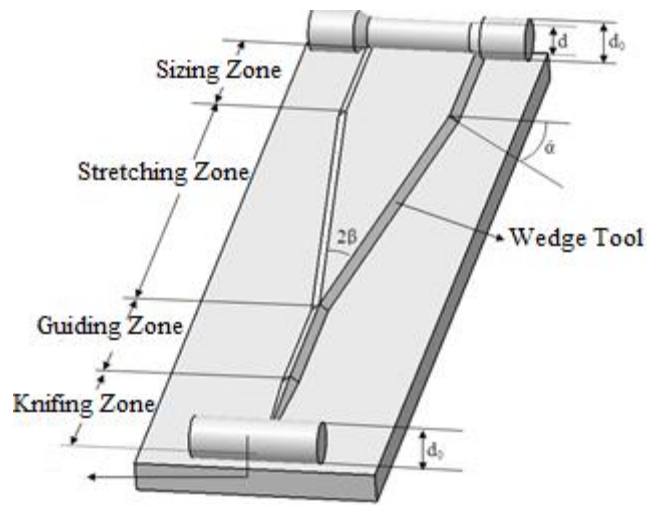


Figure 4.18 Three dimensional model of a wedge die.

The temperature of the work piece and surrounding air has been determined as 1200°C and 20°C respectively. The contacts between the tools and hot billet material are periodically repeated during process is resulting an increased temperature of the tools. Owing to heat transfer between the tools and work piece, initial temperatures of the tools have been determined as 200°C .

The step interval of die displacement for finite element calculations was adjusted with die displacement of 0.15 mm for all simulations. This option has been allowed for at least 1500 simulation steps and thus high sensitive load-stroke diagrams were obtained.

4.5 ANALYSIS of NUMERICAL RESULTS

4.5.1 The Effect of Stretching Angle (β) on Rolling Loads

In the following Figures 4.19 and 4.20, detailed graphics of tangential and radial loads are presented respectively to illustrate the effect of stretching angle with respect to forming angle and reduction ratio.

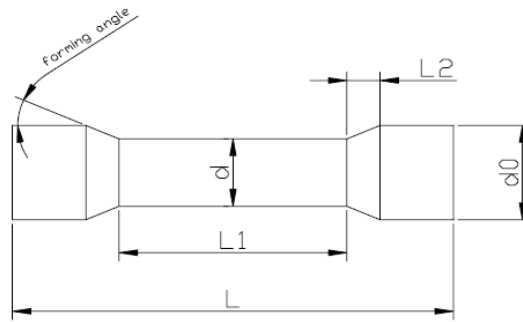


Figure 4.19 Final Geometry of Workpiece

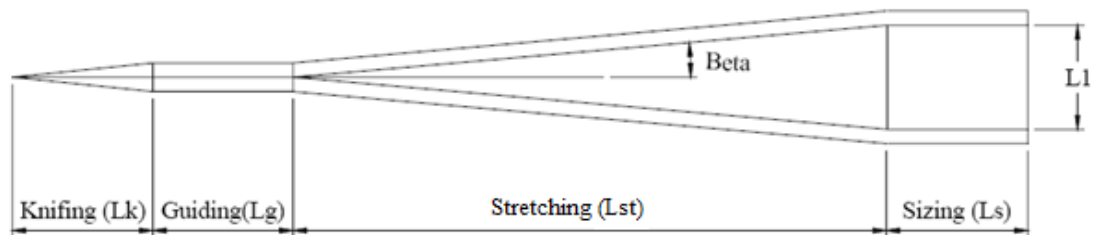


Figure 4.20 Wedge Geometry

$$L=42,6 \text{ mm} \quad L1=32,6 \quad L2=5,49 \quad d_0=14 \text{ mm} \quad d1=10 \text{ mm}$$

$$\text{Knifing zone (Lk)} = 2\pi r_0$$

$$Lk = 44 \text{ mm}$$

$$\text{Guiding zone (Lg)} = 2\pi r_0$$

$$Lg = 44 \text{ mm}$$

$$\text{Stretching zone (Lst)} = L1 / 2 \tan \beta$$

$$Lst = 31,6 / 2 \tan 4 \quad Lst = 31,6 / 2 \tan 6 \quad Lst = 31,6 / 2 \tan 8 \quad Lst = 31,6 / 2 \tan 10$$

$$Lst = 227,33 \text{ mm} \quad Lst = 150,47 \text{ mm} \quad Lst = 225,71 \text{ mm} \quad Lst = 89,77 \text{ mm}$$

$$\text{Sizing zone (Ls)} = \pi * D$$

$$\text{Sizing zone (Ls)} : \pi * 10 \quad Ls = 31,41 \text{ mm}$$

$$L_T = L + Lk + Lg + Lst$$

$$L_T = 44 + 44 + 227,33 + 31,41$$

$$L_T = 346,74$$

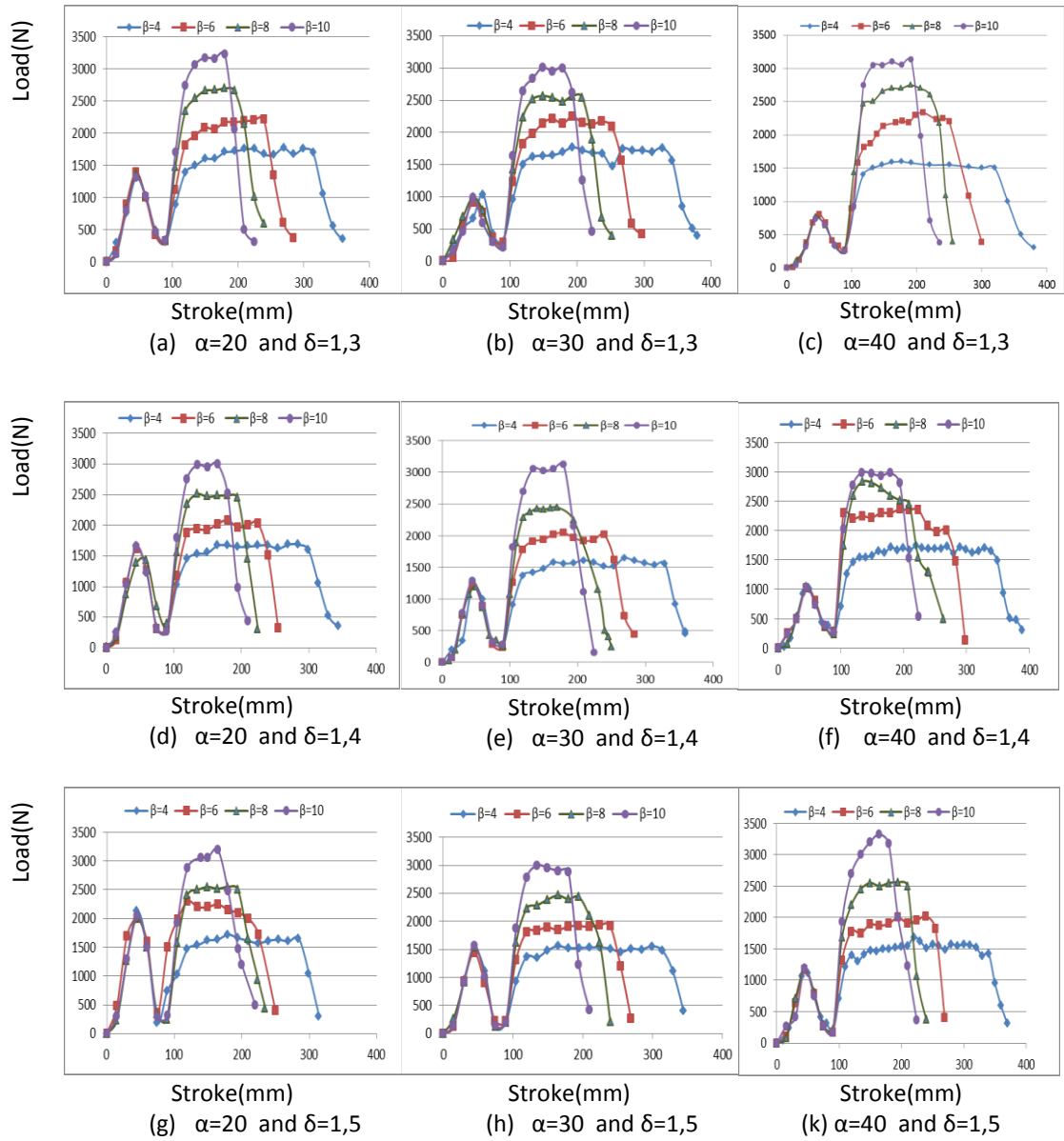


Figure 4.21 Tangential Loads According to Stretching Angle

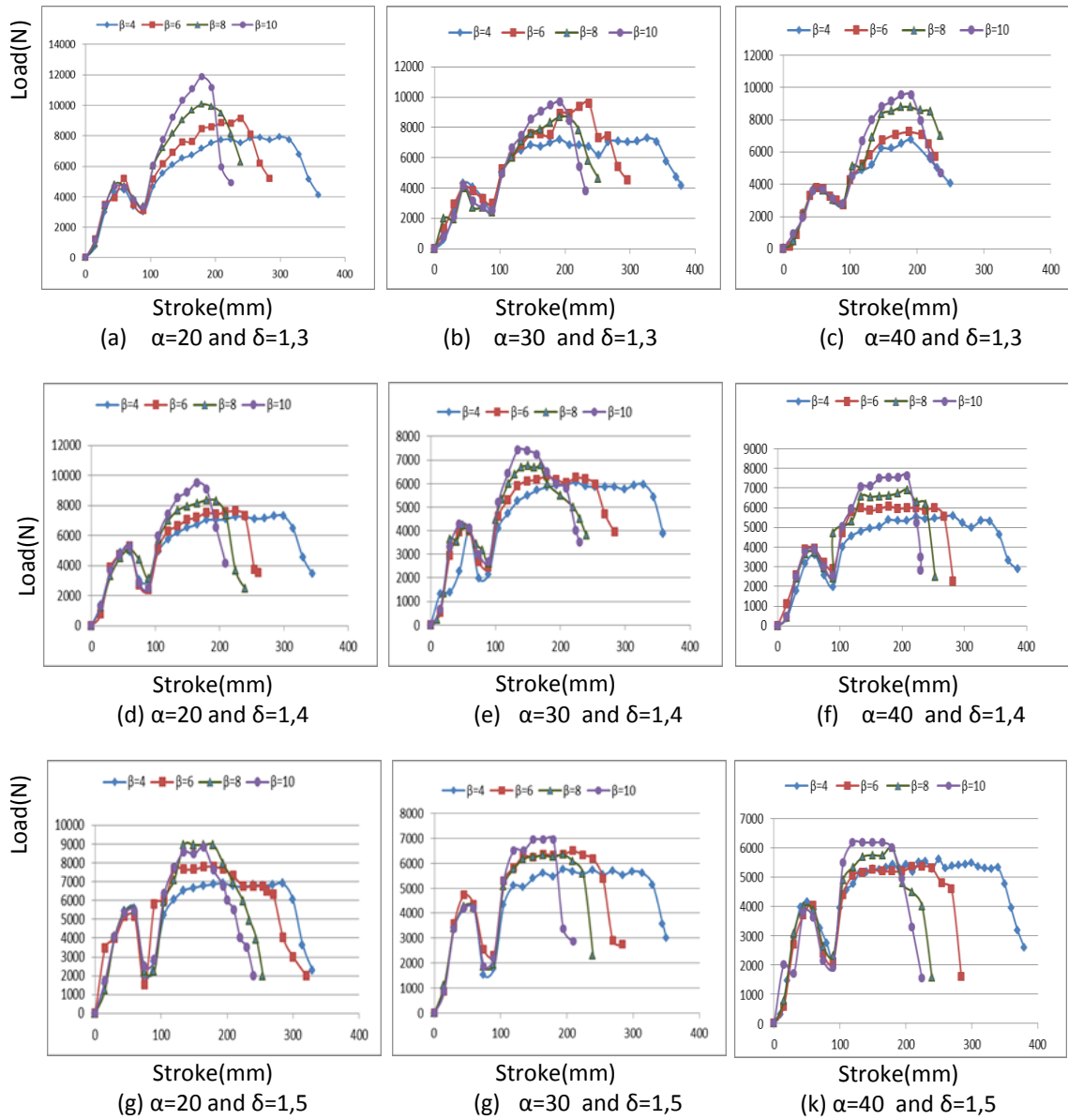


Figure 4.22 Radial Loads According to Stretching Angle (β)

From Figures 4.19 (a, b and c) it is seen that in knifing zone, tangential load values decrease while the forming angle increases. Increment of forming angle from 20° to 40° results decrement in tangential load values from 1500N to 800N around, while reduction ratio remains unchanged.

It is apparent that, increment in reduction ratio results the increment in tangential load throughout the knifing zone as shown in Figure 4.19 (d, e, f). But, reduction ratio has no or little effect in stretching zone.

From Figure 4.19 it is also clear that the die length is directly related with the stretching angle. Greater stretching angles can be regarded as an advantage due to shorter tool requirement however this preference will cause to higher forming loads. The other conclusion is that the stretching angle has no effect on knifing zone while it has greater effects on stretching zone.

Augmentation of the stretching angle (β) causes greater tangential and radial force requirements due to more metal flow per unit length since metal flow and axial extension of the billet material expose cross wedge rolling tools to greater resistance. All graphs in Figure 4.19 show that maximum tangential loads are achieved in the stretching zone for the highest stretching angle value.

The other note is that, in both guiding and sizing zones have the smallest tangential load values.

Radial load graphs depending on forming angles are demonstrated in Figures 4.20 (a, b and c). The main distinguishing feature of radial load is that it is approximately four times greater than tangential load in the same conditions. This is mainly due to the rotational compression of the workpiece external surface by the mounting dies. The other point observed in stretching zone is that in stretching zone, tangential load almost remains stable while radial load is not.

4.5.2 The Effect Forming Angle (α) on Rolling Loads

In the following Figures 4.21 and 4.22, detailed graphics of tangential and radial loads are presented respectively to illustrate the effect of forming angle with respect to stretching angle and reduction ratio.

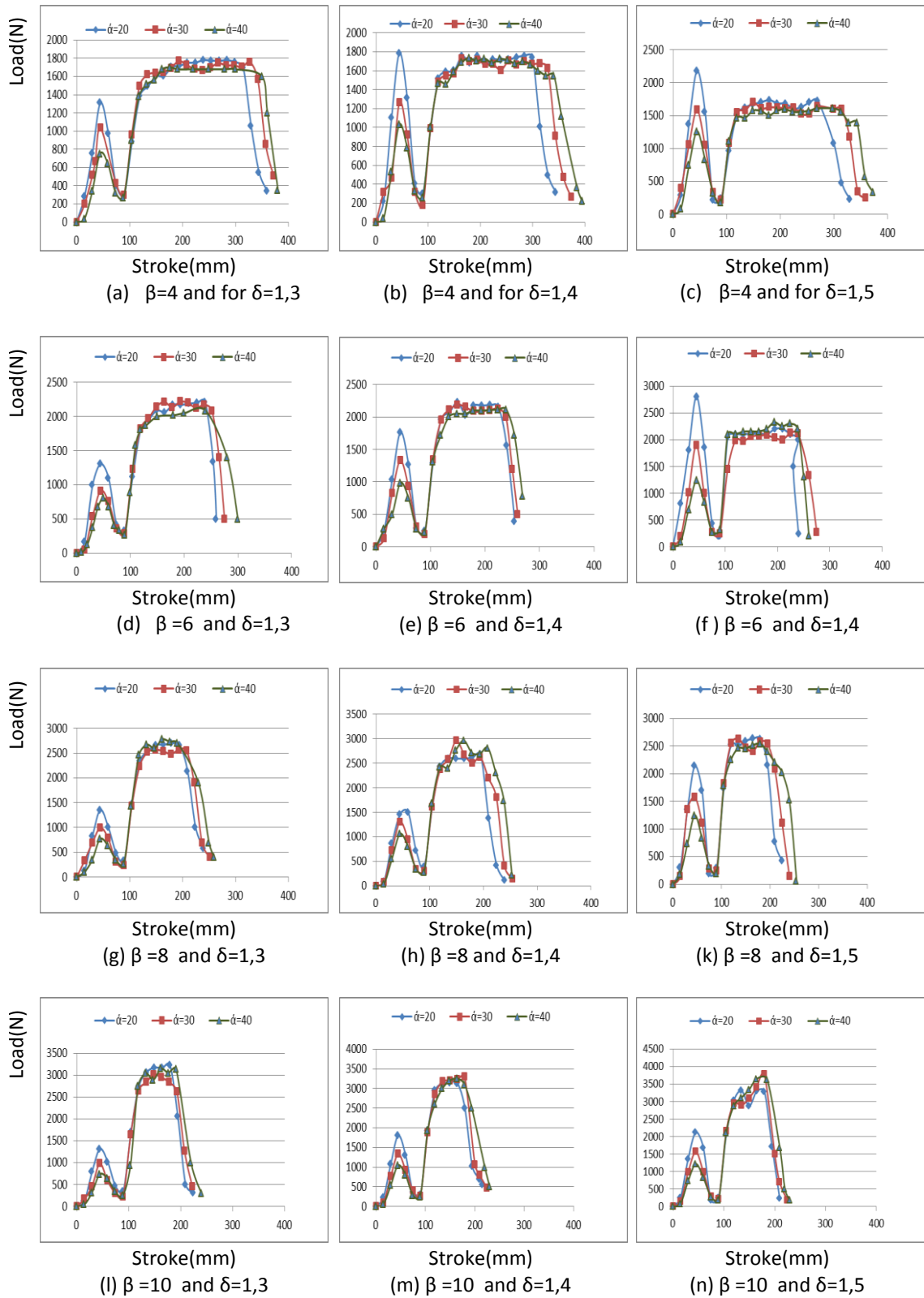


Figure 4.23 Tangential Loads According to Forming Angle (α)

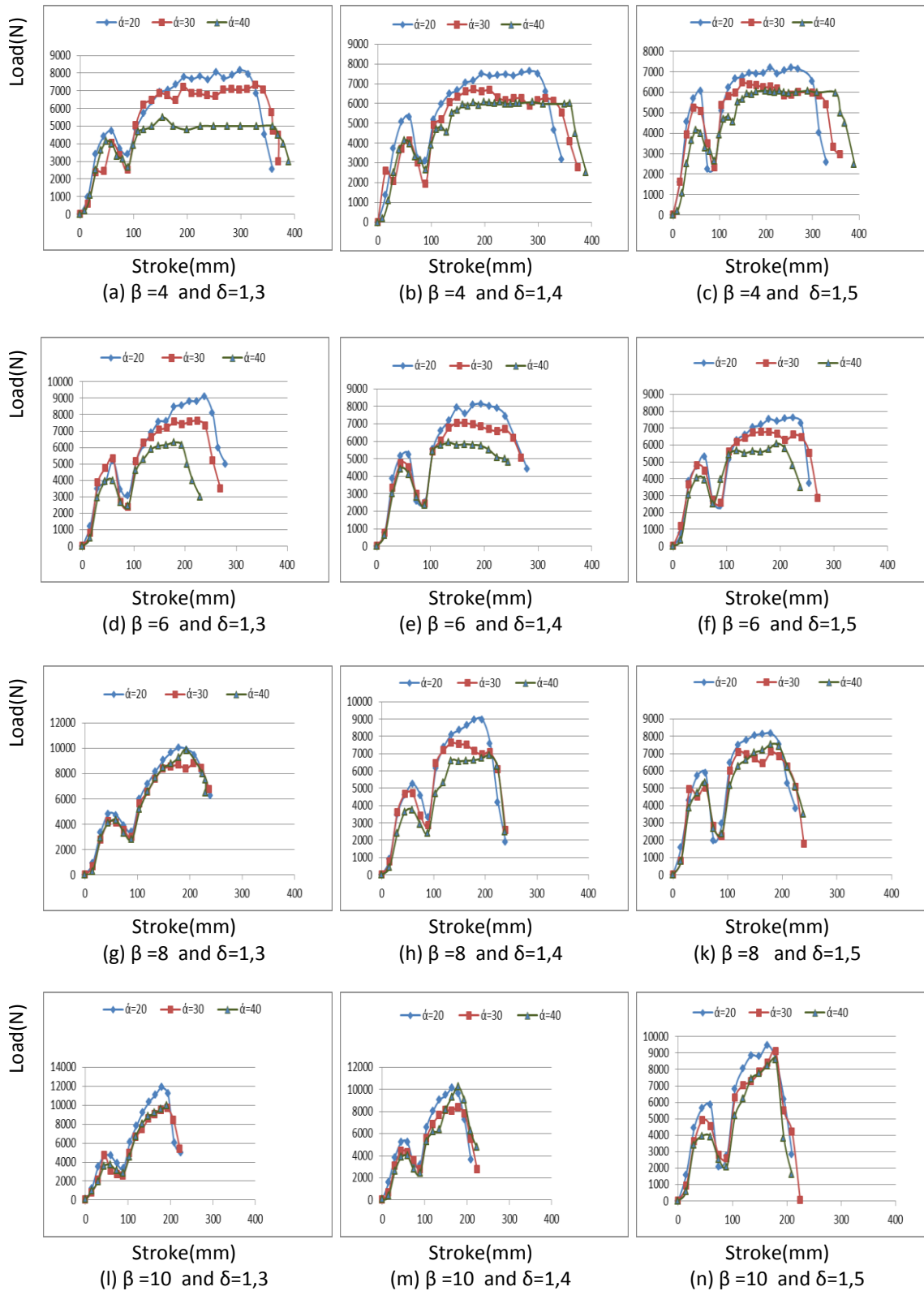


Figure 4.24 Radial Loads According to Forming Angle (α)

The forming angle (α) determines the side width of the wedges. It is apparently seen that forming angle has a main effect especially in knifing zone. As it is seen from Figure 4.21, all graphs denote that smaller values of forming angle results the higher tangential forces. This is mainly due to the workpiece and die contact surface.

As expected, in stretching zone all graphs collide with one another. Thus it can be concluded that forming angle has no or little effect on tangential load in stretching zone. While the forming angle increasing, width of the guiding zone decreases and as a theoretical approach, augmentation of the forming angle up to 90^0 causes disappearance of width of the guiding zone. As it is also reported from the literature [21], determination of excessive forming angle could cause surface cracks on the guiding zone owing to tools can lose their ability to withstand tangential or radial force by reduction of tool strength.

The effect of the forming angle on the tangential and radial load has different understanding and diversity of angles doesn't alter the load stripes significantly. In spite of this remark, it can be mentioned that increased radial and tangential loads accompany the augmentation of forming angle. Additionally, load fluctuation is the cause of larger forming angle.

4.5.3 The Effect of Reduction Ratio (δ) on Rolling Loads

In Figures 4.23 and 4.24, detailed graphics of tangential and radial loads are presented respectively to illustrate the effect of reduction ratio with respect to stretching angle and forming angle.

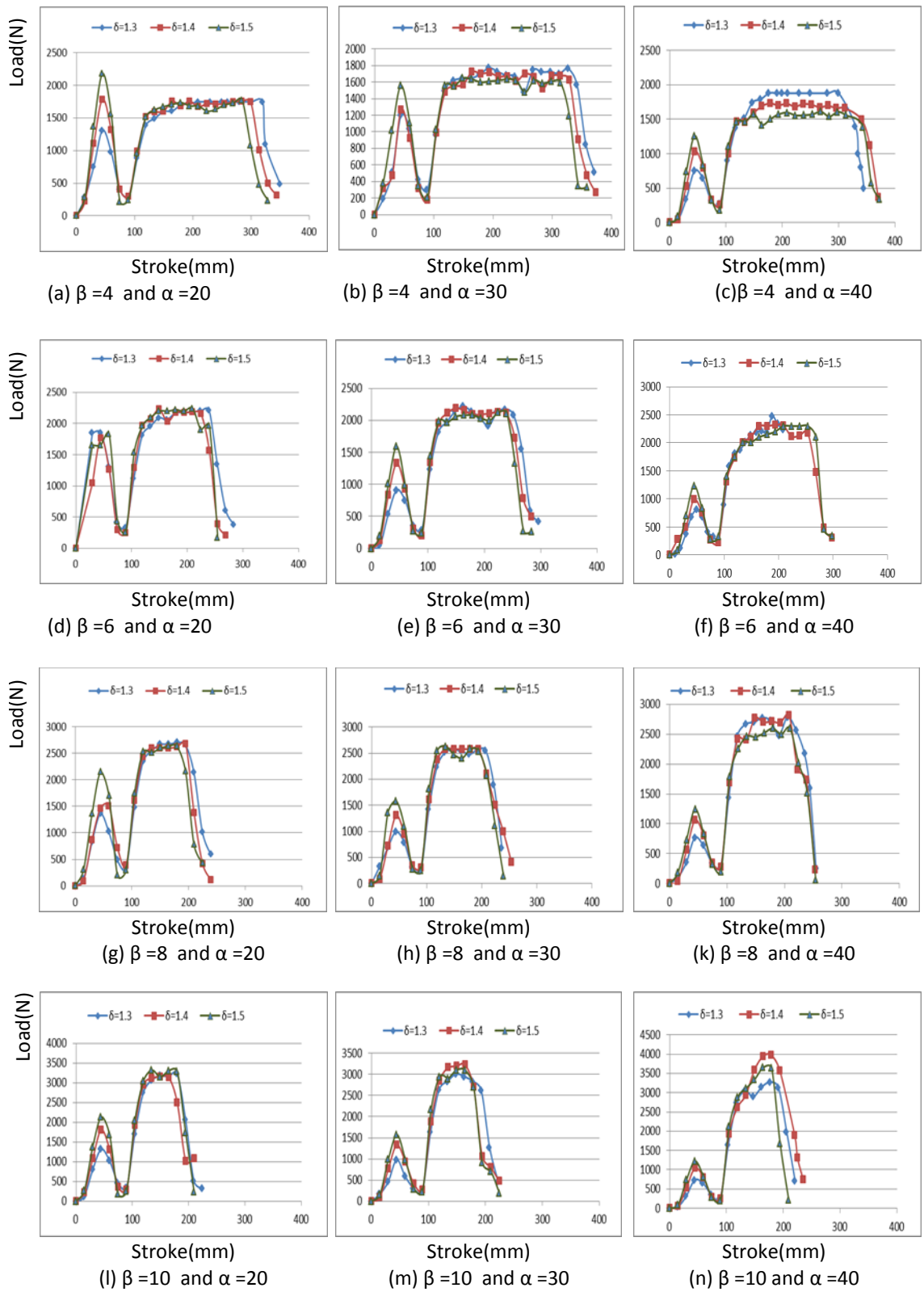


Figure 4.25 Tangential Loads According to Reduction Ratio (δ).

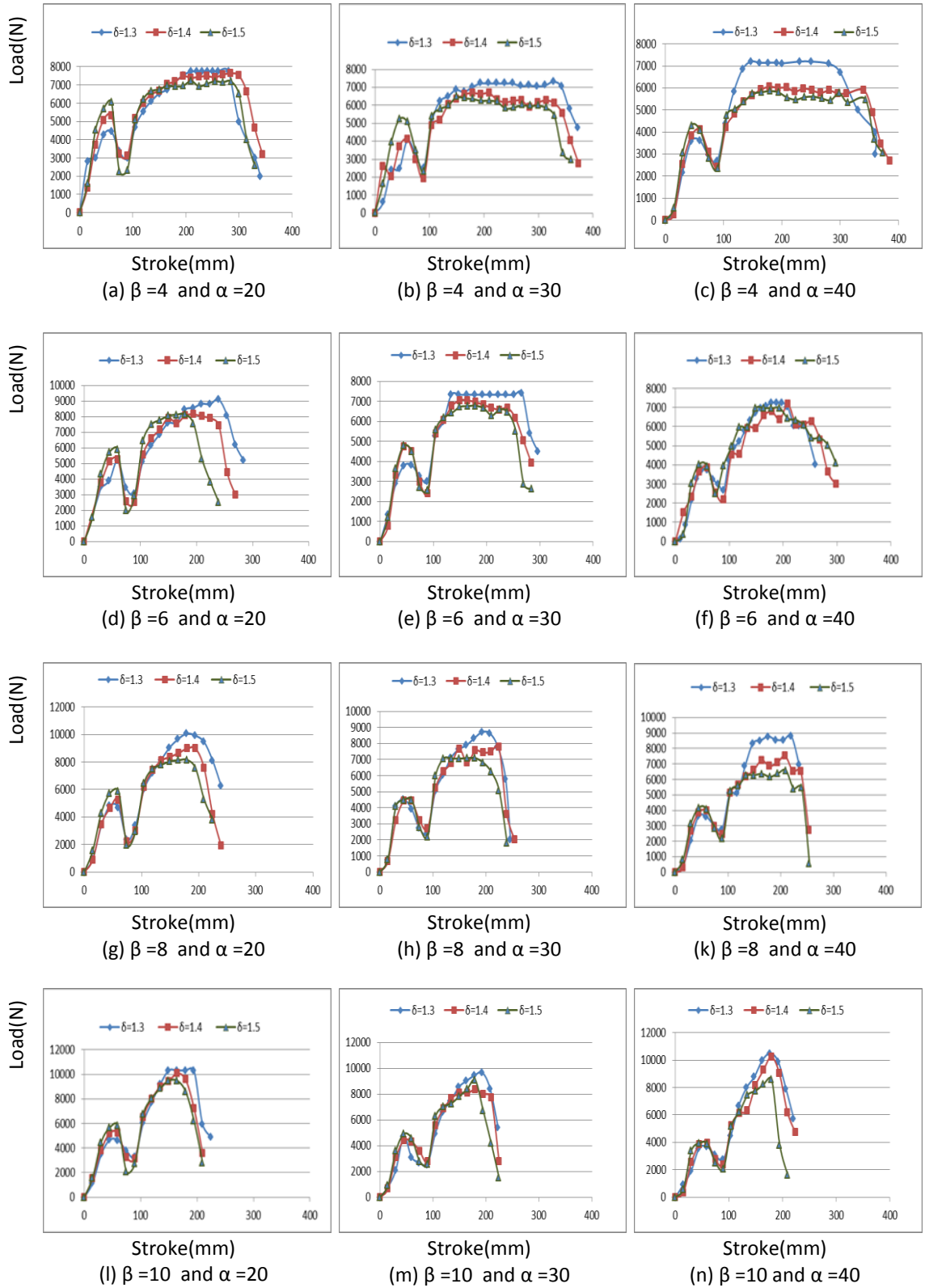


Figure 4.26 Radial Loads According to Reduction Ratio (δ).

Reduction ratio is the one of the most important technical parameters in cross wedge rolling operations and it is pertaining to wedge thickness. Greater reduction ratio can be achieved by merely utilizing thicker wedges which are facing one another while the initial diameter of the cylindrical billet material doesn't change. It is reported that [18,35], just like greater stretching angle, thicker wedges also can be considered as an advantage due to provides much more reduction in diameter but tendency of constitute slippage defects or internal cracks should be taken into consideration.

It has been found that radial and tangential load strips remain almost constant throughout the guiding and sizing zones while they increase throughout the knifing and stretching zones. It can be observed that from the Figures 4.23 and 4.24 the tools having greater reduction ratio needs much more forming load.

4.5.4 The Effect Tool Velocity (V) on Rolling Loads

In the following Figures 4.25 and 4.26, detailed graphics of tangential and radial loads are presented respectively to illustrate the effect of tool velocity with respect to forming angle and reduction ratio.

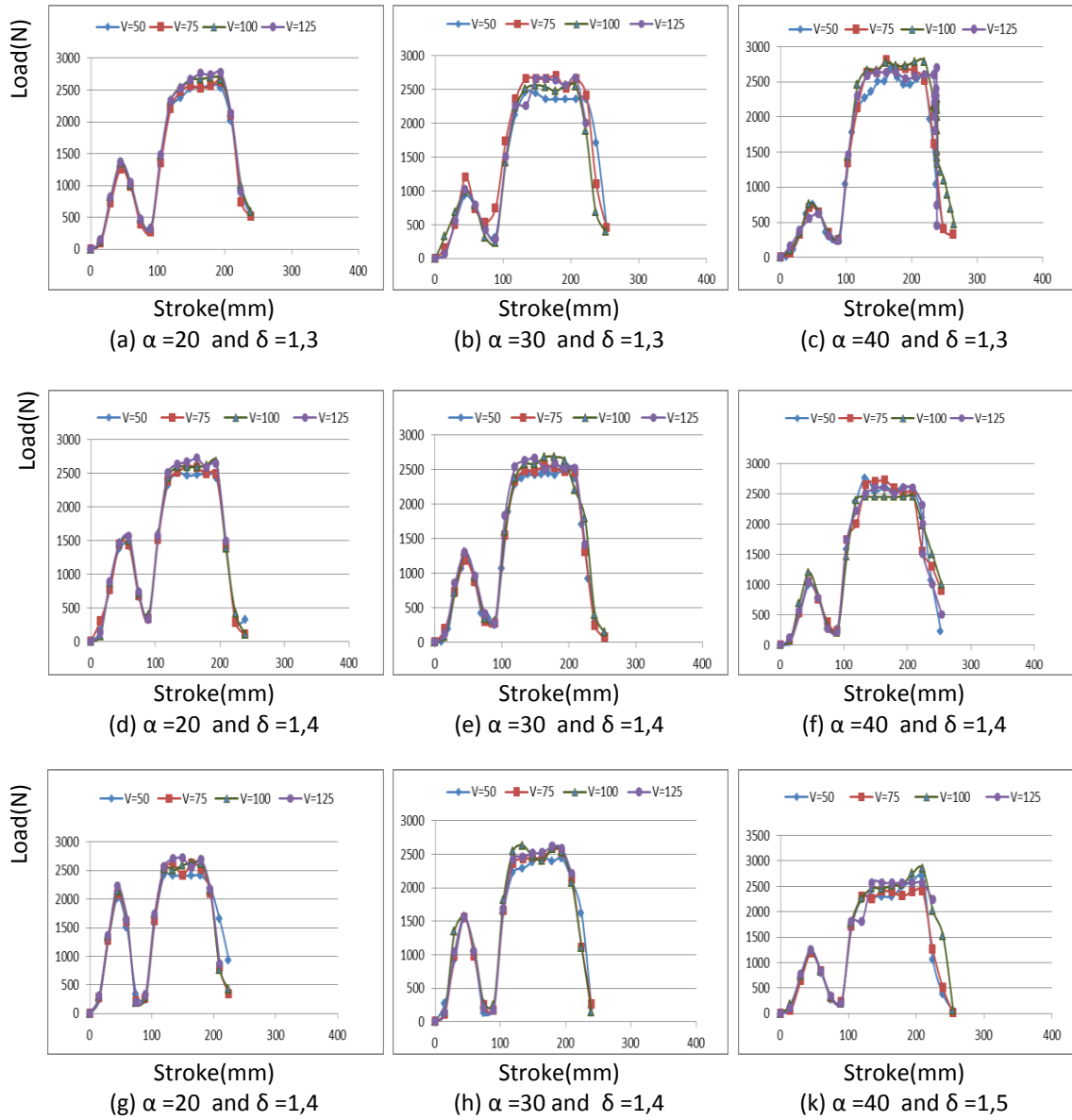


Figure 4.27 Tangential Loads According to Die Velocity (V)

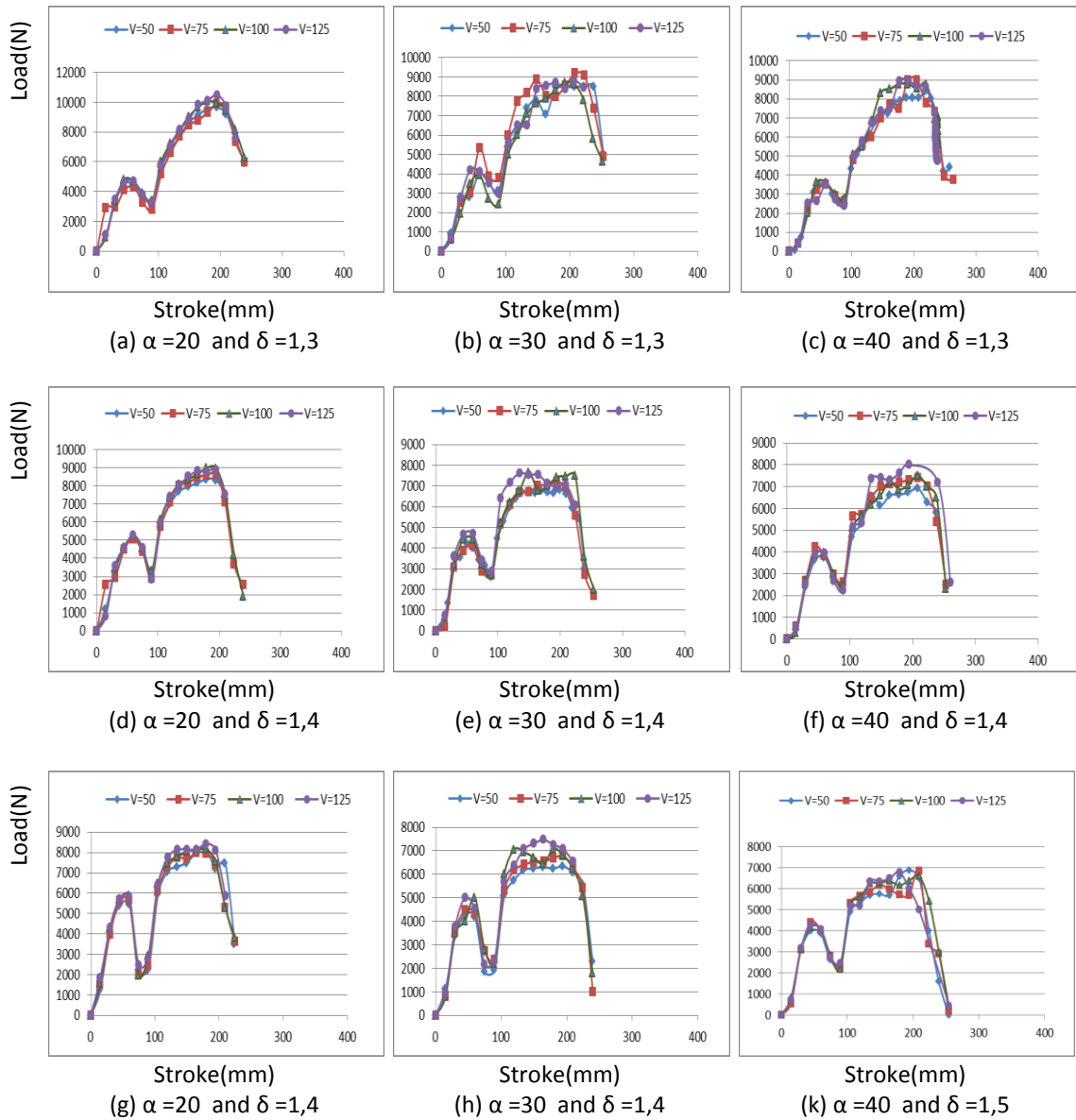


Figure 4.28 Radial Loads According to Die Velocity (V)

It has been found that load graphs are not so affected significantly by the alteration of tool velocities in cross wedge rolling operations. It is also validated with the literature that rapid movement may be carried out in order to provide time saving but excessive rapidity of tools might cause facing with some situation that isn't desired like uncontrolled slippage and internal defects of billet material [23]. Furthermore, velocities of top and bottom dies could be designated different from each other even, one of the dies can be determined as fixed while the other is active [34].

Within this study more than 300 different graphics were held but in order to sake of brevity only one part of the graphics are given in this chapter. The all other remaining are provided in Appendix of this thesis.

CHAPTER 5

MODELING AND ANALYSIS OF CROSS WEDGE ROLLING PROCESS

5.1 INTRODUCTION

In this chapter feed-forward artificial neural network (FF-ANN), analysis of variance (ANOVA) and TAGUCHI methods are implemented to cross wedge rolling process.

5.2 ARTIFICIAL NEURAL NETWORK

Intelligent manufacturing systems (IMS) are intelligent computer programs that use knowledge and reasoning techniques to solve problems that are difficult enough requiring significant human expertise for their solution. In the extreme, these systems are capable of producing various parts economically. Moreover IMS concentrates on explicitly representing an expert's knowledge about a class of problems and providing a separate reasoning mechanism that operates on this knowledge to produce a solution. The design and implementation of this system is one of the major challenges facing the today's manufacturing engineers in the realization of the IMS [33].

In this chapter, establishing a model as well as analyzing the effects of relevant process parameters on required tangential and radial loads were examined. Based on the obtained results, the best optimal combination of parametric setting which leads to the minimum required load was then revealed and recommended. Forming load was then predicted by a trained network model of Neural Network tool Box (NNTool) of MATLAB software. The overall results indicate the feasibility and effectiveness of the proposed approach in a real manufacturing environment and eliminate the need to carry out expensive as well as time consuming trial and error experimentations to reach to the optimum operating conditions.

Artificial Neural Networks (ANNS) have gained popularity as a tool for incorporating knowledge in the IMS. The adopted neural network model for simulation of quantified predicate creativity follows the most common type of ANN. The term neural network was traditionally used to refer to a network or circuit of biological neurons[34]. An Artificial Neural Network (ANN) is an information processing paradigm that is inspired by the biological nervous systems, such as the brain. By referring to the following Figure 5.1, a schematic illustration of a biological neuron is presented. Each neuron has a body, an axon, and many dendrites.

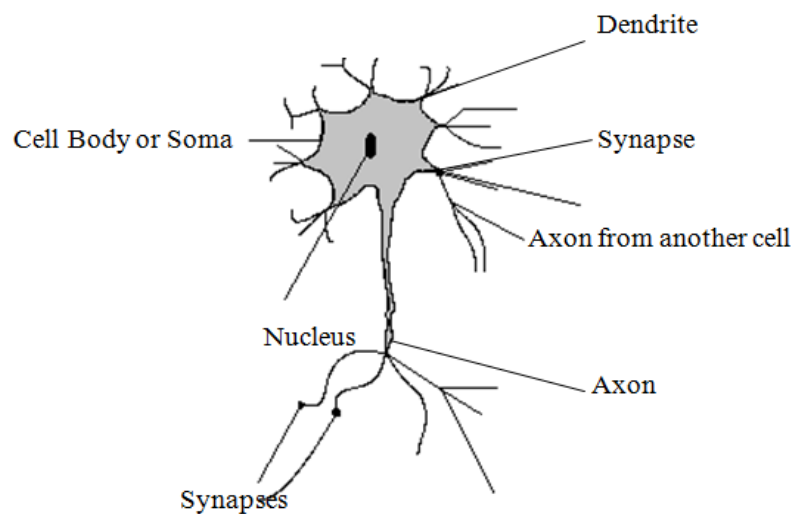


Figure 5.1 Illustration of a Biological Neuron

Processing paradigm is composed of a large number of highly interconnected processing elements (neurons) working in connection to solve specific problems. ANNs, like people, learn by example. An ANN is configured for a specific application, such as pattern recognition or data classification, through a learning process. Learning in biological systems involves adjustments to synaptic connections that exist between the neurons Figure 5.2.

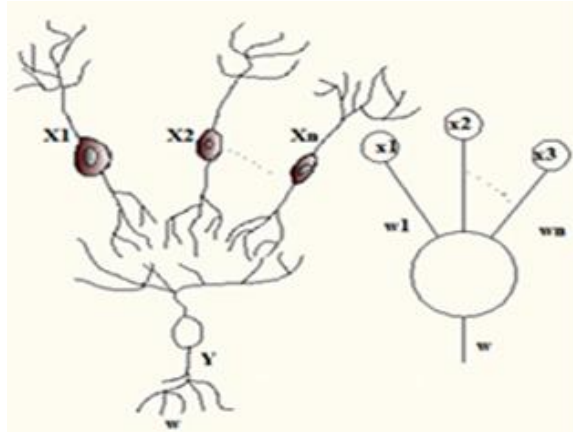


Figure 5.2 Biological Neuron and Artificial Neural Network

Representations with circles FF-ANN consist of an input layer, one or more hidden layers and output layer. As shown in Figure 5.3 the first input layer is the first layer and accepts symptoms, signs, and experimental data. Hidden layer is placed data between the input and output layer. The hidden layer processes the data. It receives from the input layer, and sends a response to the output layer. The output layer accepts all responses from the hidden layer and produces an output vector. Each layer has a certain number of processing elements which are connected by connection links with adjustable weights. These weights are adapted during the training process, most commonly through the back propagation algorithm, by presenting the neural network with examples of input–output pairs exhibiting the relationship the network is attempting to learn [35]. After a neuron performs its function, it passes its output to all of the neurons in the output layer.

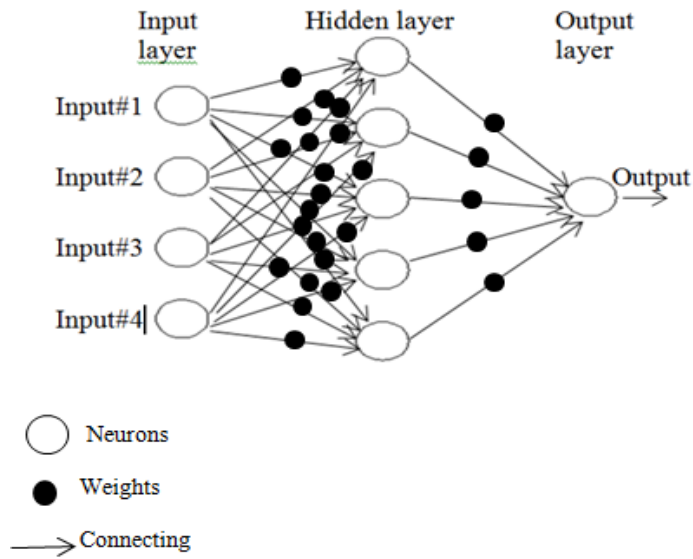


Figure 5.3 A Simplified Schematic Diagram for a (FFANN) Model

Figure 5.4 shows the type of neural networks functions. In this study, sigmoid function was selected as a network function.

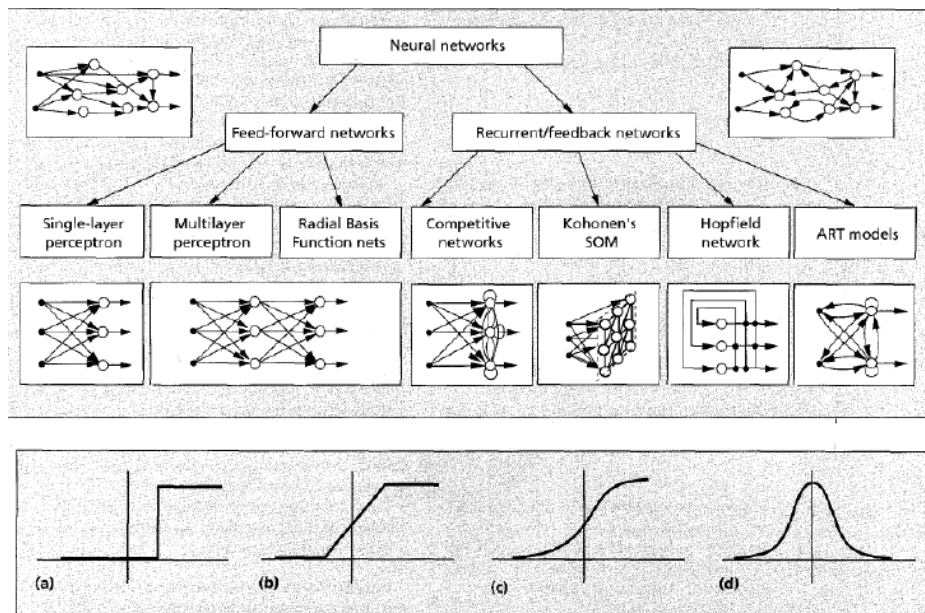


Figure 5.4 Type of Networks and Functions [36]

Activation functions: (a) threshold, (b) piecewise linear (ramped), (c) sigmoid, (d) gaussian

Once a network has been structured for a particular application, that network is ready to be trained. To start this process the initial weights are chosen randomly. Then, the training, or learning, begins.

The total input to the layer neuron i , x_i , is the summation of the weight (w_{ij}), which is associated with the connection between the neuron i and neuron j , multiplied by the input value received from the preceding layer neuron, x_j , for each connection path.

$$x_i = w_{io} + \sum_{j=1}^N w_{ij} \cdot x_j$$

$N =$ the number of inputs
 $w_{io} =$ the bias of neuron

The output from neuron i , V_i is given by $V_i = f(x)$, f is activation function.

5.3 PREDICTION OF CWR LOADS USING NEURAL NETWORK

In this section neural network capability for load prediction of the cross wedge rolling process forming angle (α), stretching angle (β), reduction ratio (δ) and die velocity (v) is investigated. Input–output data for the neural network training 96 numerical results were used to train the neural network model. Also other 48 numerical results were utilized to test the network model prediction accuracy. Tables 5.1 shows relevant process parameters and their levels considered in the present research.

Table 5.1 CWR Process Parameters and Their Levels

Parameters	Notion	Levels	Values
Forming angle	α	3	20, 30, 40
Stretching angle	β	4	4, 6, 8, 10
Reduction ratio	δ	3	1.3, 1.4, 1.5
Die velocity	V	4	50, 75, 100, 125

In order to predict the CWR die load, several feed-forward fully connected neural networks were investigated considering different topologies (various numbers of hidden layers and neurons) and activation functions for each network structure. Each network was trained separately, and amongst all, the best one was characterized by the global lowest mean square error. Finally, a four layer neural network with 4 nodes in the input layer, 10 nodes in both the first and second hidden layer, and 4 nodes in the output layer was selected as the best network structure. Figure 5.5 shows the feed forward artificial neural network structure.

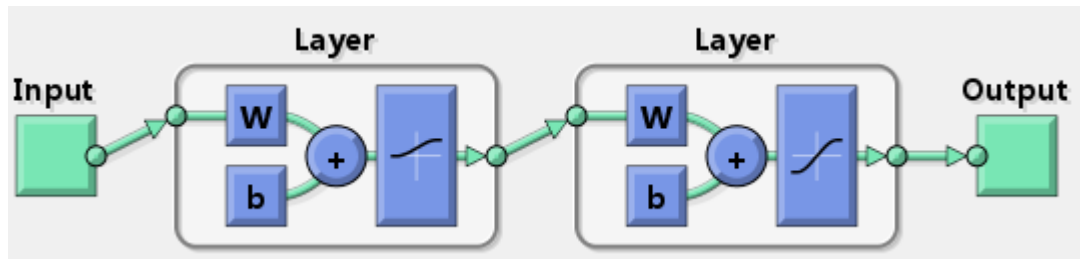


Figure 5.5 Selected Structure for the FF-ANN Model

In this study, the non-linear log-sigmoid transfer function was used as the activation

function in all hidden and output neurons: $f(x) = \frac{1}{1+e^{-x}}$

Normalization of input data is a crucial matter to consider especially when the input parameters have completely different ranges. Hence, all inputs share equal contribution to the network training procedure via normalization [35,37]. The normalization can be done with following formula:

$$(x_{norm}) = \frac{x - x_{min}}{x_{max} - x_{min}} \times 0,8 + 0,2$$

Figure 5.6 shows the selected input data, target data, transfer function and the number of neurons.

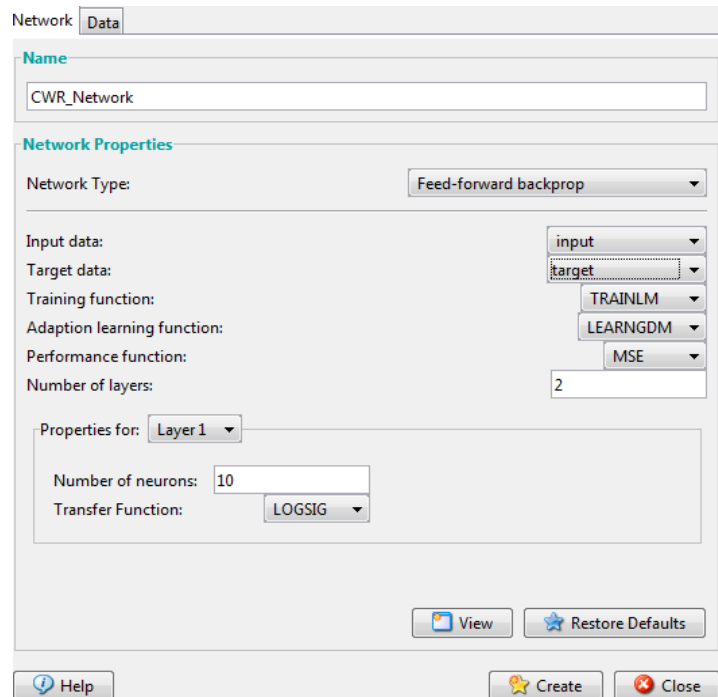


Figure 5.6 Establishment of the FF-ANN Model

Figure 5.7 shows the training of FF-ANN model screen. This window displays the training progress and allows interruption of training at any point by clicking “Stop Training”.

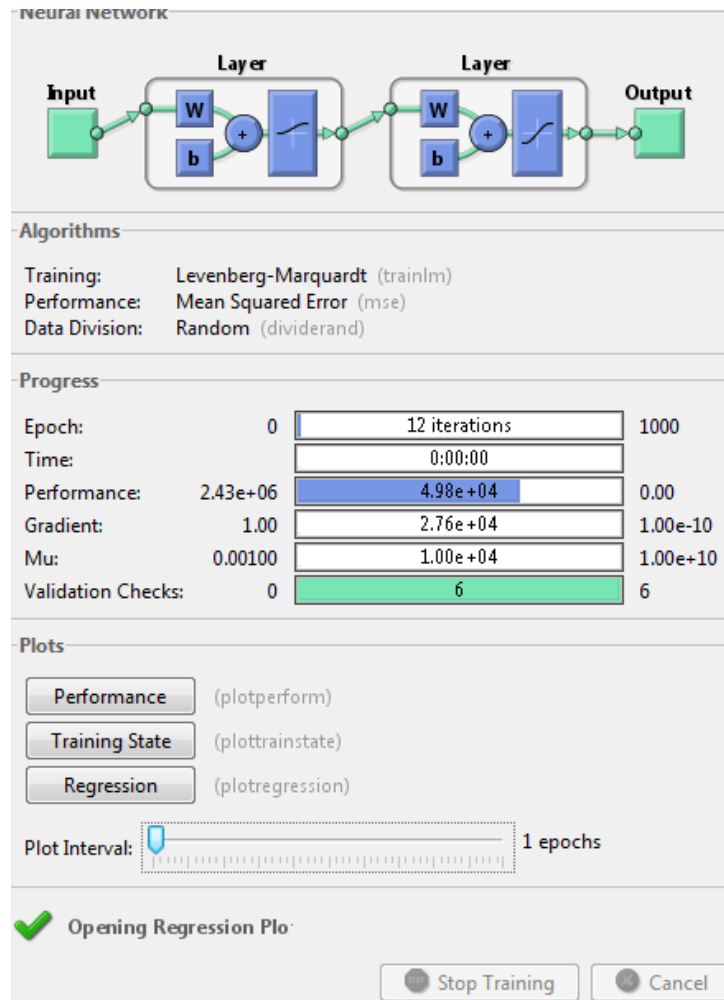


Figure 5.7 Training of the FF-ANN Model

Figure 5.8 illustrates the learning behavior of the selected network. The responses obtained from the neural model have been compared with the desired FEM simulations results.

The best validation performance is obtained at 6 validation checks and 12 epochs. Performance training window (Figure 5.8) shows the plot of training errors, validation errors, and test errors. In this training, the result is reasonable since the final mean square error is small. The test set error and the validation set error has similar characteristics. No significant over fitting has occurred after 12 epochs.

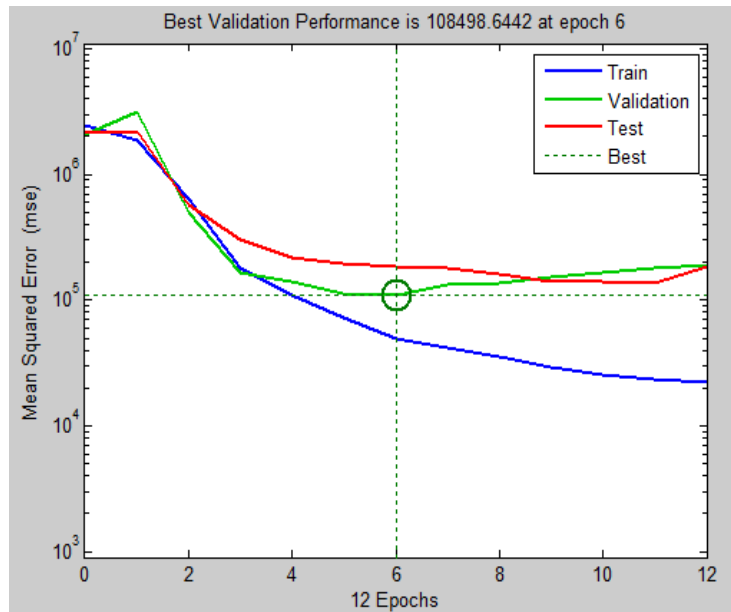


Figure 5.8 Validation Performance

The following regression plots display the network outputs with respect to targets for training, validation, and test sets (Figure 5.9). For this problem, the fit is reasonably good for all data sets, with R values in each case of 0.98 or above.

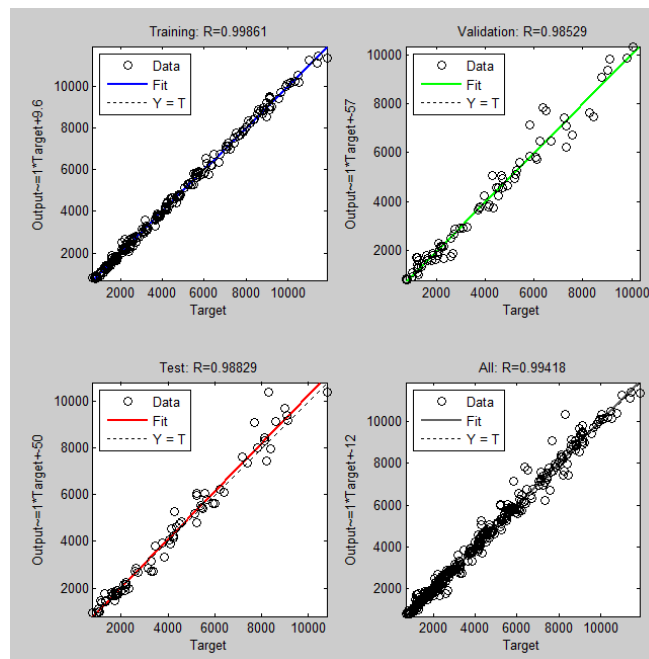


Figure 5.9 Regression Plots

The graphical results for knifing and stretching zones are depicted in Figures 5.10 and 5.11 respectively. It is obvious that FEM results and the predicted load values have very close relation to each other.

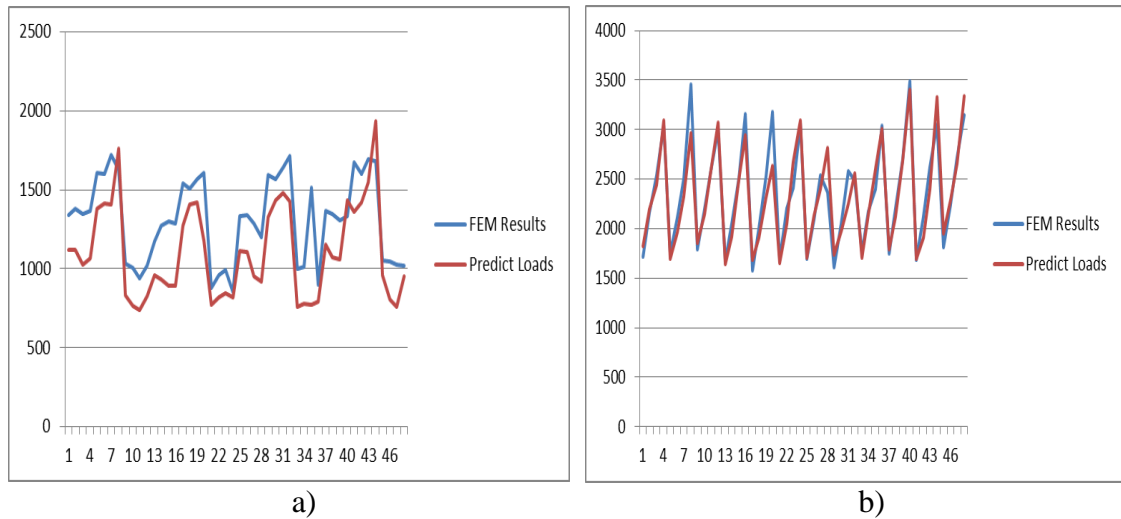


Figure 5.10 Tangential Load Comparison for FEM and ANN Results

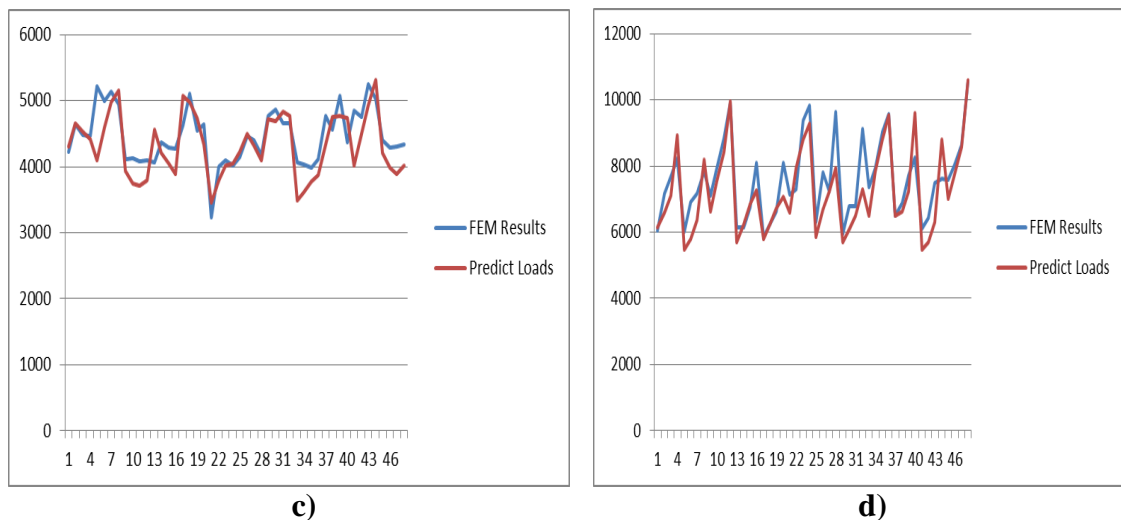


Figure 5.11 Radial Load Comparisons for FEM and ANN Results

5.4 DESIGN OF EXPERIMENTS

Although, cross wedge rolling is a developing method in the past decades, there is a gap in the literature to understand the relationships between the influencing factors. Because, any changes in the input factors affect the output functional performance. It is important to note that all variables do not affect the performance in the same manner.

Some may have strong influences on the output performance, some may have medium and some have no influence at all.

The objective of a carefully planned design of experiment is to understand which set of variables in a process affects the performance most and then determine the best levels for these variables to obtain satisfactory output functional performance in products. In this design, three levels of forming angle(α), four levels of stretching angle (β), three levels of reduction ratio (δ) and four levels of die speed (V) are used to plan numerical simulations.

All parameters alternatives to set up numerical simulations are shown in Figure 5.12.

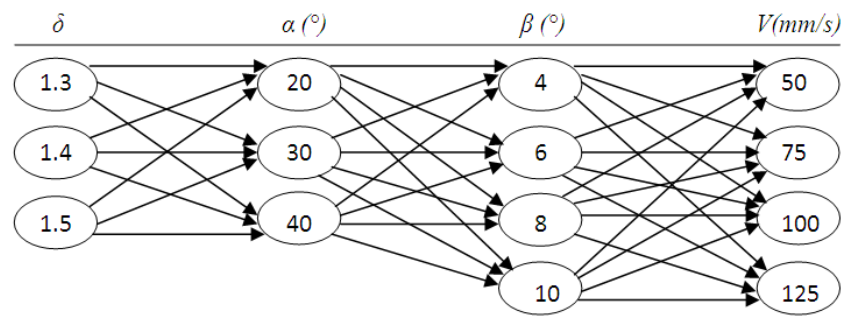


Figure 5.12 Parameter Alternatives of Numerical Simulations

Simulations were conducted in a series of trials which produce quantifiable outcomes to explore or estimate the knowledge of cross wedge rolling process. Exploration refers to understanding the parameters from the process estimation [14].

The experiment was performed using a factorial experimental design so those interactions between the independent variables could be effectively investigated.

5.4.1 Analysis of Working Conditions Using ANOVA

ANOVA is a statistical technique for determining the degree of difference or similarity between two or more groups of data. It is based on the comparison of the average value of a common component [13]. Analysis of variance (ANOVA) with a speech issues in resulting analysis is of importance to interpret the results. Test planning and analysis (DOE), in this sense plays a guiding role, DOE is based on the analysis of variance. In the present study, Minitab program was used for experimental design. Minitab program

is commonly used to calculation of statistical procedures. Firstly the custom factorial design and the next, custom responses for design of experiment are selected, since there is a many of independent variables used in ANOVA. ANOVA, of independent variables interact among themselves and presents how these interactions are used to analyze the effects on the dependent variable.

The analysis of variance divides the total variation in the response variable (y). For the most of the response surfaces, the functions for the approximations are polynomials because of simplicity, though the functions are not limited to the polynomials. In the case of four variables (forming angle, stretching angle, redaction ratio and die speed) the response surface multiple regression model is expressed as follow which is fit using the MINITAB software package.

$$E(y)=\beta_0+ \beta_1X_1+ \beta_2X_2+ \beta_3X_3+ \beta_4X_4 \quad (1)$$

Estimate value of S is obtained as follows

$$S^2 = MSE = \frac{SSE}{n-k-1} \quad (2)$$

Where S is the error of (y) and k is the number of nonconsist terms in RS model. Total sum of squares expressed as follows.

$$\text{Total SS} = \sum y_i^2 = \frac{(\sum y_i)^2}{n} \quad (3)$$

SSR = (sum of squares for regression) measures the amount of variation explained by using regression equation.

SSE = (sum of squares for error) measures the residual variation in the data that is not explained by the independent variables. So that;

$$\text{Total SS}=\text{SSR}+\text{SSE} \quad (4)$$

The degrees of freedom (DF) for these sums squares are found using the following argument. There are (n-1) total degrees of freedom and k regression degrees freedom, leaving (n-1)-k degrees of freedom for error.

The main Squares (MS) are calculated as MS=SS/DF

Statistical analysis techniques such as ANOVA can be used to check the fitness of a RS model and to identify the main effects of design variables. The major statistical parameters used for evaluating model fitness are the (y) variable, R^2 , adjusted R^2 and mean square error (MSE). These parameters are not totally independent of each other and are calculated as;

$$R^2 = \left(\frac{SSR}{\text{Total SS}} \right) 100\% \quad (5)$$

$$R^2(\text{adj}) = \left(1 - \frac{\text{MSE}}{\text{Total} \frac{SS}{n-1}} \right) 100\% \quad (6)$$

Usefulness of the regression is tested by an equivalent F-test. F-test is the regression equation that uses information provided by the predictor variables x_1 , x_2 , x_3 and x_4 substantially better than the simple predictor (y) that does not rely on any of the x value. F-test statistic is found as follows.

$$F = \frac{MSR}{MSE} \quad (7)$$

Variance of analysis for knifing and stretching zones is presented in Tables 5.2, 5.3, 5.4 and 5.5 obtained by Minitab program in accordance with the tangential and radial loads. As can be seen from these tables, four inputs (α , β , δ , V) among all parameters, especially α and δ are highly significant in knifing zone inside 95% of confidence interval (p-values less than 0.05). The smaller the p-value, the more significant is the corresponding data. On the contrary, the main effect of α on the rolling load is found as insignificant due to its 0.524 p-values, that is higher than 0.05. P-value of β in stretching zone implies that it has great significance which is greater than 95%.

Table 5.2 Tangential Load Analysis for Knifing Zone (F_{1t})

Source	DF	Seq SS	Adj SS	Adj MS	F	P
β	3	1860344	1860344	620115	1,34	0,264
α	2	10383167	10383167	5191583	11,21	0,000
δ	2	3800134	3800134	1900067	4,10	0,019
V	3	1664401	1664401	554800	1,20	0,313
Error	133	61568642	61568642	462922		
Total	143	79276687				
		S = 680,384	R-Sq = 22,34%	R-Sq(adj) = 16,50%		

Table 5.3 Tangential Load Analysis for Stretching Zone (F_{3t})

Source	DF	Seq SS	Adj SS	Adj MS	F	P
β	3	38394328	38394328	12798109	305,11	0,000
α	2	54497	54497	27249	0,65	0,524
δ	2	276953	276953	138476	3,30	0,040
V	3	1317270	1317270	439090	10,47	0,000
Error	133	5578881	5578881	41946		
Total	143	45621928				
		S = 204,808	R-Sq = 87,77%	R-Sq(adj) = 86,85%		

Table 5.4 Radial Load Analysis for Knifing Zone (F_{1r})

Source	DF	Seq SS	Adj SS	Adj MS	F	P
β	3	469542	469542	156514	1,97	0,122
α	2	27428992	27428992	13714496	172,39	0,000
δ	2	14103291	14103291	7051645	88,64	0,000
V	3	2118245	2118245	706082	8,88	0,000
Error	133	10580728	10580728	79554		
Total	143	54700798				
		S = 282,054	R-Sq = 80,66%	R-Sq(adj) = 79,20%		

Table 5.5 Radial Load Analysis for Stretching Zone (F_{3r})

Source	DF	Seq SS	Adj SS	Adj MS	F	P
β	3	150436545	150436545	50145515	182,96	0,000
α	2	47968345	47968345	23984173	87,51	0,000
δ	2	71709147	71709147	35854573	130,82	0,000
V	3	7563187	7563187	2521062	9,20	0,000
Error	133	36451960	36451960	274075		
Total	143	314129185				
		S = 523,522	R-Sq = 88,40%	R-Sq(adj) = 87,52%		

There are $n=144$ trials and $k=143$ independent predictor variables. It can verify that the total degrees of freedom $(n-1)=143$, is divided into $k=10$ for regression and $(n-k-1)=133$ for error. For the real estate data in Table 5.1, tangential load calculation step for knifing zone is taken as a sample and presented as follows. For the sake of brevity, the other calculation steps are not tabulated but results are presented in Table 5.6.

Total SS=SSR+SSE

Total SS=277677225+36451960=314129185

$$S^2 = \text{MSE} = \frac{\text{SSE}}{n-k-1} = 274074,88$$

$$R^2 = \left(\frac{SSR}{\text{Total SS}} \right) 100\% = \left(\frac{314129185}{350581145} \right) 100\% = 88,39 \%$$

$$R^2(\text{adj}) = \left(1 - \frac{MSE}{\text{Total} \frac{SS}{n-1}} \right) 100\% = \left(1 - \frac{274074,88}{\frac{314129185}{143}} \right) 100\% = 87,52\%$$

$$F = \frac{MSR}{MSE} = \frac{50145515}{274074,88} = 182,96$$

General speaking, the larger values of $R^2(\text{adj})$, and smaller the value of MSE, the better the fit. In situations where the number of design variables is large, it is more appropriate to look at $R^2(\text{adj})$. Because R^2 always increases as the number of terms in the model is increased, while $R^2(\text{adj})$ actually decreases if unnecessary terms are added to the model. In the following Table 5.6, the ANOVA results and the multiple regression values are compared. It is found that there is highly correlation between ANOVA and R^2 . Also, F-test value of 182,96 declares that at least one of the predictor variables is contributing significant information for the prediction of load requirement.

Table 5.6 Comparison of ANOVA and R^2

		ANOVA	Multi Regression	Difference
Knifing zone (tangential)	R^2	22,34	22,33	0,01
	$R^2(\text{adj})$	16,49	16,49	0
Knifing zone (radial)	R^2	80,66	80,65	0,01
	$R^2(\text{adj})$	79,20	79,20	0
Stretching zone (tangential)	R^2	87,77	87,77	0
	$R^2(\text{adj})$	86,85	86,85	0
Stretching zone (radial)	R^2	88,40	88,39	0,01
	$R^2(\text{adj})$	87,52	87,52	0

5.4.2 Main Effects Plots

The Main Effects Plot (MEP) means of factor levels. The reference line is the overall mean of the data. It is used visualize the magnitudes of main effects. This plot shows the average outcome for each value of each variable, combining the effects of the other variables as if all variables were independent. Relationships between the parameters (α , β , δ and V) have vital importance since they are playing an important role in determining the level of plastic deformation. Contact area between the workpiece and the die surface is controlled by the forming angle (α). Contact area increases with the

smaller forming angle. Stretching angle (β) determines the axial deformation of the workpiece. Larger stretching angles result more elongation of the workpiece and shortens the die length. Reduction ratio (δ) directly effects the radial load requirement.

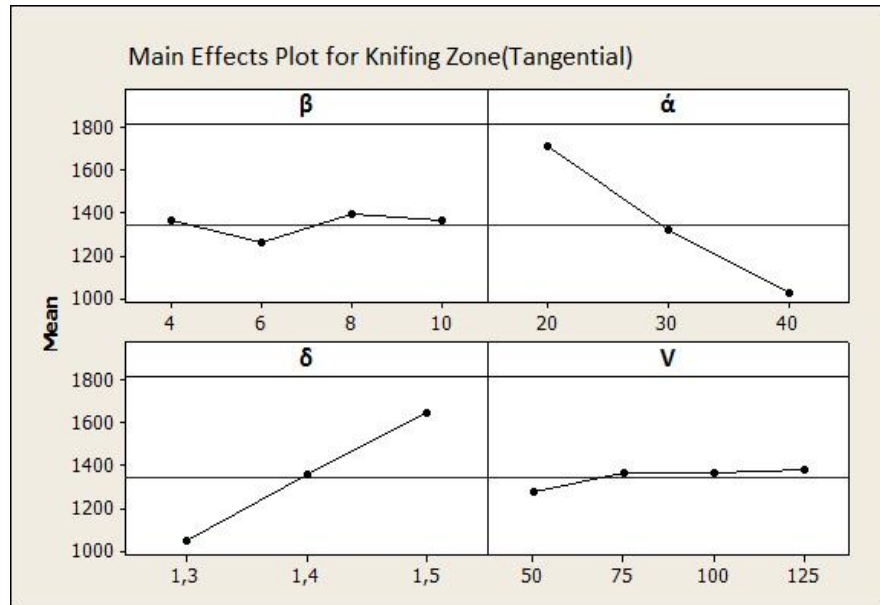


Figure 5.13 Tangential Loads MEP Charts for Knifing Zone

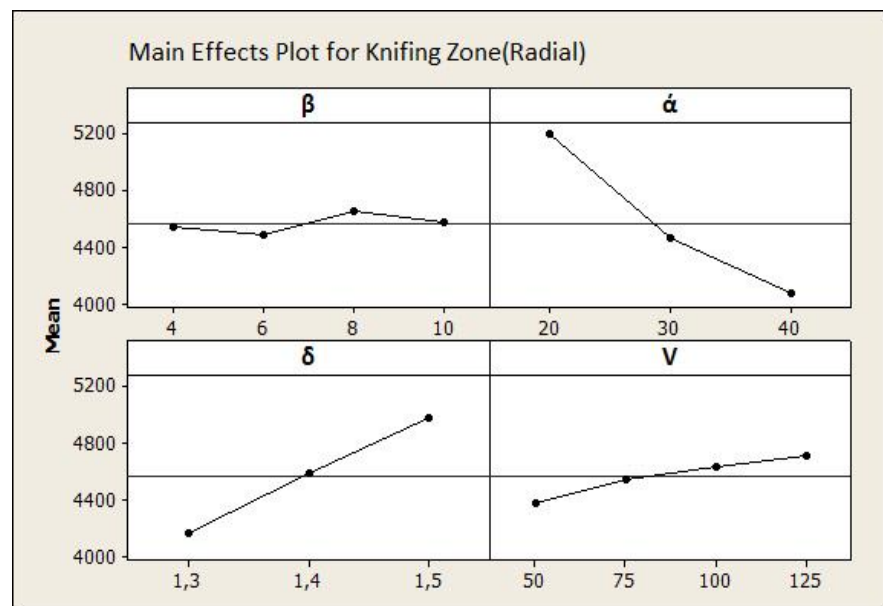


Figure 5.14 Radial Loads MEP Charts for Knifing Zone

The larger value of the reduction ratio causes the larger radial compression of the workpiece between the die platens. In the following Figures 5.13, 5.14, 5.15 and 5.16, the tangential and radial load MEP charts for knifing and stretching zones are demonstrated respectively.

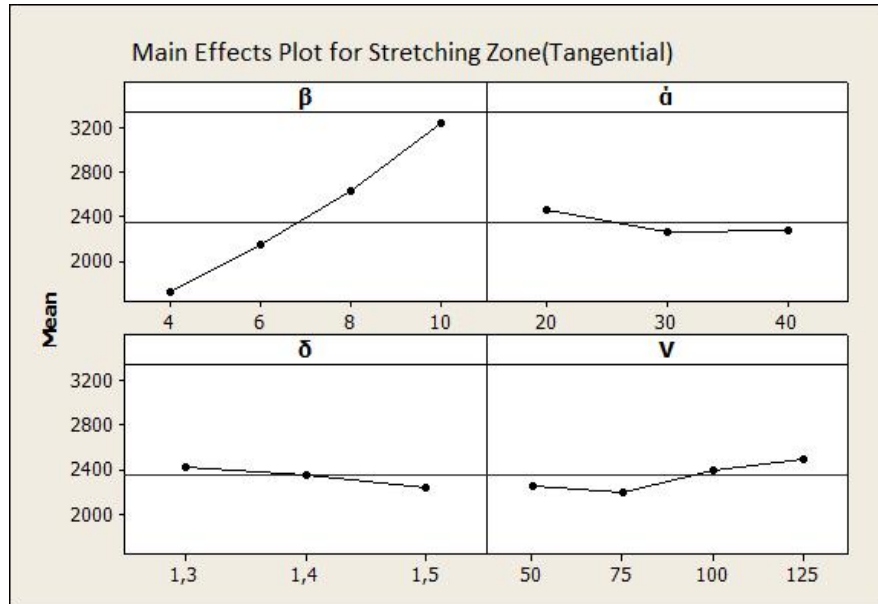


Figure 5.15 Tangential Loads MEP Charts for Stretching Zone

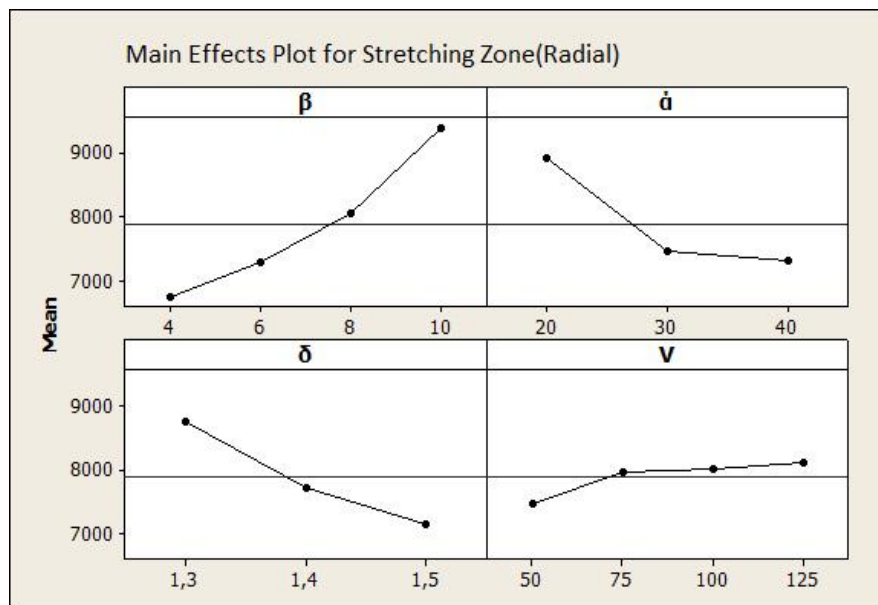


Figure 5.16 Radial Loads MEP Charts for Stretching Zone

It is seen that the tangential and radial load main effects plots show the same behavior for knifing zone. Spreading angle (β) has a lower effect on rolling load, since it has no influence on knifing zone. It is interesting note that increment in the forming angle, from 20^0 to 40^0 , causes to considerable decrease in rolling load. However, reduction ratio (δ) values over then 1.3 have an increasing effect on rolling load. Also, it is noted that die speed (V) has the fewest effect on the rolling load whatsoever. Contrary to the knifing zone, tangential and radial load main effects plots for stretching zone are different as shown in Figure 5.14. In stretching zone, spreading angle has the highest impact on both tangential and radial load. However, different forming angles are effective for the radial load, whereas forming angle has no effect on tangential load. In the same way, reduction ratio plays an important role on the radial load whereas it has no effect on tangential load.

To sum up, based on the predicted forming load values by finite element method and analysis of variance test (ANOVA), it was observed that decreasing spreading angle and increasing forming angle are accompanied by reduction of denoted maximum radial and tangential loads. However, higher relative reduction values in the CWR process are associated with increased values of radial loads resulting from contact surface increase.

5.4.3 Interaction Plots for Knifing and Stretching Zones

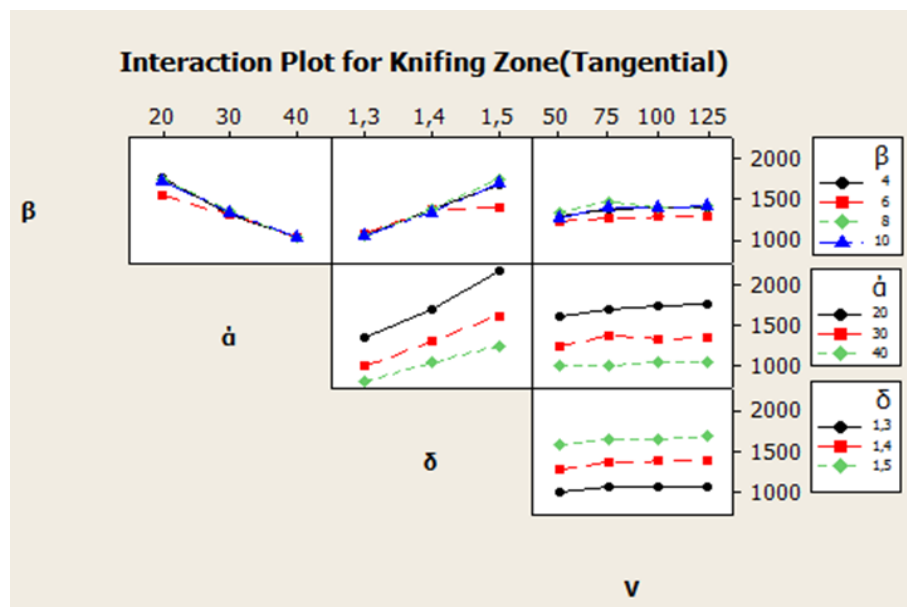


Figure 5.17 Tangential Loads Interaction Plots for Knifing Zone

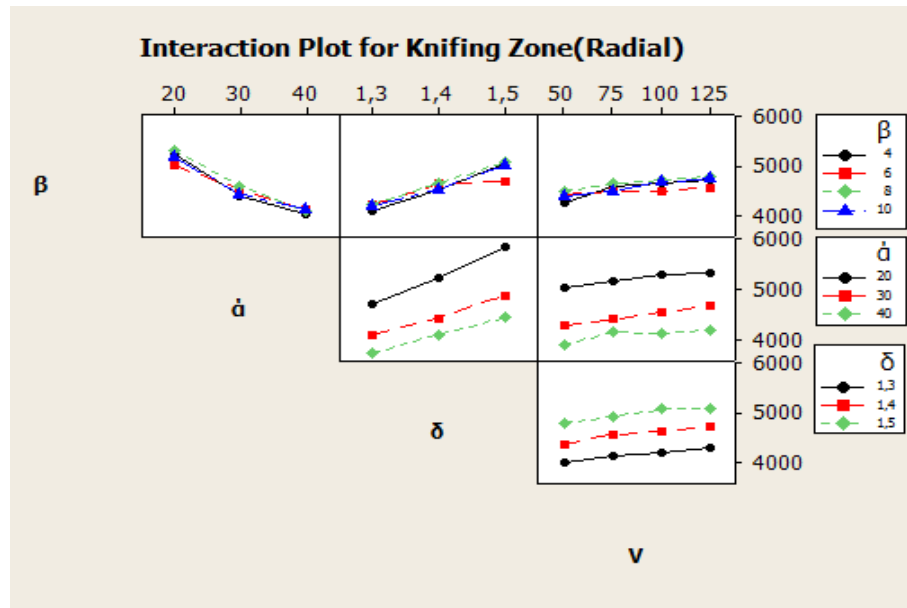


Figure 5.18 Radial Loads Interaction Plots for Knifing Zone

Another graphic statistical tool used in this study is called an Interaction Plot. This tool is used for identifying the interactions between factors. This type of chart illustrates the effects between variables which are not independent. Figure 5.15, 5.16, 5.17 and 5.18 present the interaction plots between cross wedge rolling parameters for knifing and stretching zones respectively.

Interactions between the parameters show similar effects for tangential and radial loads in knifing zone. Nearly parallel lines in knifing zone indicate a very weak interaction especially between die speed and the other parameters. The significant interaction is indicated by the lack of parallelism of the lines in the interaction plots. It should be noted that the objective function is the rolling force and reaching to the least possible amount is of paramount importance. Therefore, interaction plots should be taken into consideration carefully in order to find the overall working conditions leading to the minimum required rolling load.

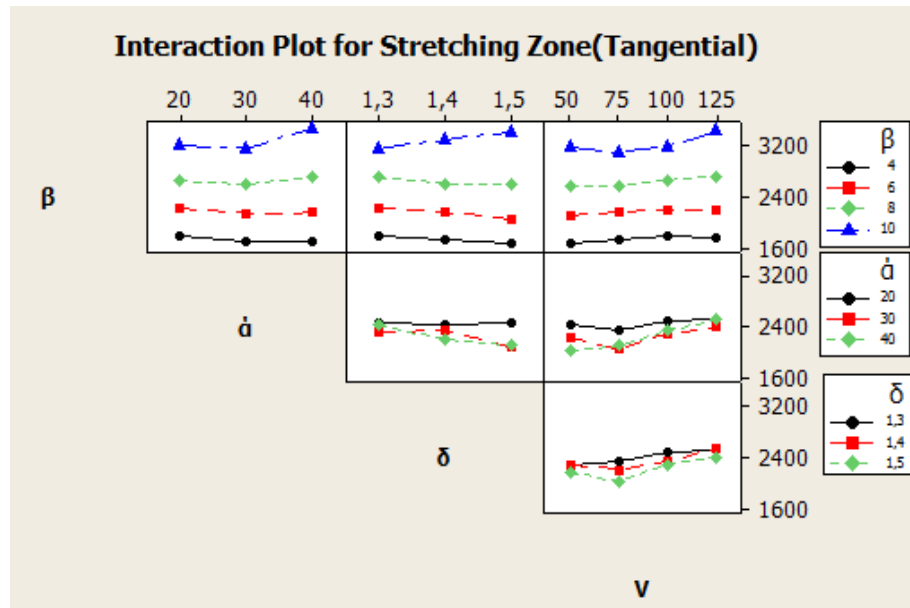


Figure 5.19 Tangential Loads Interaction Plots for Stretching Zone

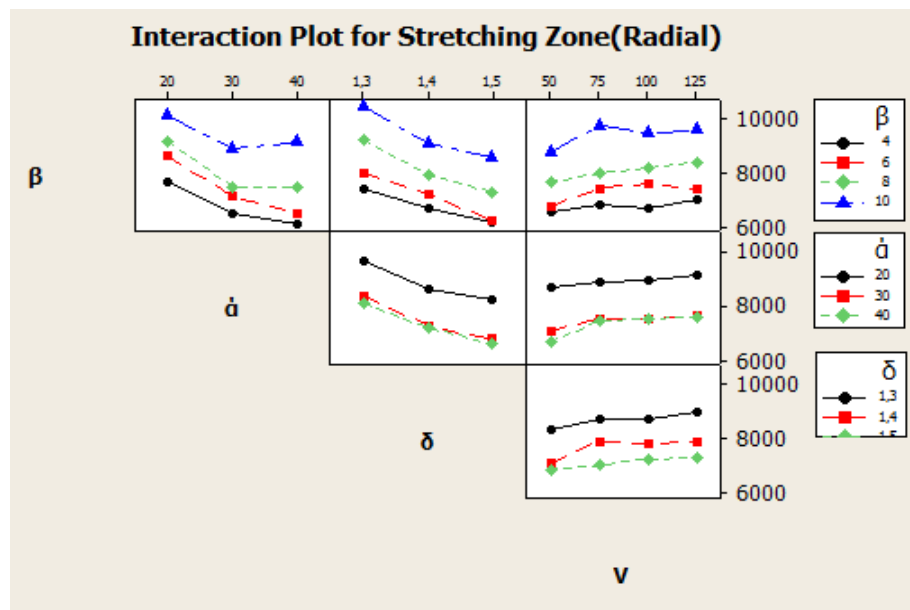


Figure 5.20 Radials Load Interaction Plots for Stretching Zone

As it is seen from Figure 5.15 the rolling load decreases as the forming angle moves from low value (20) towards high (40). On the other hand, Figure 5.16 shows totally different picture. In Figure 5.16, low value of stretching angle and high value of reduction ratio and forming angle is desired and such interesting point is that without the statistical design this conclusion could not have been drawn.

It is revealed that combination of high forming angle (40^0) along with the lowest possible reduction ratio (1.3) and stretching angle ($\beta=4$) results in minimum rolling force in both tangential and radial directions in knifing zone. This finding is in conflict with the MEP charts of stretching zone illustrated in Figure 5.14. In stretching zone main objective parameter influencing the rolling force is stretching angle (β). Increment of stretching angle from 4^0 to 10^0 causes the great amount of rolling force.

The other remarkable parameter is reduction ratio. In knifing zone increment in the reduction ratio from 1.3 to 1.5 increases the rolling load approximately 50% in tangential load and 25% in radial load. On the other hand, in stretching zone reduction ratio has almost no effect on tangential load. Also, contrary to knifing zone rolling force decreases 25% with the increment in reduction ratio for radial load.

Interaction plots revealed that the low value of stretching angle and high value of forming angle and reduction ratio has the dominant contribution on the wedge rolling load requirement, while die speed is less significant. In all cases, radial loads are higher than tangential loads, and therefore, tools must be designed by considering the radial loads. It is discovered from MEP charts and interaction plots that parameters act differently in knifing and stretching zones. As a result, minimum load requirement should be concentrated on high forming angle and low reduction ratio in knifing zone, while low stretching angle and high reduction ratio in stretching zone.

5.5 CONTRIBUTION OF PROCESS PARAMETERS USING TAGUCHI

Taguchi method was developed by Taguchi; it is widely used in designing and analysis of experimental method to optimize the performance characteristics through the setting of process parameters [38].

Based on the simulations, four different β values were considered. But, during the simulations, it is realized that rolling load is increasing with the highest values of stretching angles. Thus in order to clarify the effect of stretching angle on rolling load, lowest value of $\beta=4$ is ignored and 6,8 and 10 degrees of β were considered for Taguchi method.

Three levels of forming angle(α), three levels of stretching angle (β) and three levels of reduction ratio (δ) are used to plan Taguchi method as shown in Table 5.7.

Table 5.7 Experiment Factors Level Using Taguchi Method

Parameters	Levels		
	1	2	3
Forming angle	20	30	40
Stretching angle	6	8	10
Reduction ratio	1,3	1,4	1,5

Taguchi method provide an integrated approach to determine the best range of designs simply and efficiently for quality, performance, and cost [3, 13].

In Taguchi method, three-stages such as system design, parameter design, and tolerance design are employed. Parameter design is the key stage, which used to obtain the optimum levels of process parameters for developing the quality characteristics and to determine the product parameter values depending optimum process parameter values [20]. Based on orthogonal arrays, the number of experiments which may lead to the increasing of the time and cost can be reduced by using Taguchi method. It employs a special design of orthogonal arrays to learn the whole parameters space with the least experiments only.

5.5.1 Defining Parameters and Design Orthogonal Array

The effect of many different parameters on the performance characteristic in a condensed set of experiments can be examined by using the orthogonal array experimental design proposed by Taguchi. Once the parameters affecting a process that can be controlled have been determined, the levels at which these parameters should be varied must be determined [39]. Determining what levels of a variable to test requires an in depth understanding of the process, including the minimum, maximum, and mid value of the parameter. Typically, the number of levels for all parameters in the experimental design is chosen to be the same to aid in the selection of the proper orthogonal array.

Knowing the number of parameters and the number of levels, the proper orthogonal array can be selected. Table 5.8 demonstrates the Taguchi orthogonal array selection chart. Using the table shown below, the name of the appropriate array can be found by looking at the column and row corresponding to the number of parameters and number of levels. Within this study, L9 array was selected since three parameters were considered with 3 levels.

Table 5.8 Orthogonal Array(I_9) Selected Table

Number of Levels	Number of Parameters (P)																														
	2	3	4	5	6	7	8	9	10	11	12	13	14	15	16	17	18	19	20	21	22	23	24	25	26	27	28	29	30	31	
2	L4	L4	L8	L8	L8	L8	L12	L12	L12	L12	L16	L16	L16	L16	L16	L16	L16	L16	L16	L16	L16	L16	L16	L16	L16	L16	L16	L16	L16	L16	L16
3	L9	L9	L9	L18	L18	L18	L18	L27	L27	L27	L27	L27	L27	L36	L36	L36	L36	L36	L36	L36	L36	L36	L36	L36	L36	L36	L36	L36	L36	L36	L36
4	L16	L16	L16	L16	L32	L32	L32	L32	L32	L32	L32	L32	L32	L32	L32	L32	L32	L32	L32	L32	L32	L32	L32	L32	L32	L32	L32	L32	L32	L32	L32
5	L25	L25	L25	L25	L25	L50	L50	L50	L50	L50	L50	L50	L50	L50	L50	L50	L50	L50	L50	L50	L50	L50	L50	L50	L50	L50	L50	L50	L50	L50	L50

According to factors level used in Taguchi, following Table 5.9 was formed for experimentation.

Table 5.9 Orthogonal Array (I_9) of Taguchi Method

Expt.	Parameters		
	Forming angle	Stretching angle	Reduction ratio
1	1	1	1
2	1	2	2
3	1	3	3
4	2	1	2
5	2	2	3
6	2	3	1
7	3	1	2
8	3	2	1
9	3	3	3

Taguchi method employs the S/N ratio to identify the quality characteristics applied for engineering design problems. Usually, the S/N ratio characteristics can be divided into three types: the-lower-the-better, the-higher-the better, and the-nominal-the-better [14]. Resulting data coming from knifing and stretching zone is denoted in Table 5.10.

Table 5.10 Result Data

Parameter	Expt No.	level	Knifing Zone		Stretching Zone		Knifing Zone SN		Stretching Zone SN	
			Tangential	Radial	Tangential	Radial	Tan.	Rad.	Tan.	Rad.
Forming angle										
Level1	1		811,6	3849,7	1826,9	7228,9	58,2	71,7	65,2	77,2
	2	20	1726,4	5447	2649,9	9116,2	64,7	74,7	68,5	79,2
	3		2256,3	5961,3	3249,8	9565,1	67,1	75,5	70,2	79,6
Level2	4		1344,7	4566,5	2210	6884,6	62,6	73,2	66,9	76,8
	5	30	1637,7	4655,5	2581,2	6793,4	64,3	73,4	68,2	76,6
	6		1021,1	4094,5	2999,2	9927,9	60,2	72,2	69,5	79,9
Level2	7		1032,7	3972,2	2104,6	6680	60,3	72	66,5	76,5
	8	40	766,8	3816,9	2765,1	8781,6	57,7	71,6	68,8	78,9
	9		1168,9	4250,9	3855,3	9137,7	61,4	72,6	71,7	79,2
Stretching angle										
Level1	1		811,6	3849,7	1826,9	7228,9	58,2	71,7	65,2	77,2
	4	6	1344,7	4566,5	2210	6884,6	62,6	73,2	66,9	76,8
	7		1032,7	3972,2	2104,6	6680	60,3	72	66,5	76,5
Level2	2		1726,4	5447	2649,9	9116,2	64,7	74,7	68,5	79,2
	5	8	1637,7	4655,5	2581,2	6793,4	64,3	73,4	68,2	76,6
	8		766,8	3816,9	2765,1	8781,6	57,7	71,6	68,8	78,9
Level2	3		2256,3	5961,3	3249,8	9565,1	67,1	75,5	70,2	79,6
	6	10	1021,1	4094,5	2999,2	9927,9	60,2	72,2	69,5	79,9
	9		1168,9	4250,9	3855,3	9137,7	61,4	72,6	71,7	79,2
Reduction ratio										
Level1	1		811,6	3849,7	1826,9	7228,9	58,2	71,7	65,2	77,2
	6	1,3	1021,1	4094,5	2999,2	9927,9	60,2	72,2	69,5	79,9
	8		766,8	3816,9	2765,1	8781,6	57,7	71,6	68,8	78,9
Level2	2		1726,4	5447	2649,9	9116,2	64,7	74,7	68,5	79,2
	4	1,4	1344,7	4566,5	2210	6884,6	62,6	73,2	66,9	76,8
	9		1168,9	4250,9	3855,3	9137,7	61,4	72,6	71,7	79,2
Level2	3		2256,3	5961,3	3249,8	9565,1	67,1	75,5	70,2	79,6
	5	1,5	1637,7	4655,5	2581,2	6793,4	64,3	73,4	68,2	76,6
	7		1032,7	3972,2	2104,6	6680	60,3	72	66,5	76,5

The S/N ratio is used to measure the deformation deviation. The S/N ratio is explained as $-10 \log(\text{MSD})$, where MSD is mean square deviation

$$\frac{1}{n} \sum_0^n \left(\frac{1}{y^2} \right)$$

for the output characteristics; n is the number of experiments (for one set of parameters, n=1) and Y is the evaluated value of designed knifing and stretching zone heights from the simulation experiments.

$$MSD = \frac{1}{n} \sum_0^n \left(\frac{1}{y^2} \right) = \frac{1}{1} \sum_0^1 \left(\frac{1}{811,6^2} \right) = 1,51815E - 06$$

Here n=1 y=0,81 S/N ratio = $-10 \log\left(\frac{1}{811,6^2}\right) = 58,2$

The overall mean S/N ratio is expressed as $\frac{\bar{s}}{s} = \frac{1}{9} \sum_1^9 \left(\frac{s}{N_i} \right) = 61,81$

Table 5.11 S/N ratio, sum of squares Values and SS_i

Zones		SN	SS	Forming angle SS _i	Stretching angle SS _i	Reduction Ratio SS _i
Knifing zone	Tangential	61,81	26,08	25,8	13,2	58,3
	Radial	68,40	10,66	37,5	15,2	39
Stretching Zone	Tangential	72,99	4,92	5,4	87,1	6,4
	Radial	78,21	5,31	7,4	72,7	11,9

The sum of squares due to variation about overall mean is $SS = \sum_{i=1}^9 \left(\frac{s}{N_i} - \left(\frac{\bar{s}}{N} \right) \right)^2$

The calculated value for this expression is 26,08 For the ith process parameters, the sum of squares due to variation about is

$$SS_j = \sum_{j=1}^3 \left(\frac{s}{N_j} - \left(\frac{\bar{s}}{N} \right) \right)^2$$

Table 5.12 Contribution of process parameters (%)

Process Parameter	Knifing Zone		Stretching Zone	
	Tangential	Radial	Tangential	Radial
Forming angle	26,5	40,9	5,5	8
Stretching angle	13,6	16,6	88,1	79
Reduction Ratio	59,9	42,5	6,5	12,9

Stretching angle has an extraordinary contribution in tangential load at stretching zone with an impact of 88,1 % and 79% radial load. In stretching zone, forming angle and reduction ratio have relatively small impacts. Adversely, stretching angle imposes less amount of forming loads. Reduction ratio and forming angle have a higher contributions in knifing zone with an amount of 59,9% and 40,9% respectively.

CHAPTER 6

DISCUSSION AND CONCLUSIONS

6.1 INTRODUCTION

In this chapter, according to numerical simulation results, the effects of some cross wedge rolling parameters such as forming angle, stretching angle, reduction ratio and die speed on load requirements at both knifing and stretching zones are discussed.

6.2 DISCUSSION AND CONCLUSIONS

In this thesis, effects of CWR process parameters on forming such as forming angle, stretching angle, reduction ratio and die speeds were investigated. In order to clarify the relationships between the parameters, many cross wedge rolling conditions were simulated by DEFORM 3D software.

The rolling force in cross wedge rolling processes can be determined when its axial, radial and tangential components are known. Axial force makes workpiece in deformation zone to extend in axial direction. This axial force stretches the workpiece in longitudinal direction. Material flow of the workpiece in longitudinal direction and steady rolling is affected by the axial force. But, axial force is not detailed within this work since it has no loading effect on wedge dies. The tangential force of rolled part acting on the die is important to prevent the slippage. On the other hand, radial load is caused by the rotational compression of the workpiece external surface by the mounting dies. Since the work focuses on the tooling design and the factors acting on the die, only tangential and radial loads were taken into consideration. In order to perform numerical simulation, workpiece material was selected as the AISI-1045 steel and wedge dies were considered as rigid materials due to their negligible elastic deformation. During the study, simulations were performed by varying the stretching angle β (4° , 6° , 8° , 10°), forming angle α (20° , 30° , 40°), reduction ratio δ (1.3, 1.4, 1.5).

ANOVA and TAGUCHI statistical techniques were employed to clarify and distinguish the level of importance of main effects and their possible dual interactions with each other. Analyses of the main effect plots and interaction plots revealed the variation trends of the rolling force with respect to both input parameters and their mutual impacts. Upon this, a set of inputs which results the minimum possible rolling force were identified. Subsequently, a feed-forward neural network based back-propagation learning algorithm having a 4-10-4 topology was developed to correlate these four different process parameters. The prediction of accuracy of the neural model was also confirmed by a new data set other than those used in training phase.

After all numerical simulations and the statistical analysis the main concluding remarks can be outlined as follows:

- Effect of Forming Angle (α):

The values of tangential and radial loads decreases with the increment of the forming angle in the range of ($\alpha=20^\circ-40^\circ$) in knifing zone since the forming angle controls the size of the contact area between the tools and the workpiece. At the stretching zone, whereas forming angle has no or little effect on the tangential load, the radial load reduces especially in the range of ($\alpha=20^\circ-30^\circ$) but almost stable between the forming angles of $\alpha=30^\circ-40^\circ$. In brief, in order to provide less amount of load, forming angle should be selected the lowest one within the range. Especially in knifing and guiding zones, a smaller forming angle signifies a sharper tool, which increases the contact area and produces a more localized plastic deformation.

- Effect of Stretching Angle (β):

At the knifing zone, it is found that neither tangential nor radial loads are influenced by stretching angle. On the contrary, stretching angle has considerable impact on both tangential and rolling loads throughout the stretching zone. Within the drawn conclusions it is found that the smallest stretching angle causes the lowest possible forming loads. But, it should be noted that the stretching angle is directly related with the die length. Larger stretching angles within the tool lead more elongation of the workpiece.

Lower values of the stretching angle are associated with a greater die length required to achieve the product geometry.

- Effect of Reduction Ratio (δ)

The larger the value of reduction ratio (δ) implies the larger compression of the workpiece between the dies. At the knifing zone, both tangential and radial loads increase with the increment in the reduction ratio in the range of ($\delta=1.3-1.5$). On the other hand, reduction ratio has almost no effect on the tangential load at the stretching zone, while the radial load decreases.

The modeling of load requirement to achieve the minimum load requirement is obligatory in CWR process. This thesis investigated a way to model the tangential and radial rolling load of knifing and stretching zones through statistical design of experiment approach. The dependency of parameters is examined and their interactions graphs are discussed. This work proposes that to achieve the low value of rolling load, concentrate should focus on the knifing and stretching zones separately. It is concluded that in knifing zone, high value of forming angle with the combination of low value of reduction ratio results in minimum load while in stretching zone has low stretching angle with high reduction ratio.

RECOMMENDATION FOR FUTURE STUDIES

Utilization of the following items will be useful for the extension of present work;

- A comprehensive experimental setup should be constructed.
- A computer program should be prepared to propose the desired wedge die geometry for all axisymmetric parts.

REFERENCES

- [1] Pater Z. (1998). Simulation of Cross Wedge Rolling Process Using the Upper Bound Method, *Scandinavian Journal of Metallurgy*, **27**, 120-127.
- [2] Yaomin D. (1998) A Numerical, Experimental, and Phenomenological Investigation of Cross-Wedge Rolling, Proquest Dissertations and Theses; *Proquest Dissertations & Theses* (PQDT) Pg. N/A
- [3] Pater Z. (2003). Tools Optimization in CWR. *Journal of Materials Processing Technology*. 176–182.
- [4] Yaomin D., Lovell M., Tagavi K. (1998), Analysis of Interfacial Slip in Cross Wedge rolling: An Experimentally Verified Finite Element Model. *Journal of Materials Processing Technology*. **80-81**, 273-281
- [5] Deng, Z., Lovell M. R., Tagavi, K. (2001). Influence of Material Properties and Rolling Speed on the Interfacial Slip Characteristics In Cross Wedge Rolling. *ASME J. of Manu. Science and Engineering*. **123**, 760-768.
- [6] Fang G., Lei L.P., Zeng P., Mater J. (2002). Three Dimensional Rigid-Plastic Finite Element Simulation For The Two-Roll Cross Wedge Rolling Process. *Journal of Materials Processing Technology*. **129**, 245–249.
- [7] Q. Li, M. Lovell, Int. J. Adv. (2004). The Establishment of A Failure Criterion in Cross Wedge Rolling. *Manufacturing Technol.* **24**, 180–189.
- [8] Pater Z., Gontarz A., Łukasik K., Weroński W. (2003). Modeling of Cross Wedge Rolling Processes, *NOT, Kiev, (in Russian)*.
- [9] Pater Z., Weron W. Kazanecki Ąski J., Gontarz A. (1999). Study of the process stability of CWR, *Journal of Materials Processing Technology*. **92-93**.
- [10] Pater Z. (1999). Numerical Simulation of The CWR Process Including Upsetting, *Journal of Materials Processing Technology*. **92-93**, 468-473.
- [11] Pater Z., Bartnicki Samołyk J., G. (2005). Numerical Modeling of CWR Process of Ball Pin. *Journal of Materials Processing Technology*. **164-165**, 1235–1240

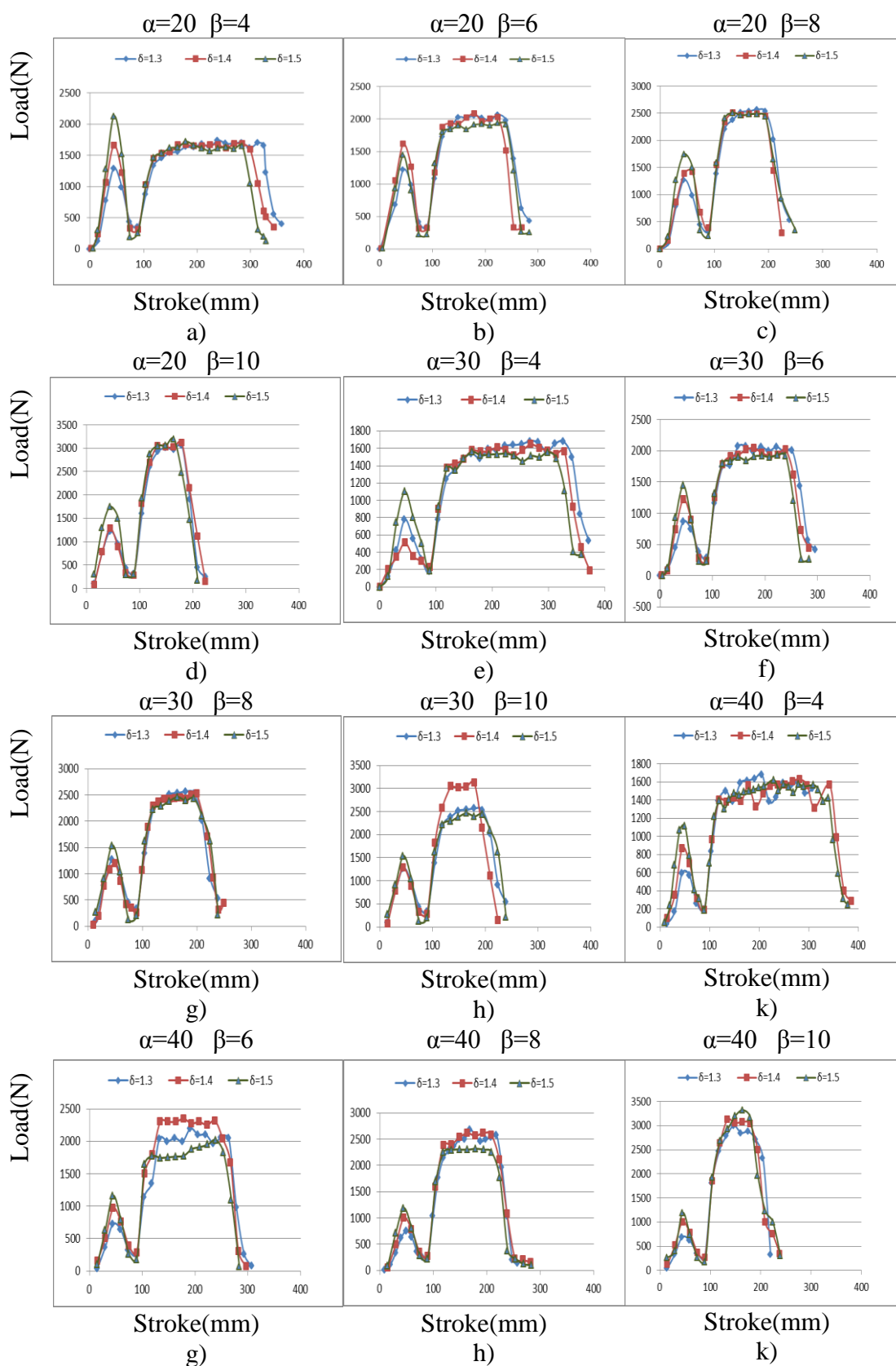
- [12] Fang G., Lei L.P., Zeng P. (2002). Three Dimensional Rigid-Plastic Finite Element Simulation For The Two Roll CWR Process s. *Journal of Materials Processing Technology*. 245-249.
- [13] Bartnicki J., Pater Z. (2005), Numerical Simulation of Three Rolls CWR of Hollowed Shafts. *Journal of Materials Processing Technology*. **164–165**, 1154–1159.
- [14] Pater Z., Bartnicki J., Gontarz A., Weronki S. (2004). Numerical Modeling of CWR of Hollowed Shafts. *Nadbystrzycka Lublin, Poland*. **36**, 20-618
- [15] Dong, Y., Tagavi, K., Lovell, M. (2000) Analysis of interfacial slip in cross-wedge rolling: a numerical and phenomenological investigation, *Journal of Materials Processing Technology*. **97**, 44-53.
- [16] Wang M., Li X., Du F., Zheng Y. (2005). Thermal Mechanical Simulation of CWR, *Materials Science and Engineering A*. **391**, 305–312
- [17] Pater Z. (2006) Finite Element Analysis of CWR. *Journal of Materials Processing Technology* 201-208.
- [18] Pater Z. (2000). Theoretical and Experimental Analysis of CWR Process. *International Journal of Machine Tools & Manufacture*. **40** 49-63.
- [19] Lovell, M.R. (2001). Evaluation of Critical Interfacial Friction in Cross Wedge Rolling. *Journal of Tribology*. **123**, 424-429
- [20] Lee H.W., Lee G.A., Yoon D.J., Choi S., Na K.H., Hwang M.Y. (2008) Optimization Of Design Parameters Using A Response Surface Method In A Cold CWR. *Journal of Materials Processing Technology*. **201**, 112-117
- [21] Metal Pres s.r.o, Stará osada 94, 664 84 Zastávka u Brna, Czech republic <http://www.metalpres.cz/english/index.htm>
- [22] Deonge Y., et al. (1998). Analysis of Interfacial Slip In Cross-Wedge Rolling: An Experimentally Verified Finite-Element Model, *Journal of Material Processing Technology*. **80-81**, 273-281,
- [23] Yaomin D,et all, (2000) Analysis of stress in cross wedge rolling with application to failure, *International Journal of Mechanical Sciences*, **42**, 1233-1253

- [24] Yaomen D. (1998), A Numerical, Experimental, and Phenomenological Investigation of Cross Wedge Rolling, *Proquest Dissertations Theses, Proquest Dissertations &Theses (PQDT)*.
- [25] Z. Pater , A. Gontarz, W. Weroński, (2006) Cross-wedge rolling by means of one flat wedge and two shaped rolls, *Journal of Materials Processing Technology*, **36**, 20-618 Lublin
- [26] Fu X. P. and Dean T. A. (1993). Past Developments, Current Applications and Trends in Cross Wedge Rolling Process, *International Journal of Machine Tools Manufacturing*. **33**, 367-400.
- [27] Yılmaz N.F., Dereli T., Çağlar A.F. (2005) Yeni Bir İleri Teknoloji Üretim Metodu: Çapraz Kamalı Haddeleme, 3. *Makina Tasarım ve İmalat Teknolojileri Kongresi, Konya*. 77-83.
- [27] Neugebauer R., et al. (2002). *Journal of Materials Processing Technology* **125-126**, 856-862.
- [28] Wang M., LI X., Feng Du S. ,(2009). CWR Using Finite Element Method, *Journal of Iron And Steel Research, International*. 38-43.
- [30] Urankar S., Lovell M., Morrow C., Lic Q., Kawada K. (2006). Development of A Critical Friction Model For Cross Wedge Rolling Hollow Shafts, *Journal of Materials Processing Technology*.
- [31] Pater Z. (1998). Simulation Of Cwr Process Using Upper-Bound Method,, *Journal of Materials*. **27**, 120-127
- [32] Bozgeyik, A. (2006). Computer Aided Evaluation of Cross Wedge Rolling Parameters. *Y. Lisans, Gaziantep*.
- [33] Zohourkari I., Assarzadeh S., Zohoor M. (2010). Modeling and Analysis of Hot Extrusion Metal Forming Process Using Artificial Neural Network and Anova Proceedings of the ASME. *10th Biennial Conference on Engineering Systems Design and Analysis ESDA2010, July 12-14, Istanbul, Turkey*.
- [34] Hopfield J. J. (1982). Neural Networks and Physical Systems With Emergent Collective Computational Abilities. *Proc. Natl Acad. Sci. USA*. **79**, 2554-2558.
- [35] Haykin, S. (1994). Neural Networks: A Comprehensive Foundation. *Macmillan College Publishing Co, New York*.

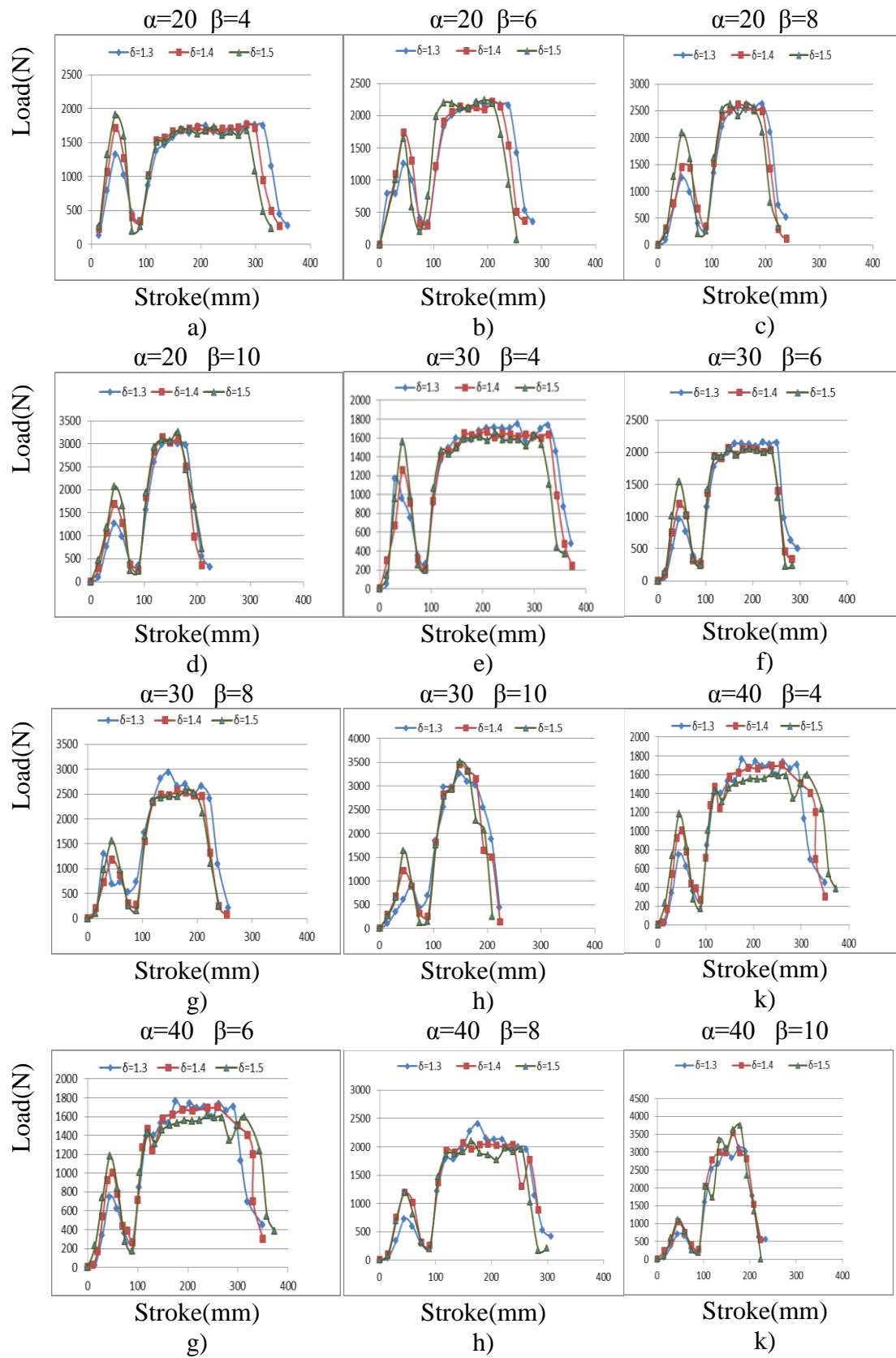
- [36][Jain, A.K., Mao Mohiuddin,K.M.,(1996) Artificial Neural Networks: A Tutorial, Theme Feature. **18**,31-44]
- [37] Demuth, H. And Beale, M. (2001). Neural Networks Toolbox for Use with MATLAB, *User's Guide*, <http://www.varpa.org/Docencia/Files/nnet.pdf>.
- [37] Pater Z. (2000). Theoretical and Experimental Analysis of Cross Wedge Rolling Process, *International Journal of Machine Tools &Manufacturer*. **40**,49-63
- [38] Hasan. O., Tamer. E., Ismail, U. (2007). Application of Taguchi Optimization Technique In Determining Plastic Injection Molding Process Parameters For a Thin Shell Part. *Materials & Design*. **28**, 1271-1278.
- [39]Design of experiments via taguchi methods: orthogonal arrays,
https://controls.engin.umich.edu/wiki/index.php/Design_of_experiments_via_taguchi_methods:_orthogonal_arrays

APPENDICES

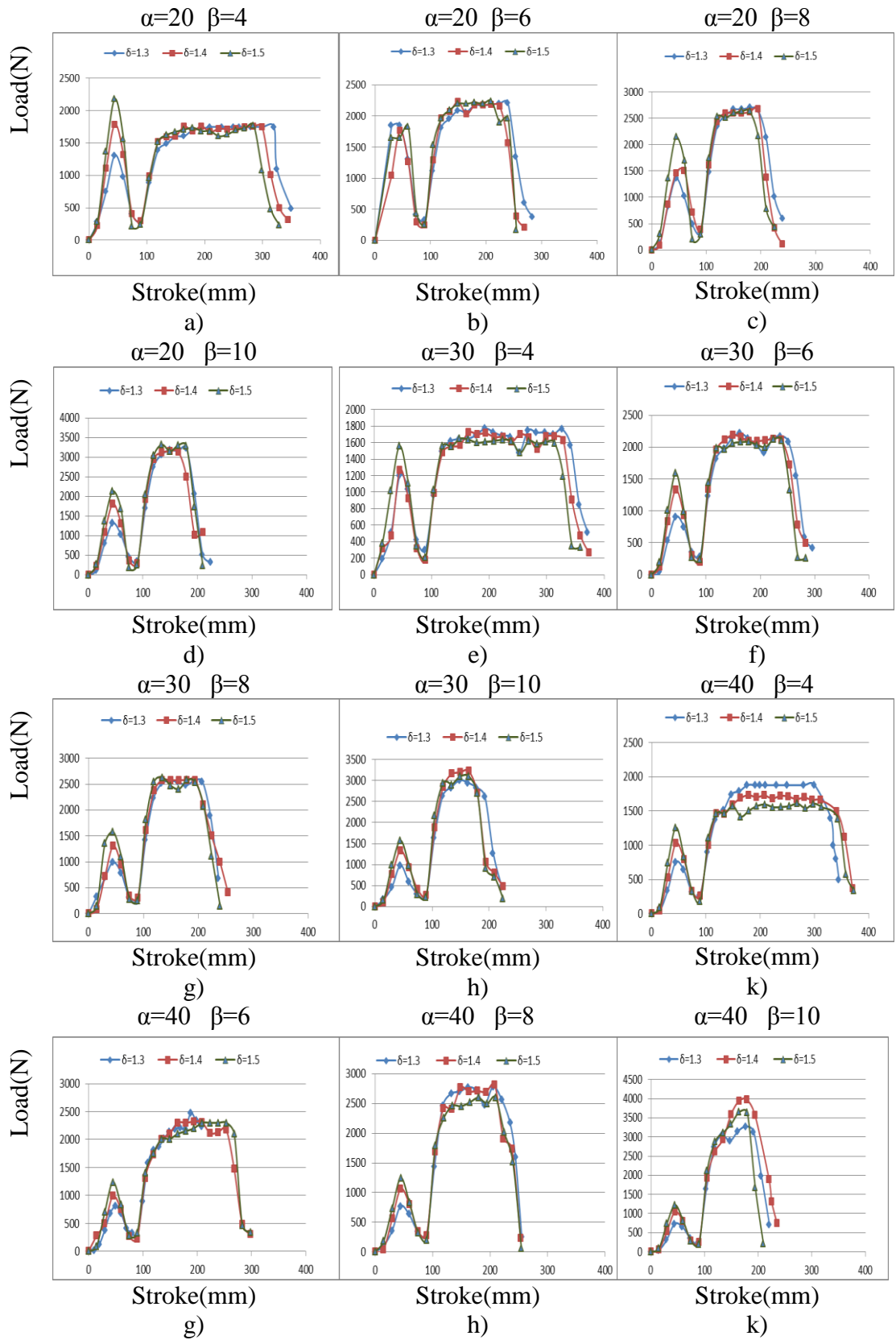
Following Figure demonstrate the variations of tangential load graphs according to various reduction ratio under $V=50$ mm/sn die velocity condition.



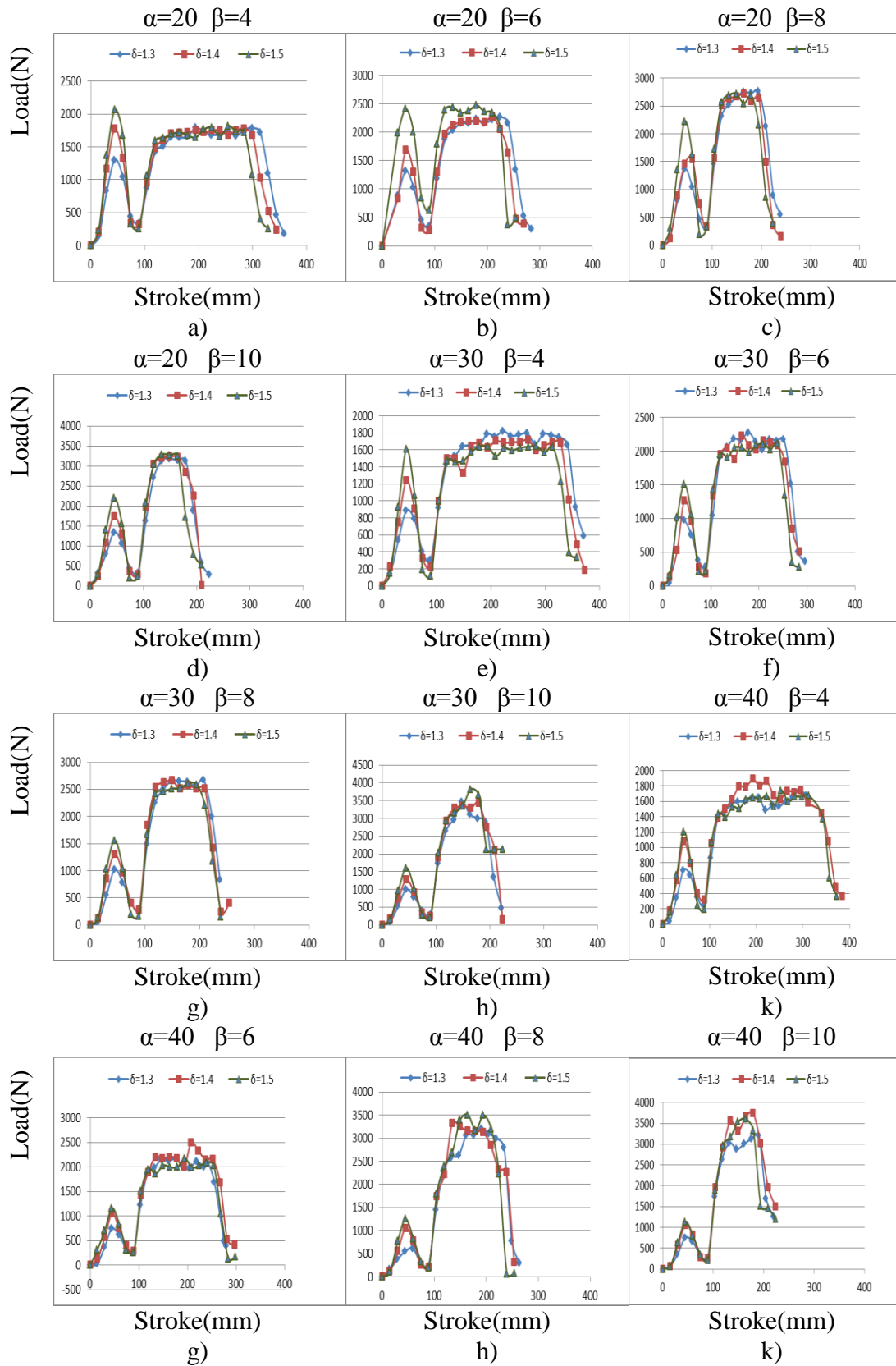
Following Figure demonstrate the variations of tangential load graphs according to various reduction ratio under $V=75\text{mm/sn}$ die velocity condition.



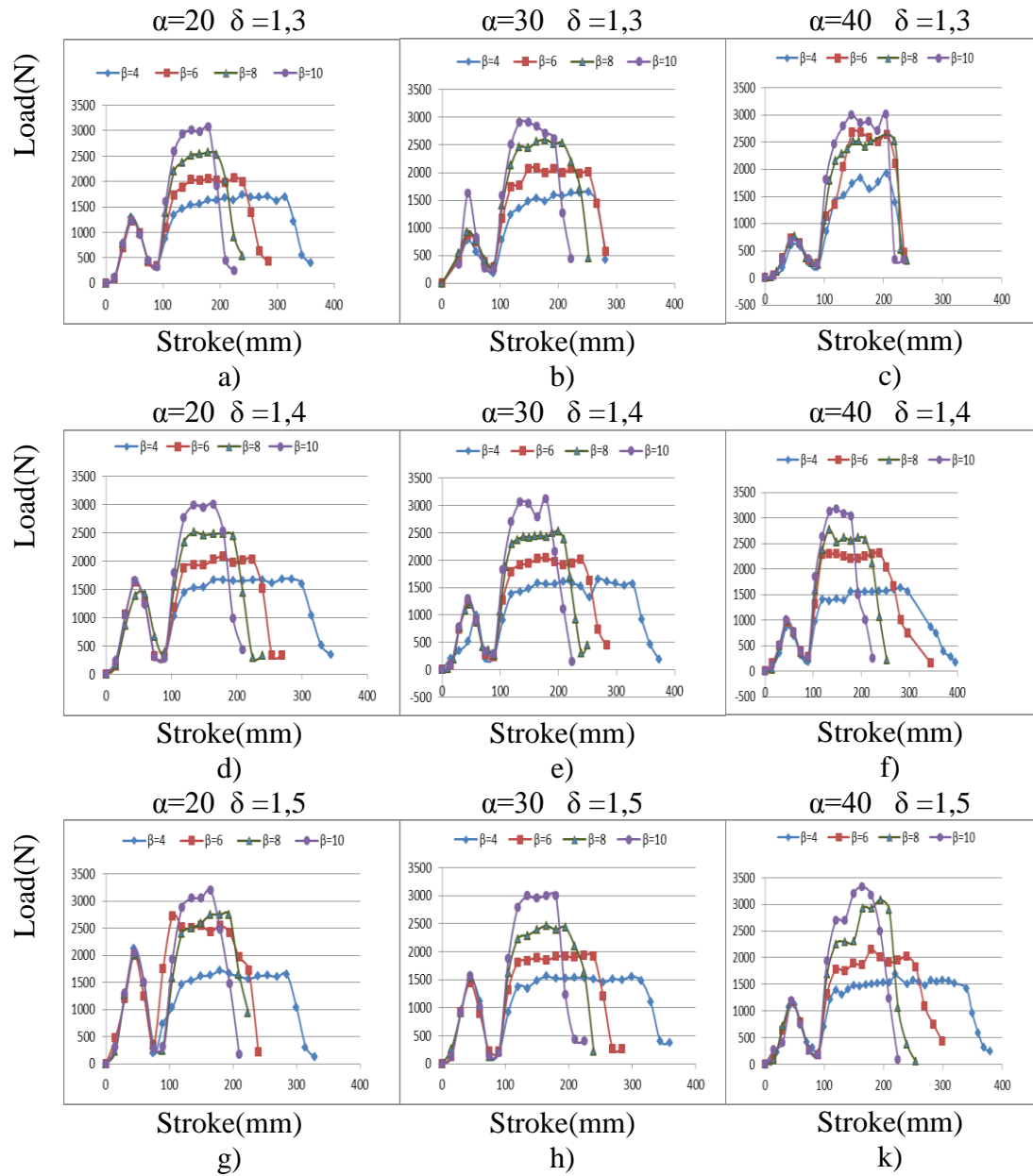
Following Figure demonstrate the variations of tangential load graphs according to various reduction ratio under $V=100$ mm/sn die velocity condition.



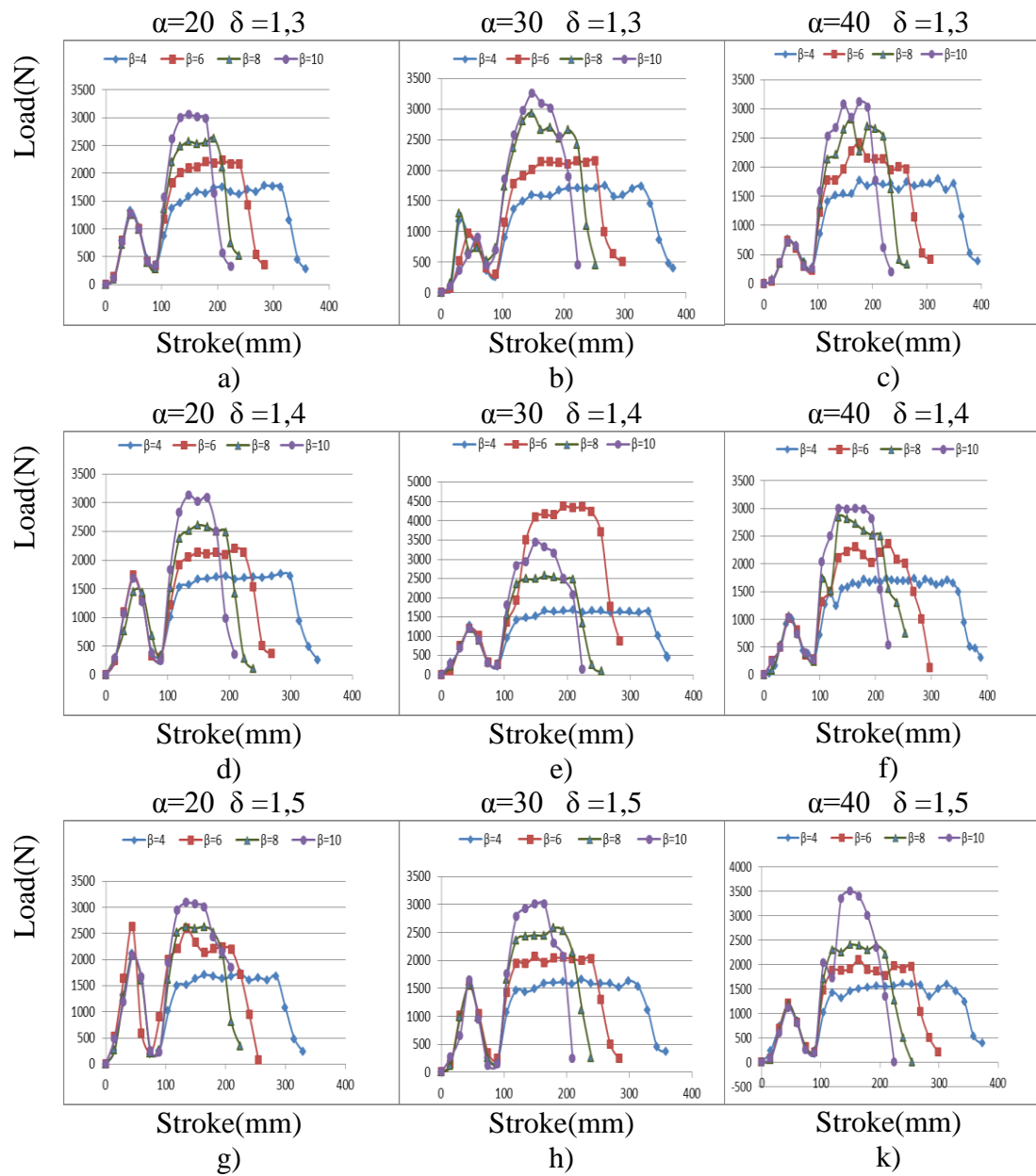
Following Figure demonstrate the variations of tangential load graphs according to various reduction ratio under $V=125\text{mm/sn}$ die velocity condition.



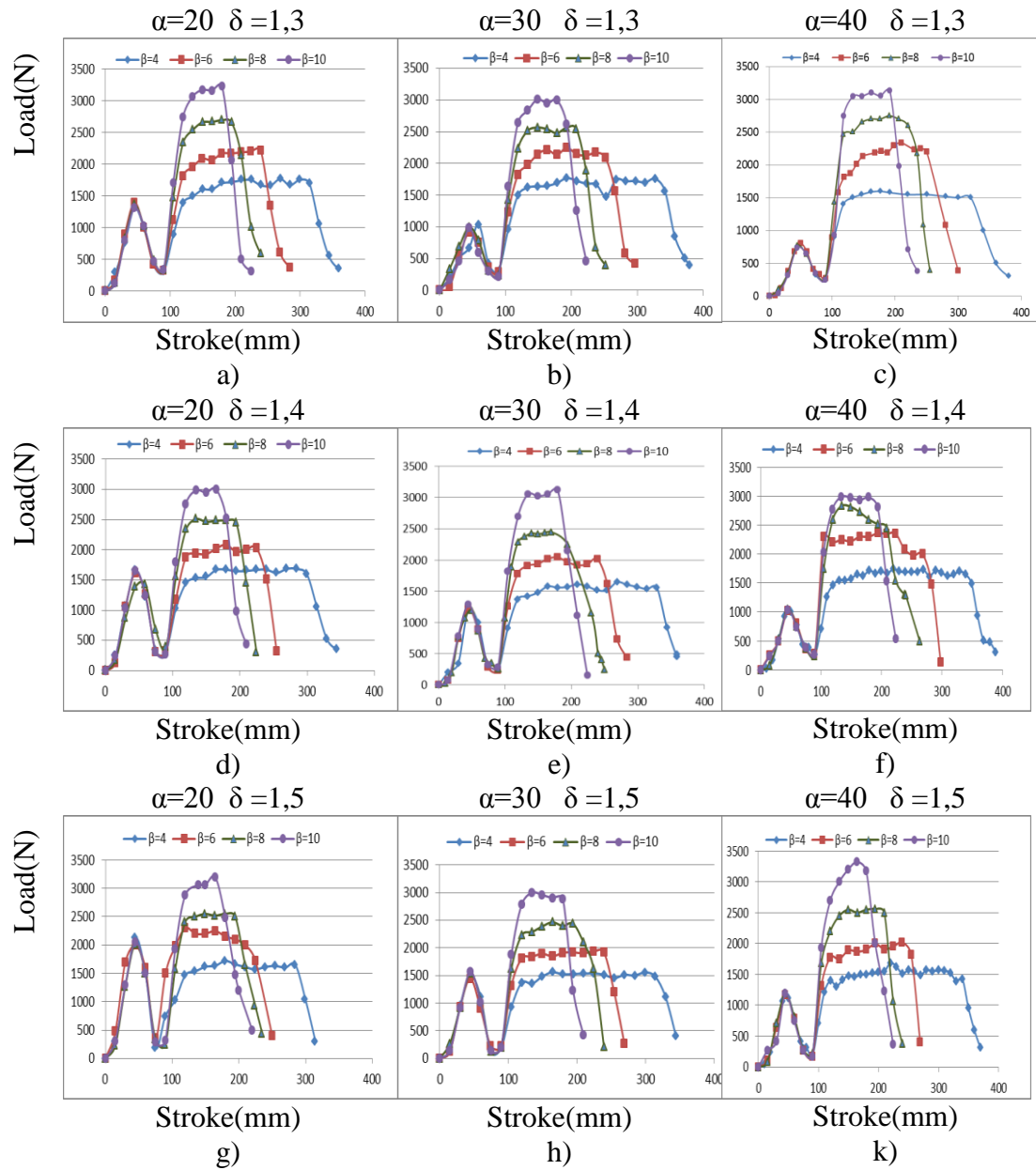
Following Figure demonstrate the variations of tangential load graphs according to various stretching angle under $V=50$ mm/sn die velocity condition.



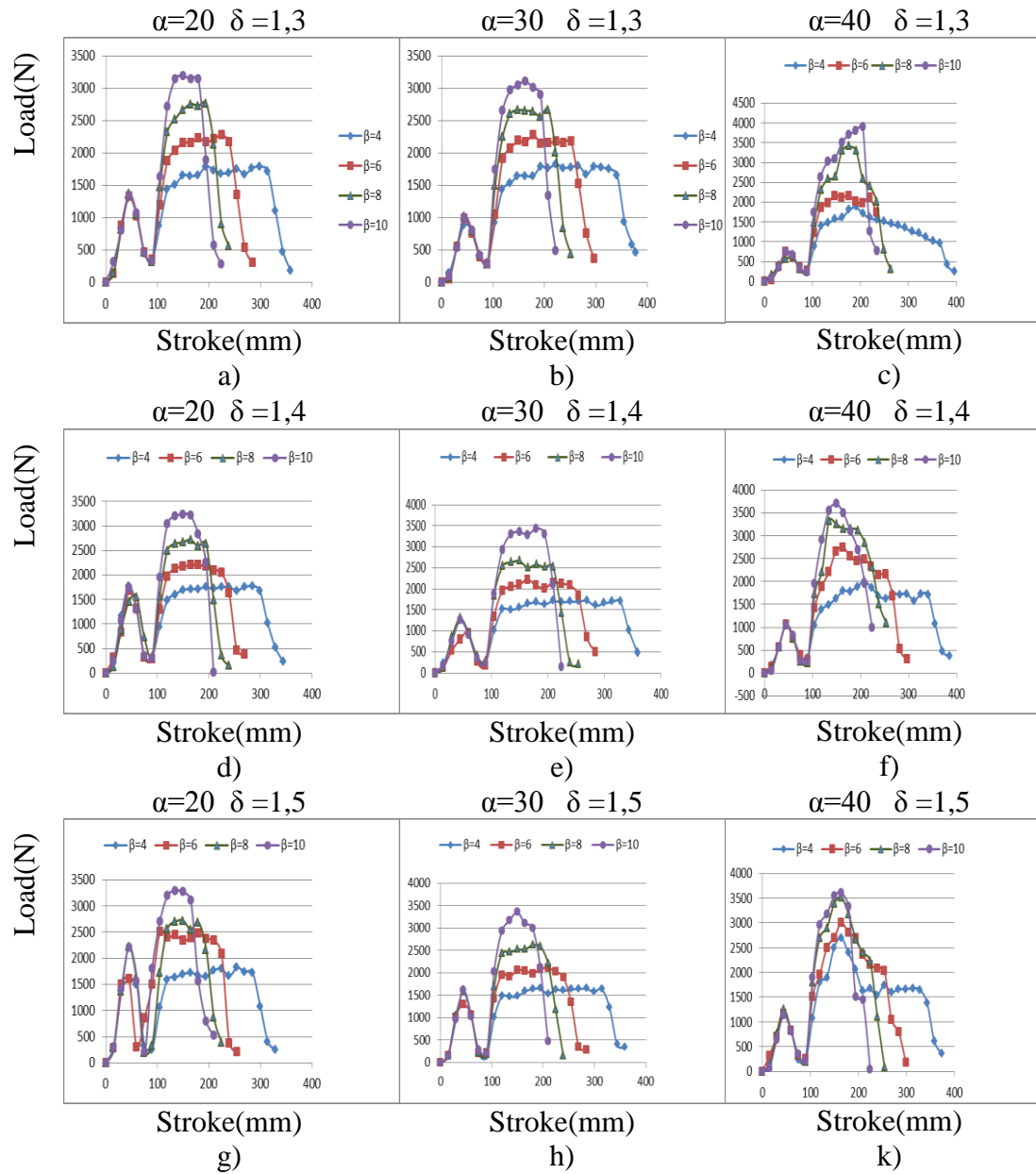
Following Figure demonstrate the variations of tangential load graphs according to various stretching angle under $V=75$ mm/sn die velocity condition.



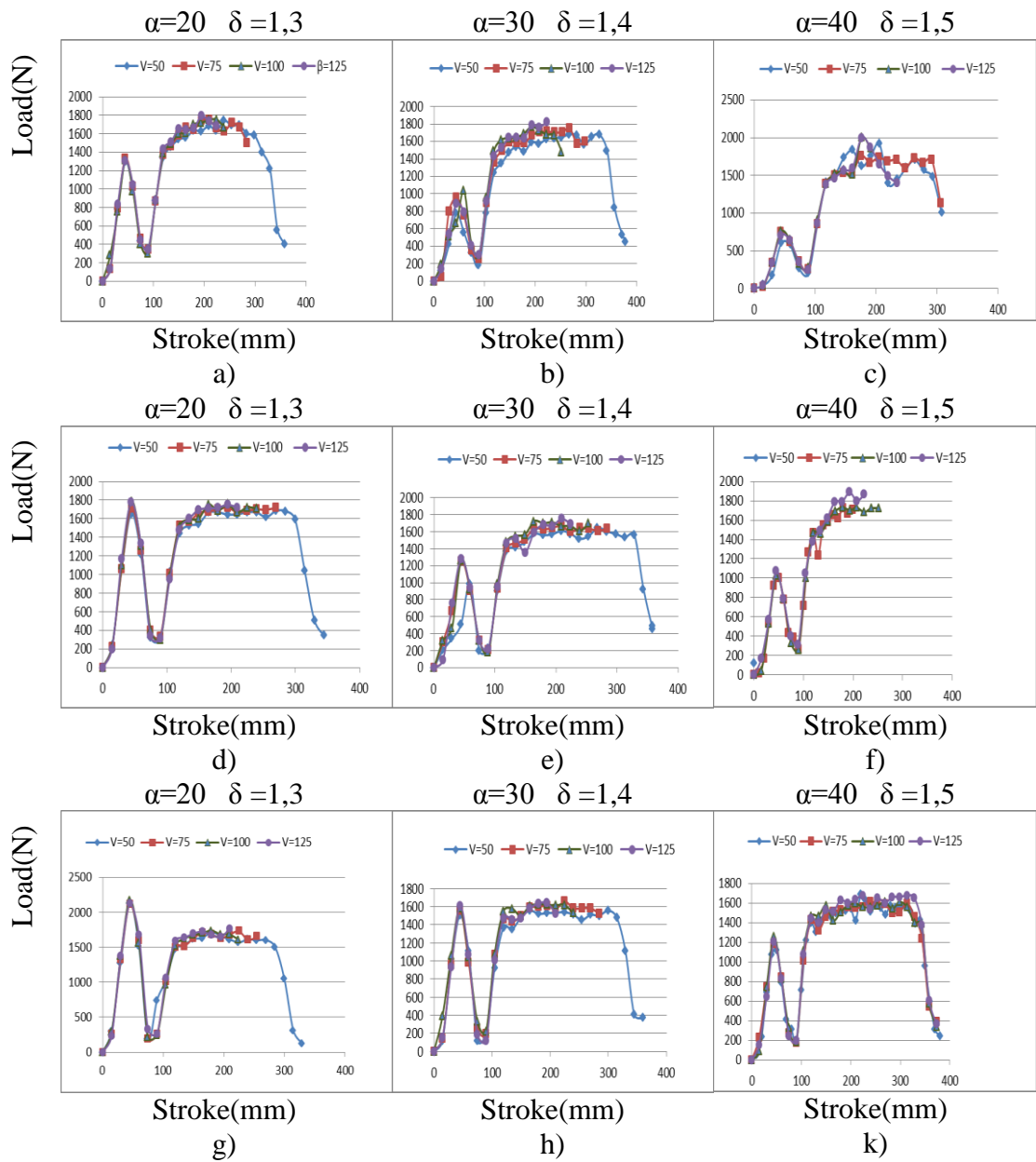
Following Figure demonstrate the variations of tangential load graphs according to various stretching angle under $V=100$ mm/sn die velocity condition.



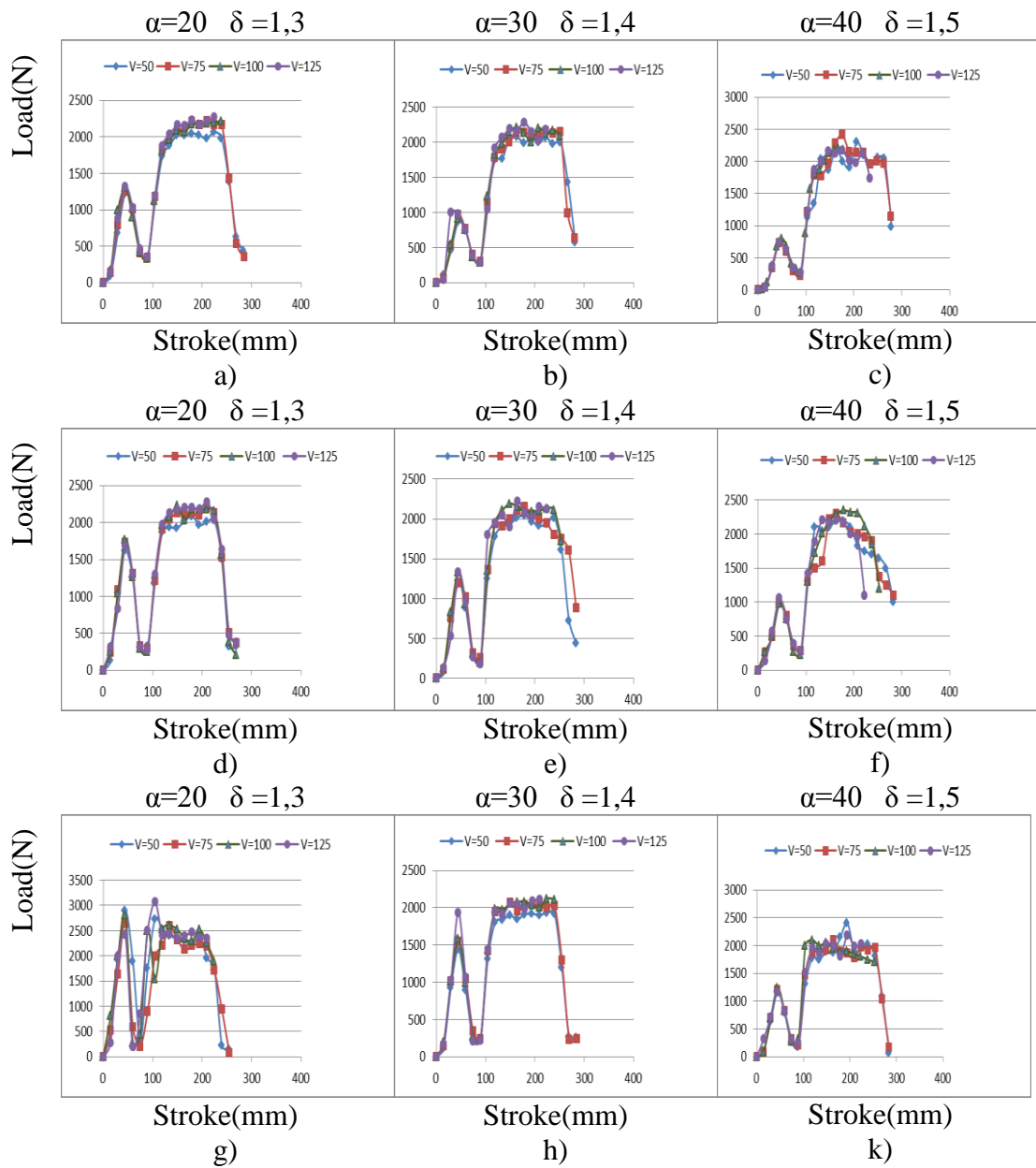
Following Figure demonstrate the variations of tangential load graphs according to various stretching angle under $V=125$ mm/sn die velocity condition.



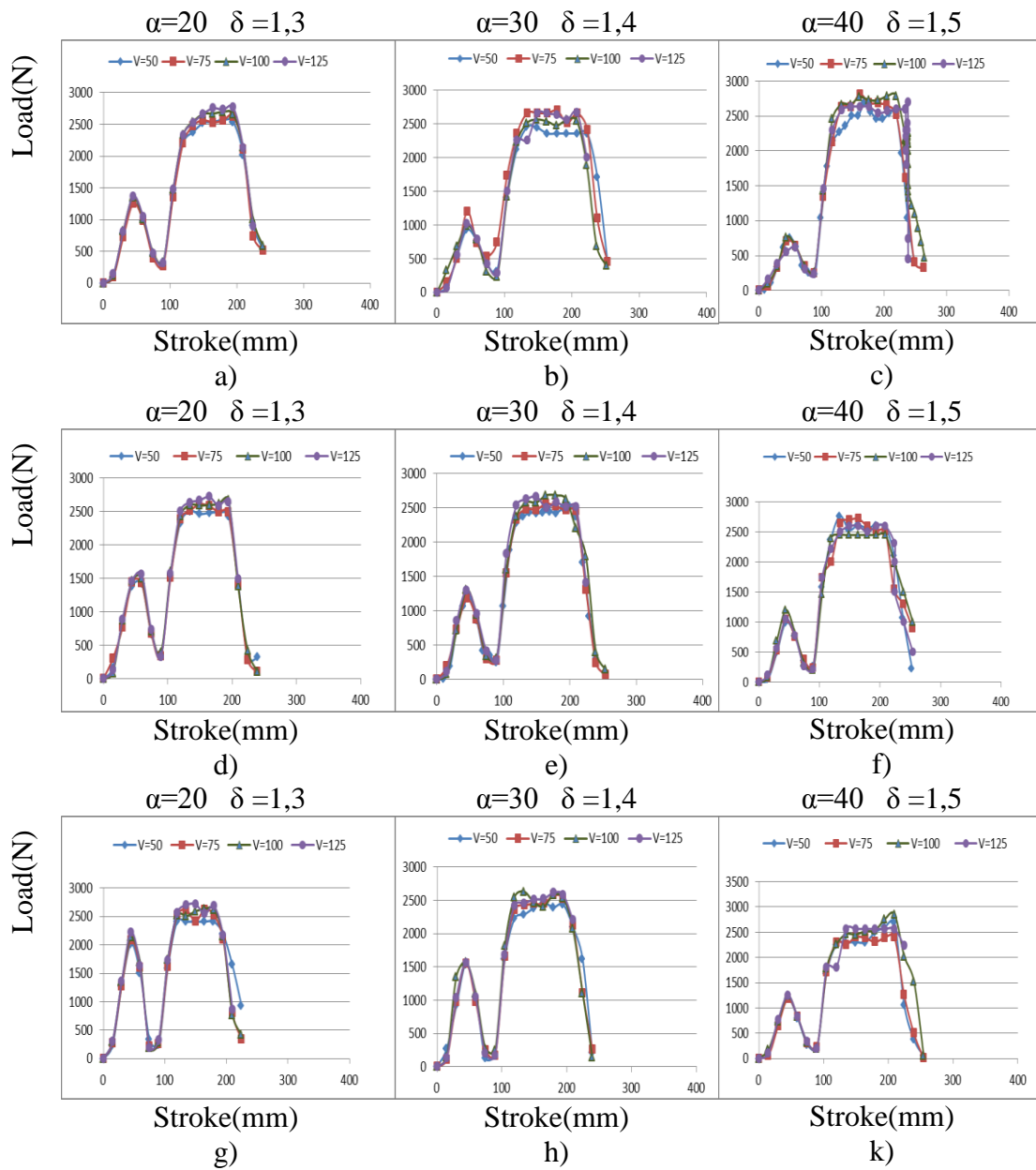
Following Figure demonstrate the variations of tangential load graphs according to various die speed under $\beta = 4^\circ$ stretching angle condition.



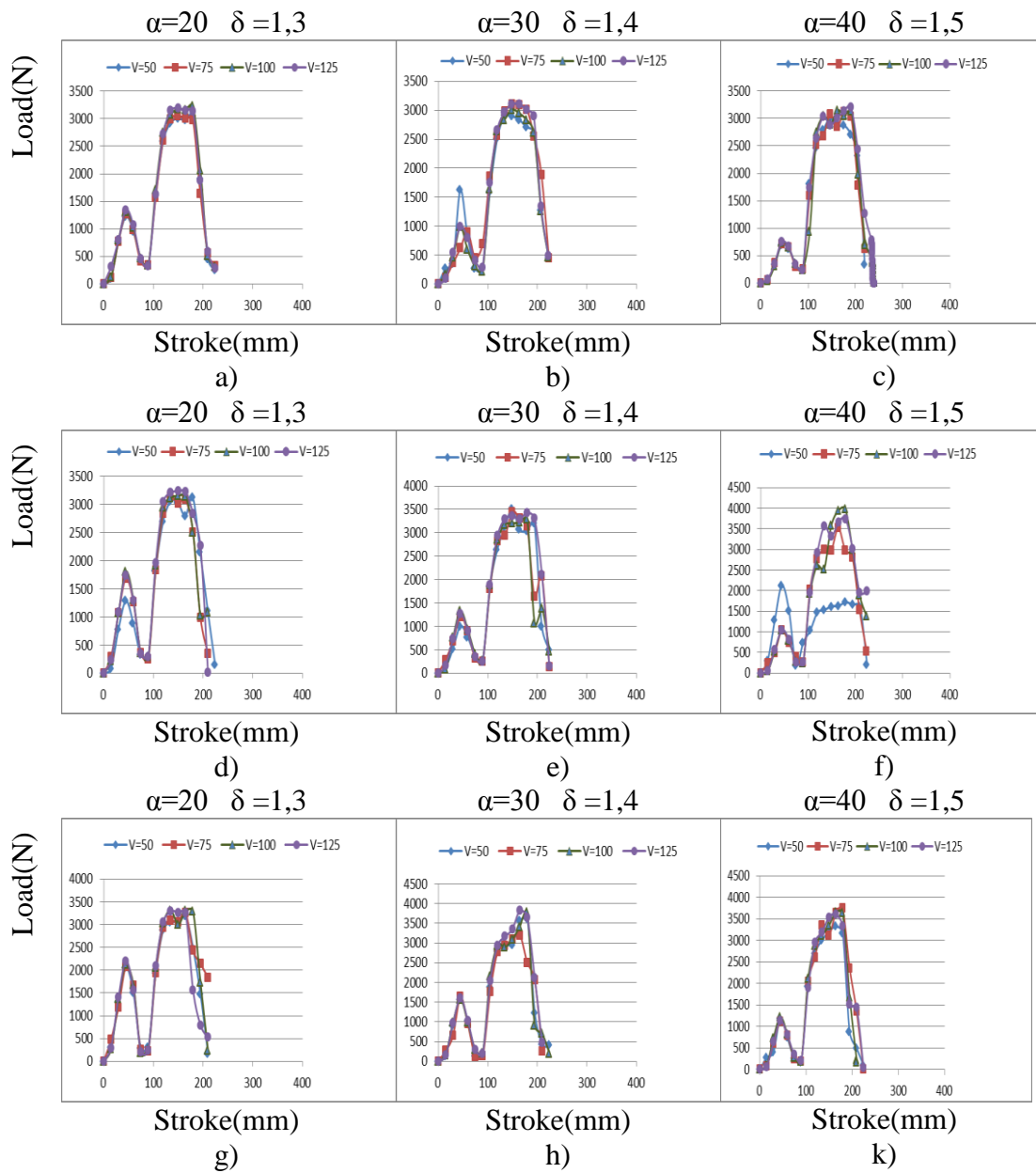
Following Figure demonstrate the variations of tangential load graphs according to various die speed under $\beta = 6^\circ$ stretching angle condition.



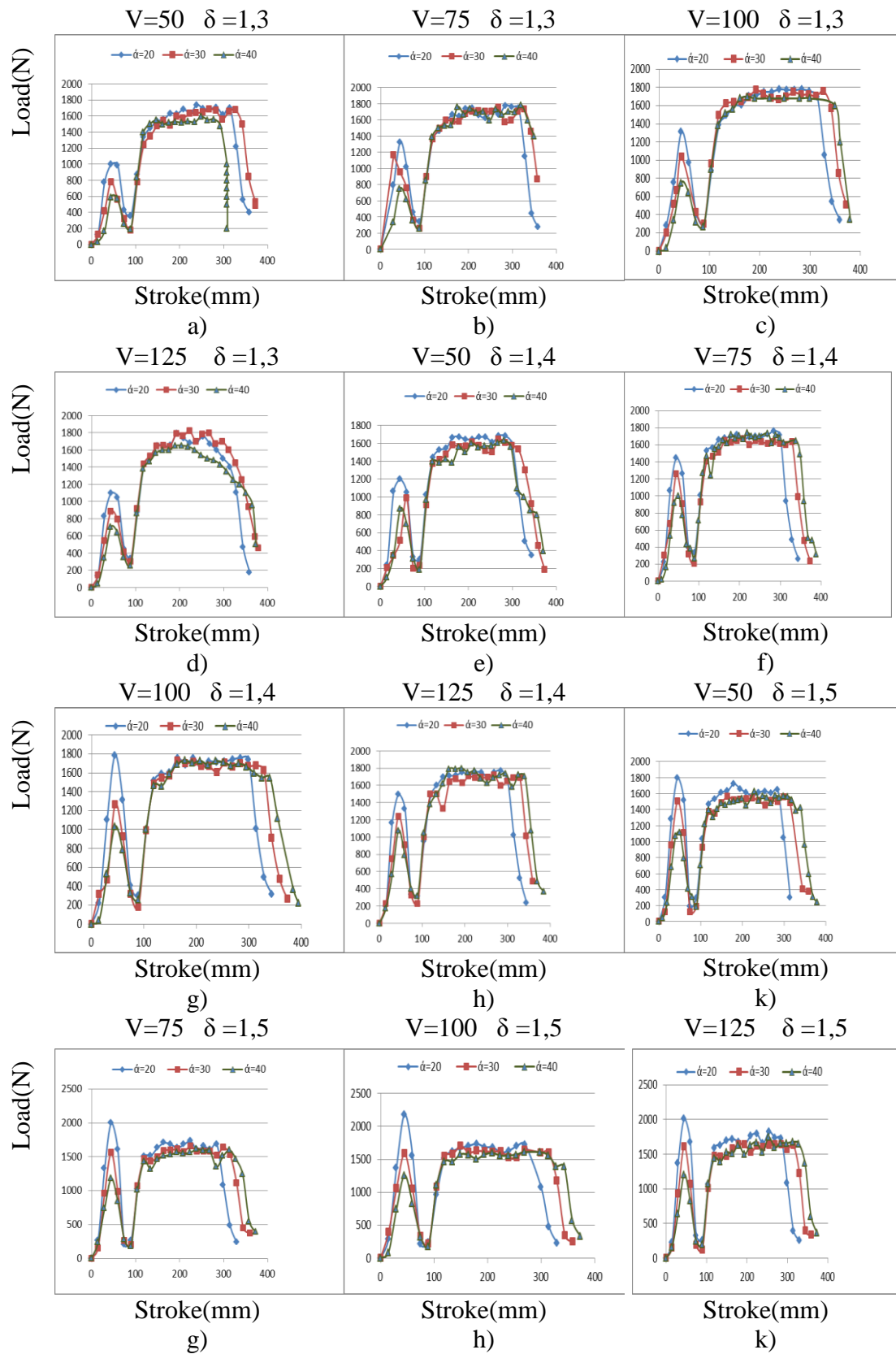
Following Figure demonstrate the variations of tangential load graphs according to various die speed under $\beta = 8^\circ$ stretching angle condition.



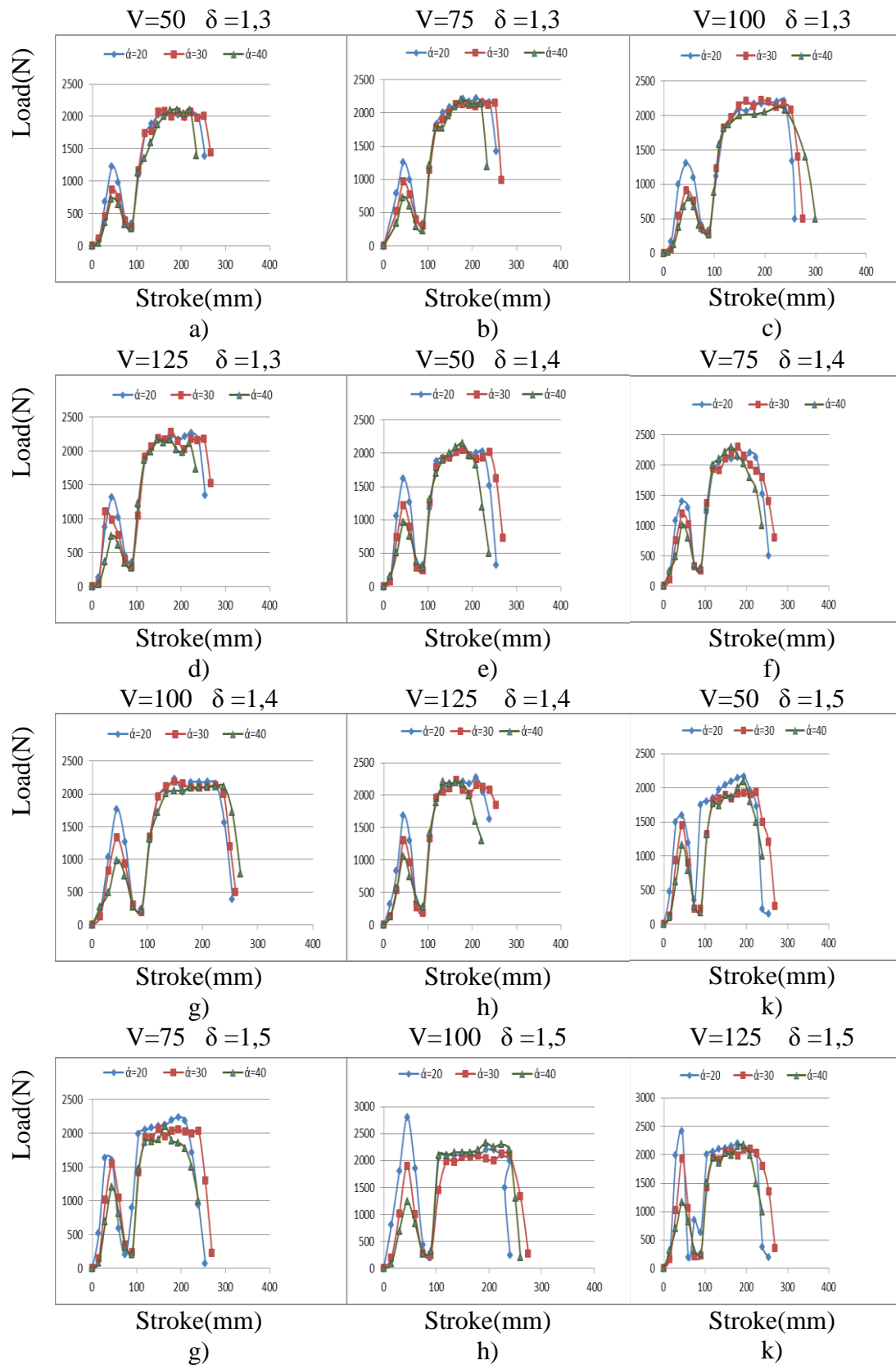
Following Figure demonstrate the variations of tangential load graphs according to various die speed under $\beta = 10^\circ$ stretching angle condition.



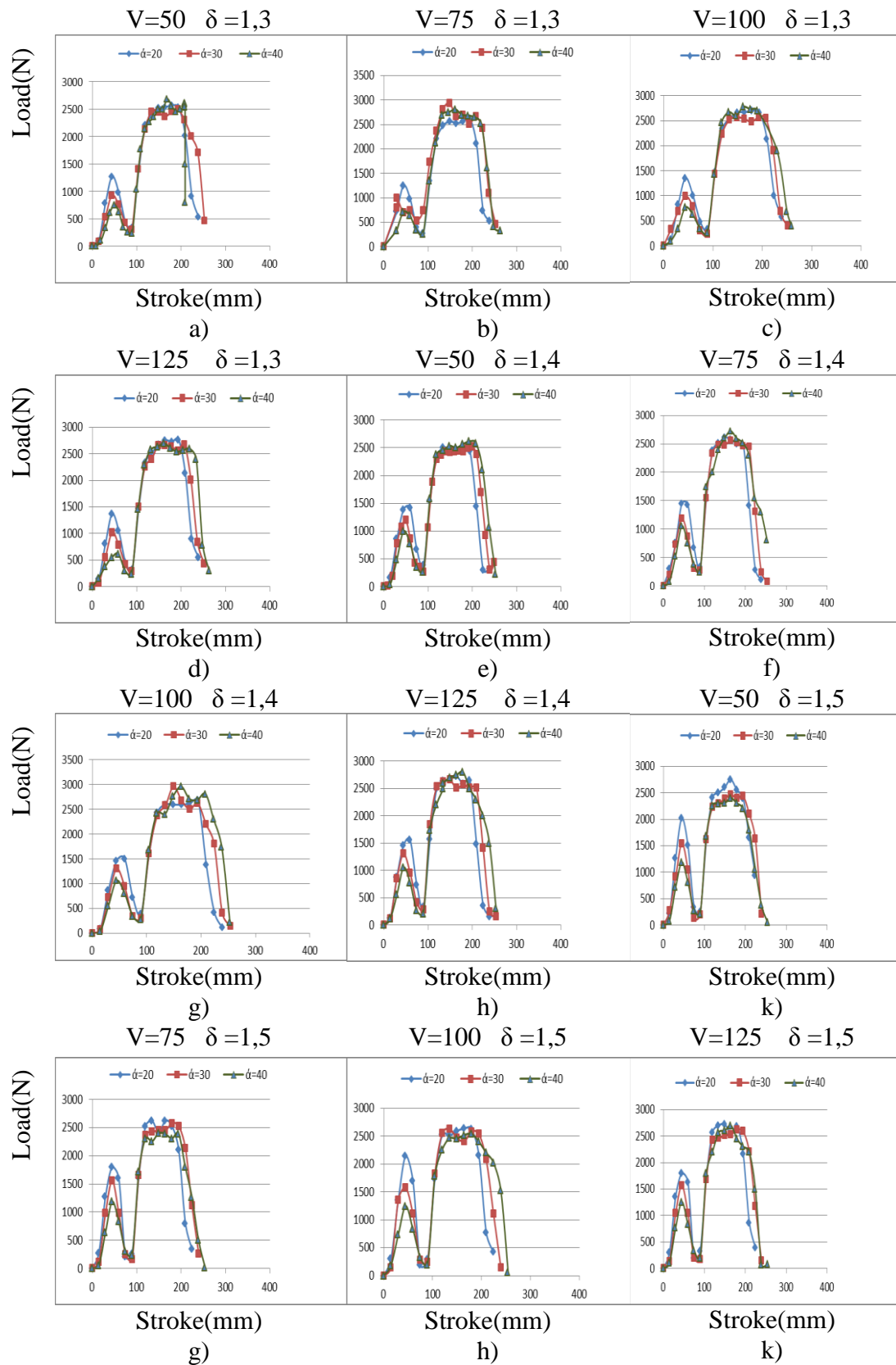
Following Figure demonstrate the variations of tangential load graphs according to various forming angle under $\beta = 4^\circ$ stretching angle condition.



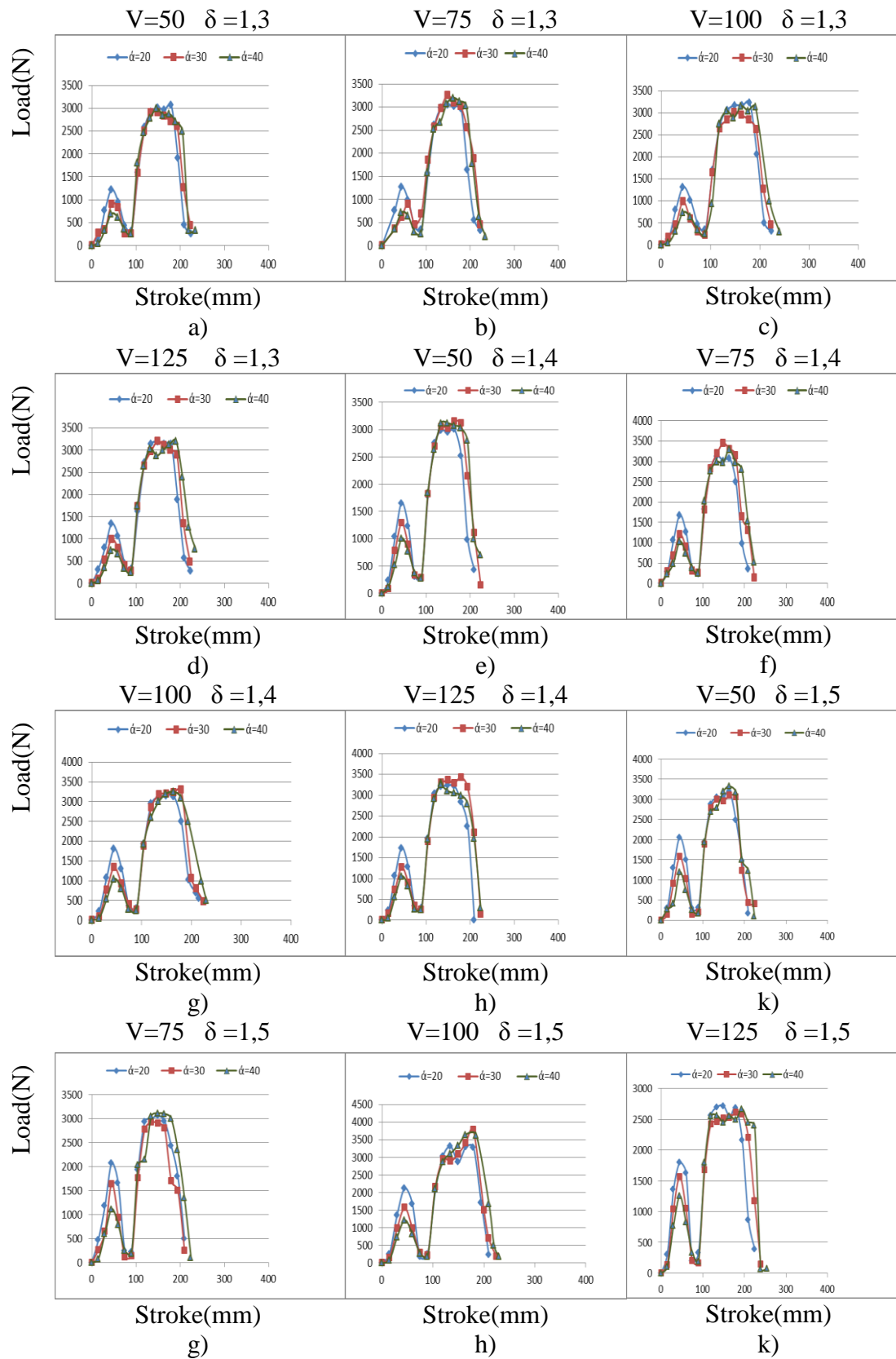
Following Figure demonstrate the variations of tangential load graphs according to various forming angle under $\beta = 6^\circ$ stretching angle condition.



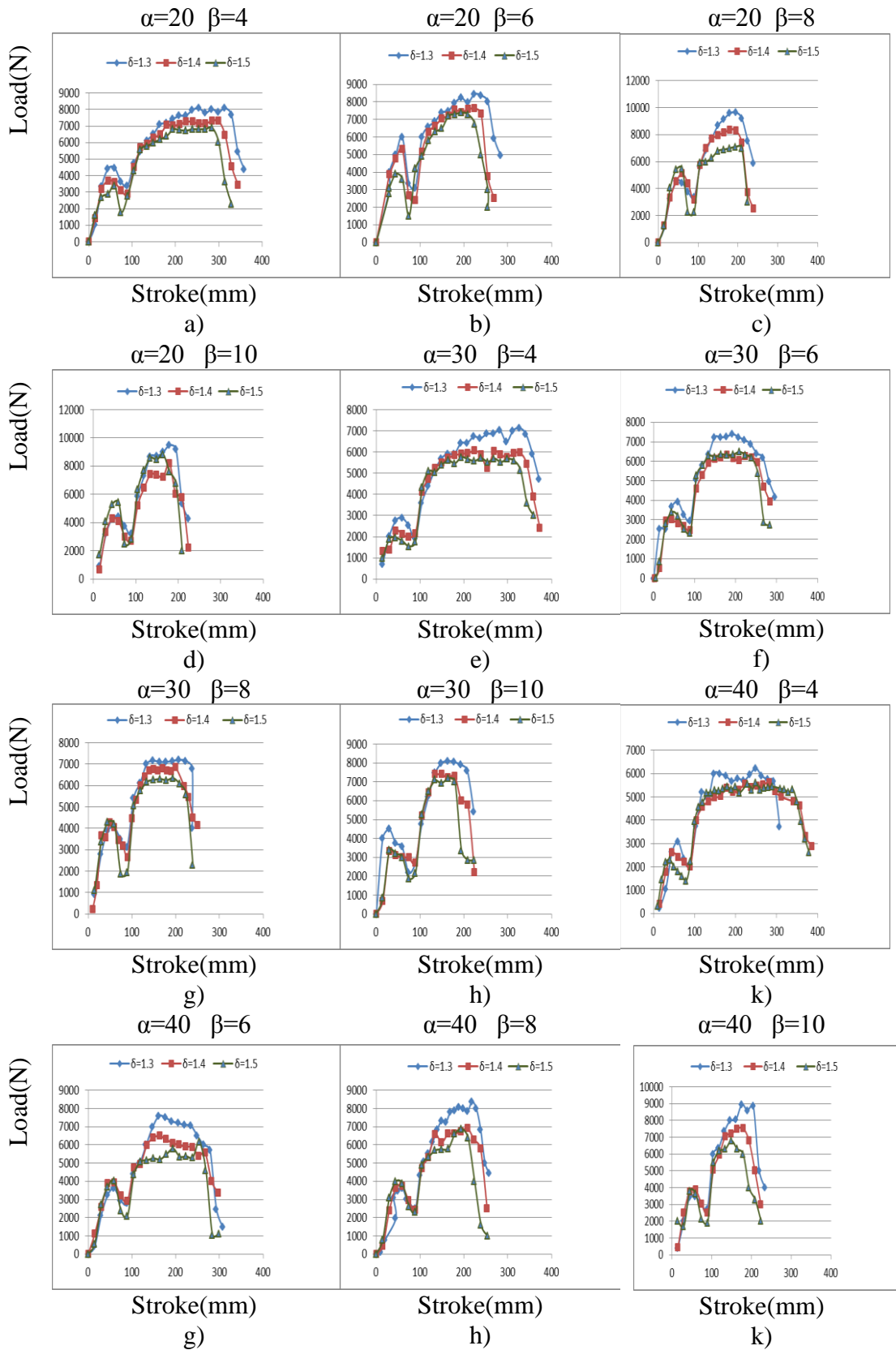
Following Figure demonstrate the variations of tangential load graphs according to various forming angle under $\beta = 8^\circ$ stretching angle condition.



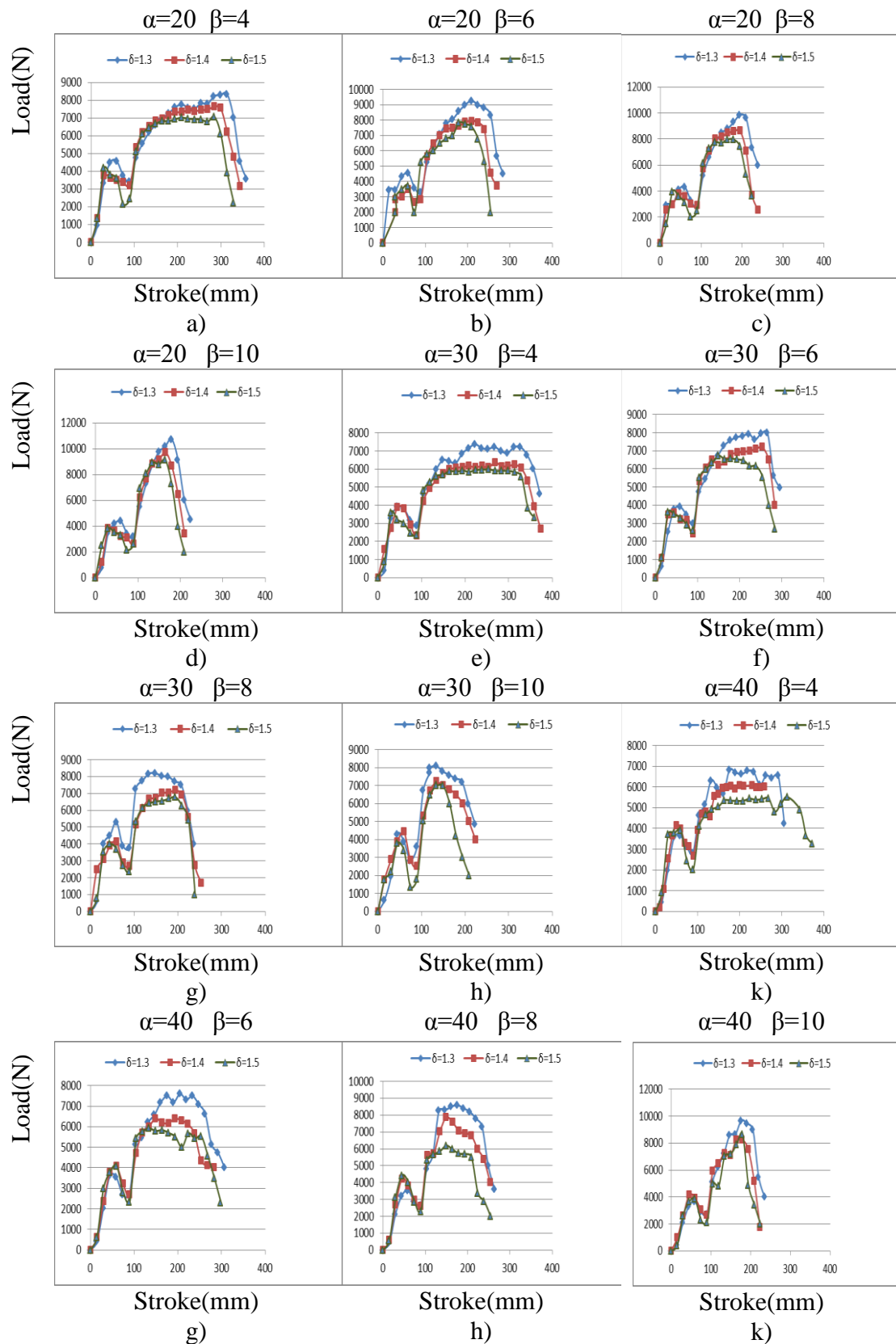
Following Figure demonstrate the variations of tangential load graphs according to various forming angle under $\beta = 10^\circ$ stretching angle condition.



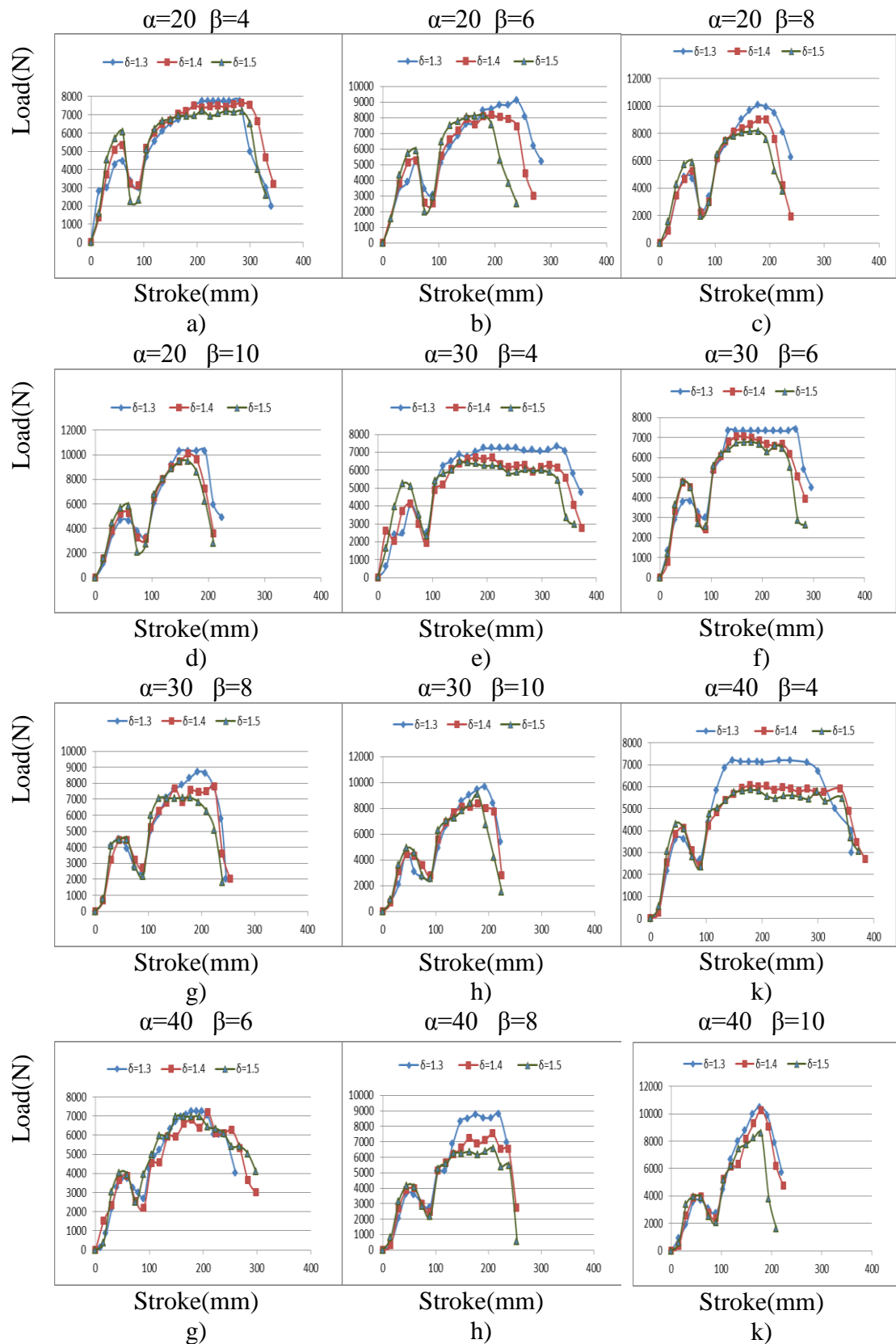
Following Figure demonstrate the variations of radial load graphs according to various reduction ratio under $V=50$ mm/sn die velocity condition.



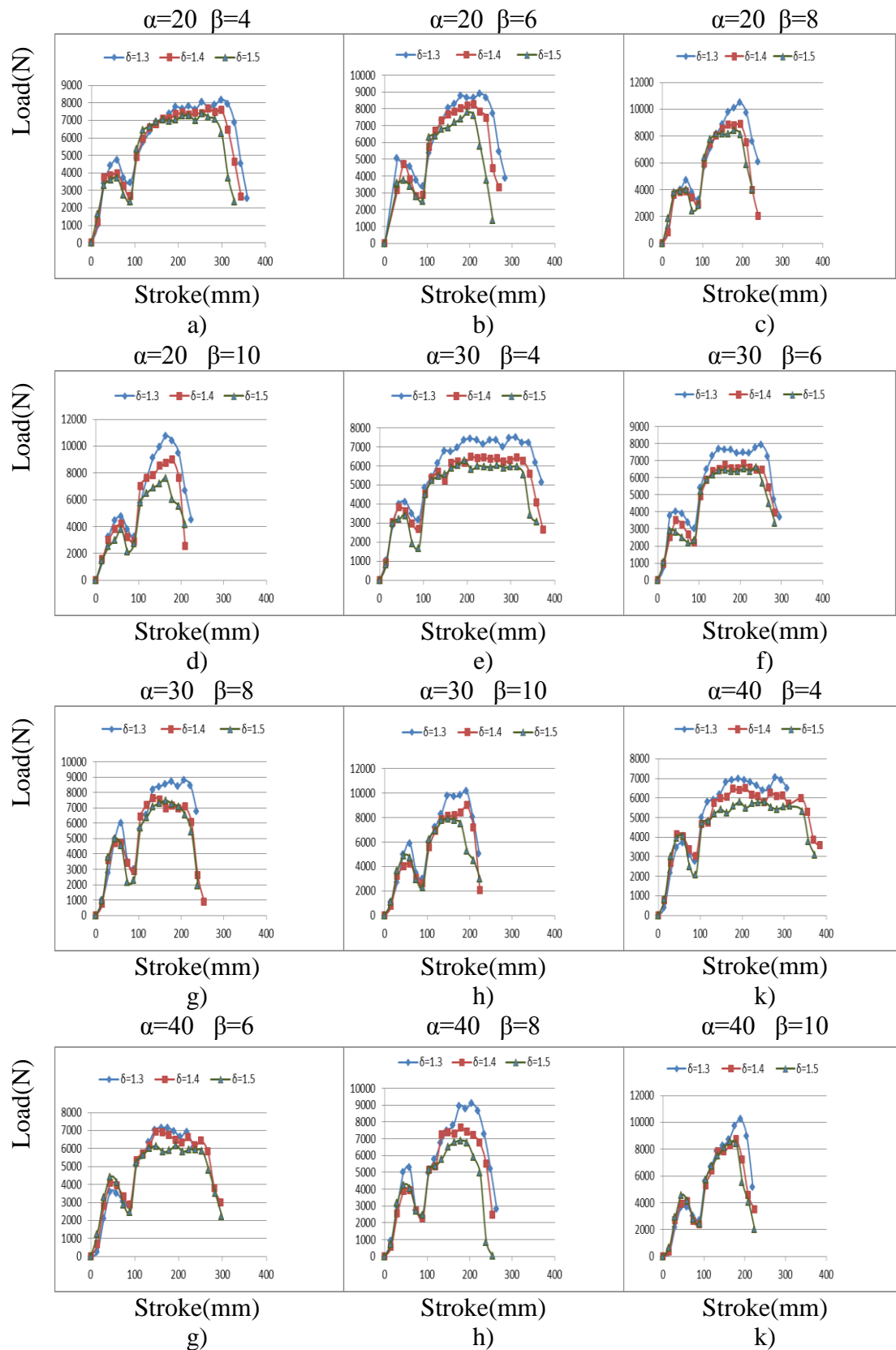
Following Figure demonstrate the variations of radial load graphs according to various reduction ratio under V=75 mm/sn die velocity condition.



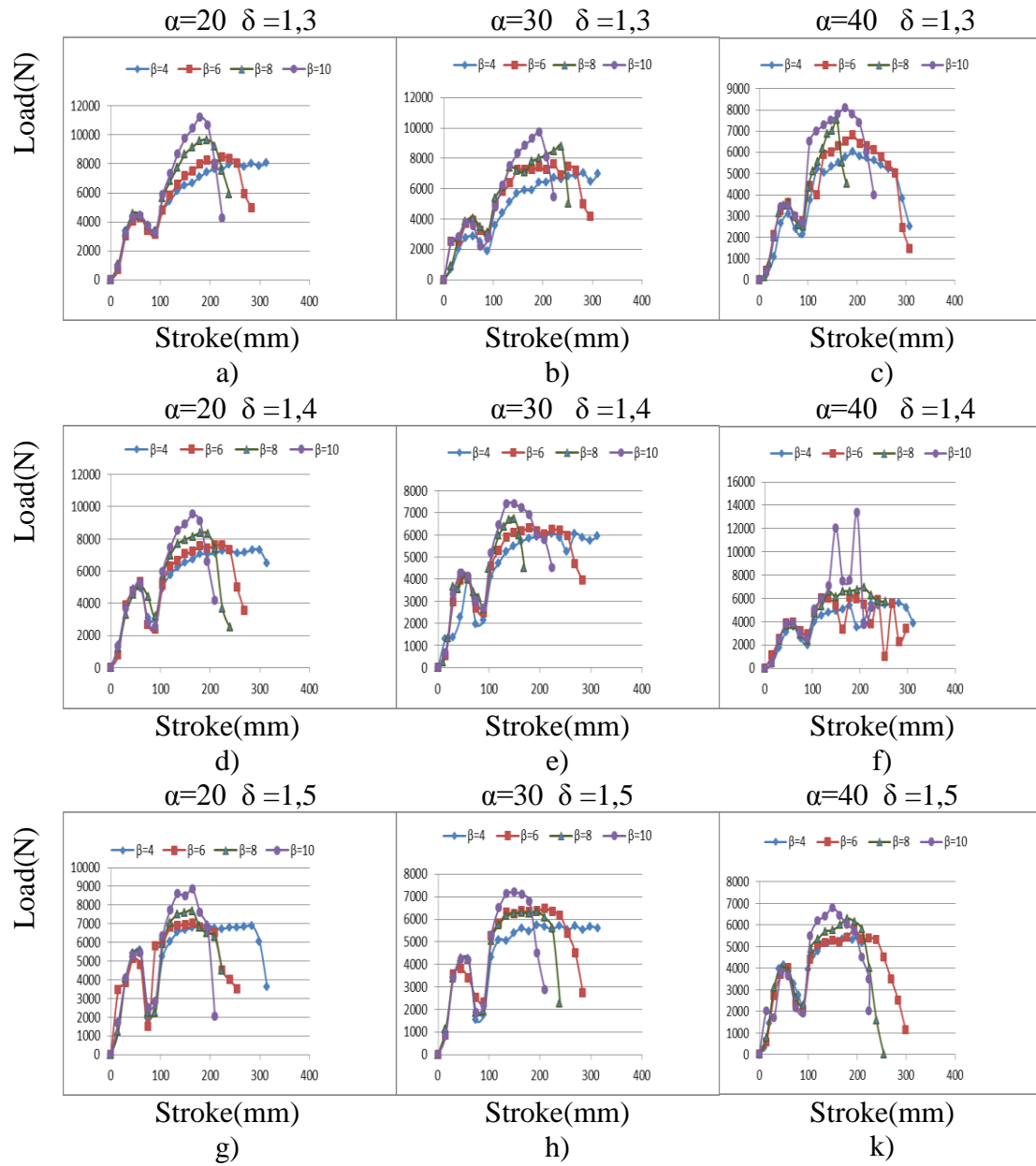
Following Figure demonstrate the variations of radial load graphs according to various reduction ratio under $V=100$ mm/sn die velocity condition.



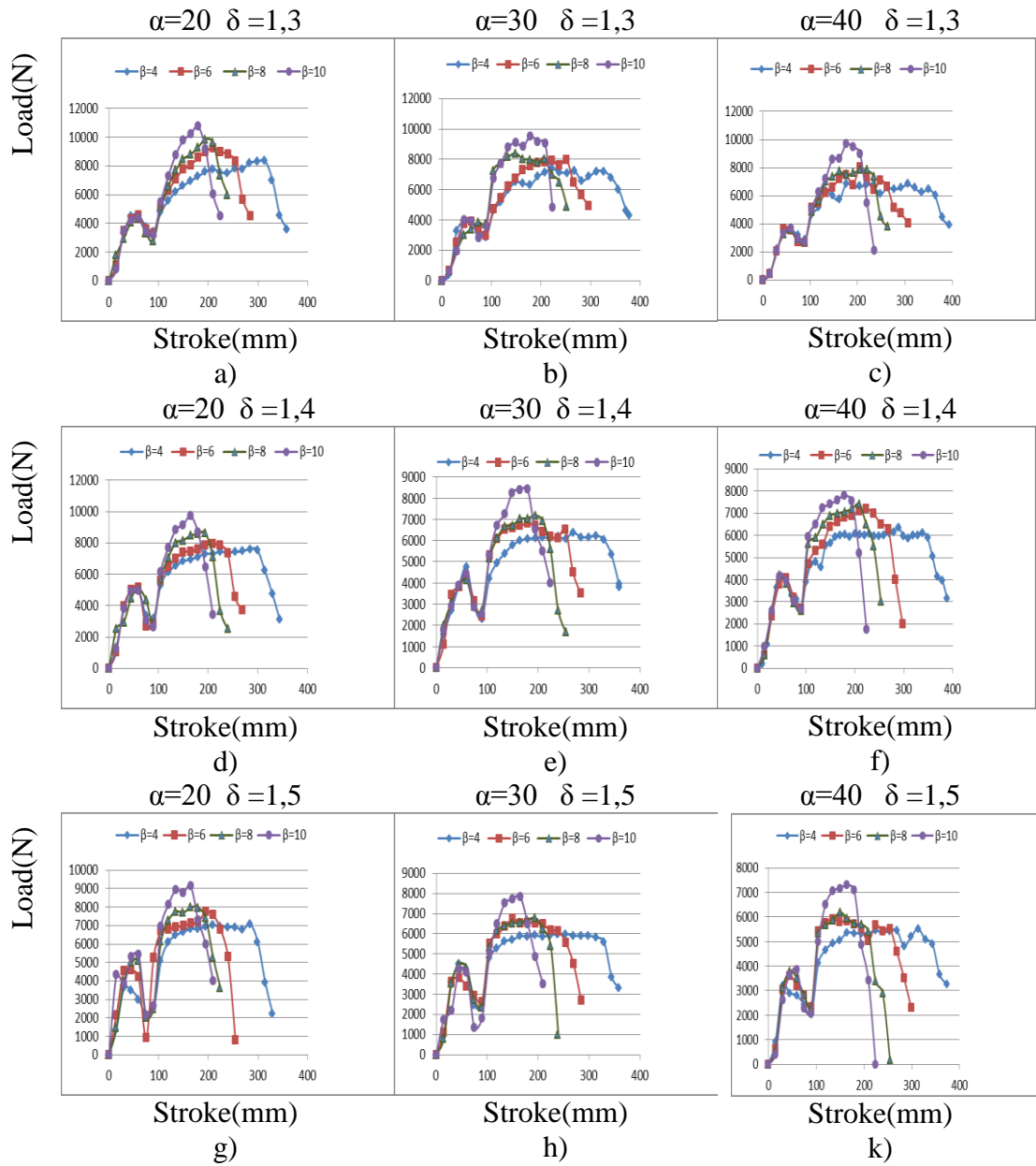
Following Figure demonstrate the variations of radial load graphs according to various reduction ratio under V=125 mm/sn die velocity condition.



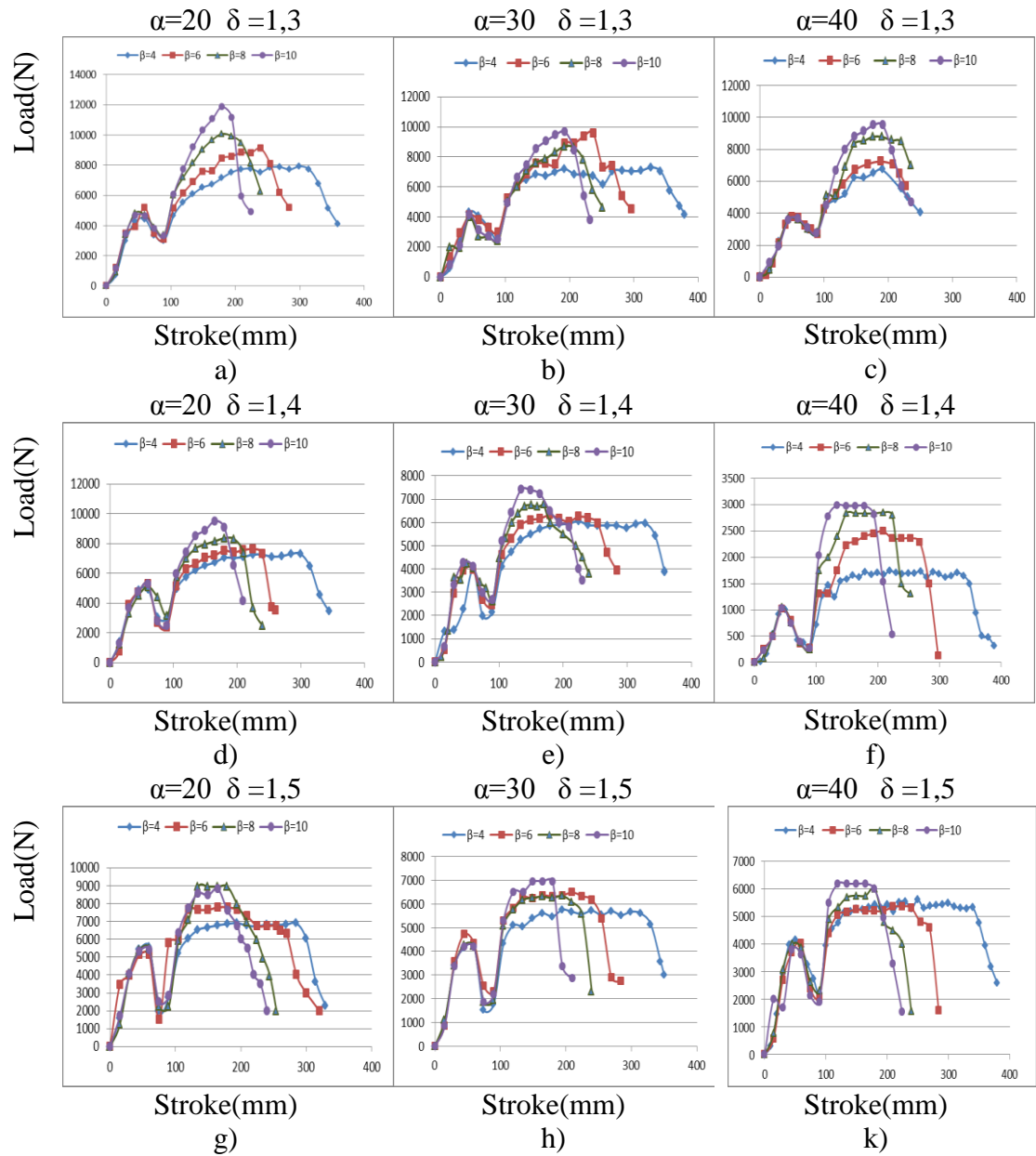
Following Figure demonstrate the variations of radial load graphs according to various stretching angle under V=50 mm/sn die velocity condition.



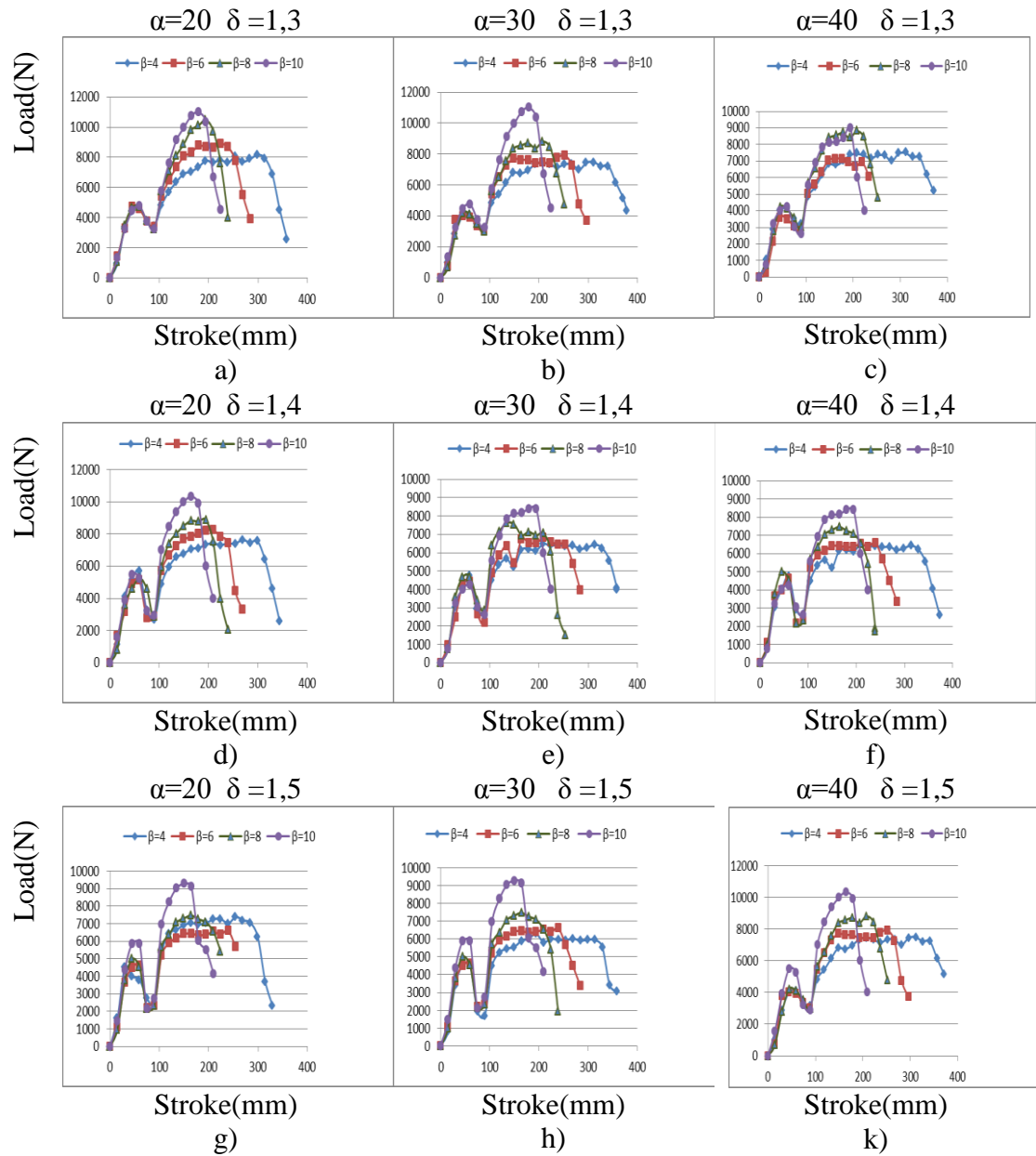
Following Figure demonstrate the variations of radial load graphs according to various stretching angle under $V=75$ mm/sn die velocity condition.



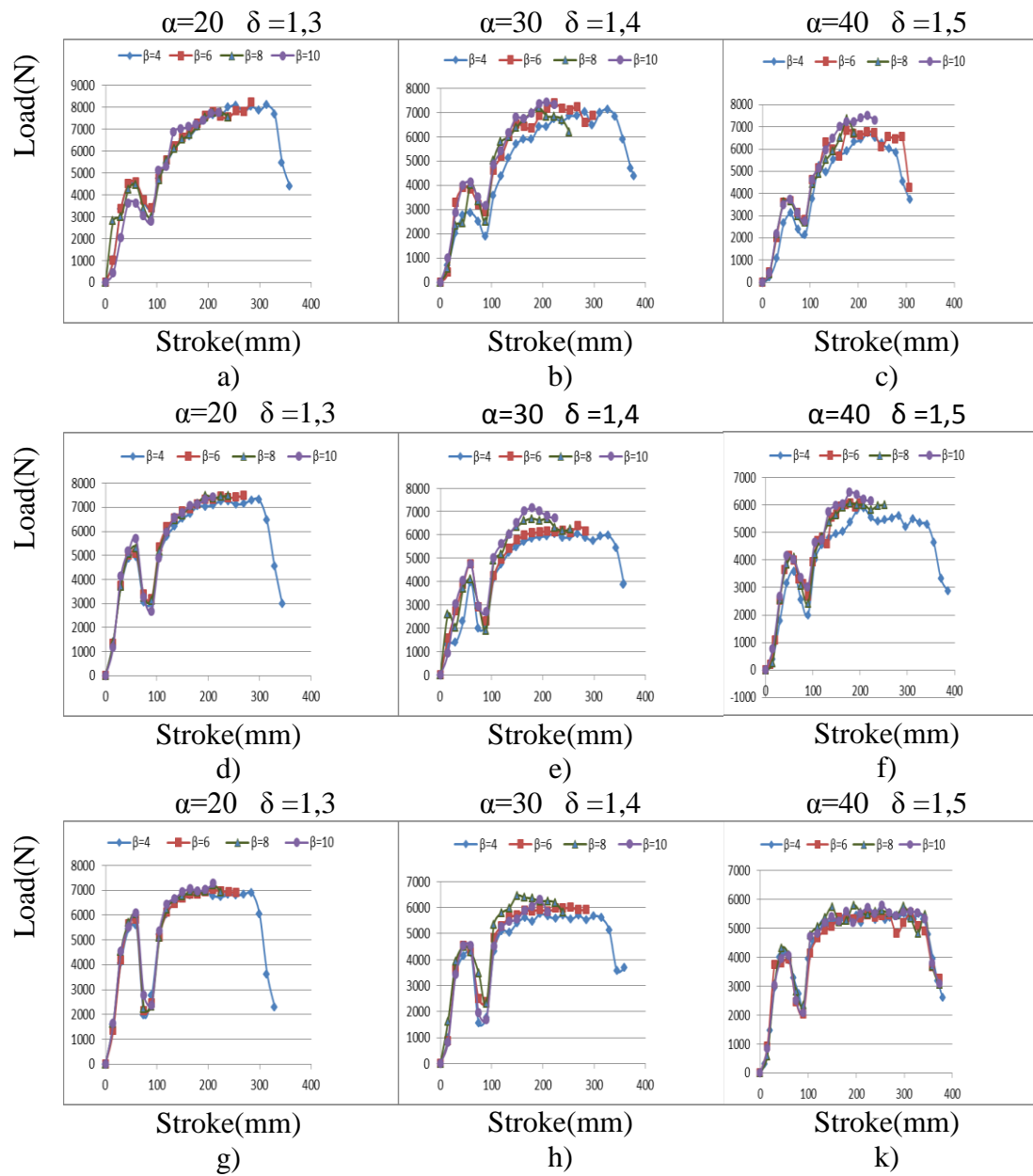
Following Figure demonstrate the variations of radial load graphs according to various stretching angle under $V=100$ mm/sn die velocity condition.



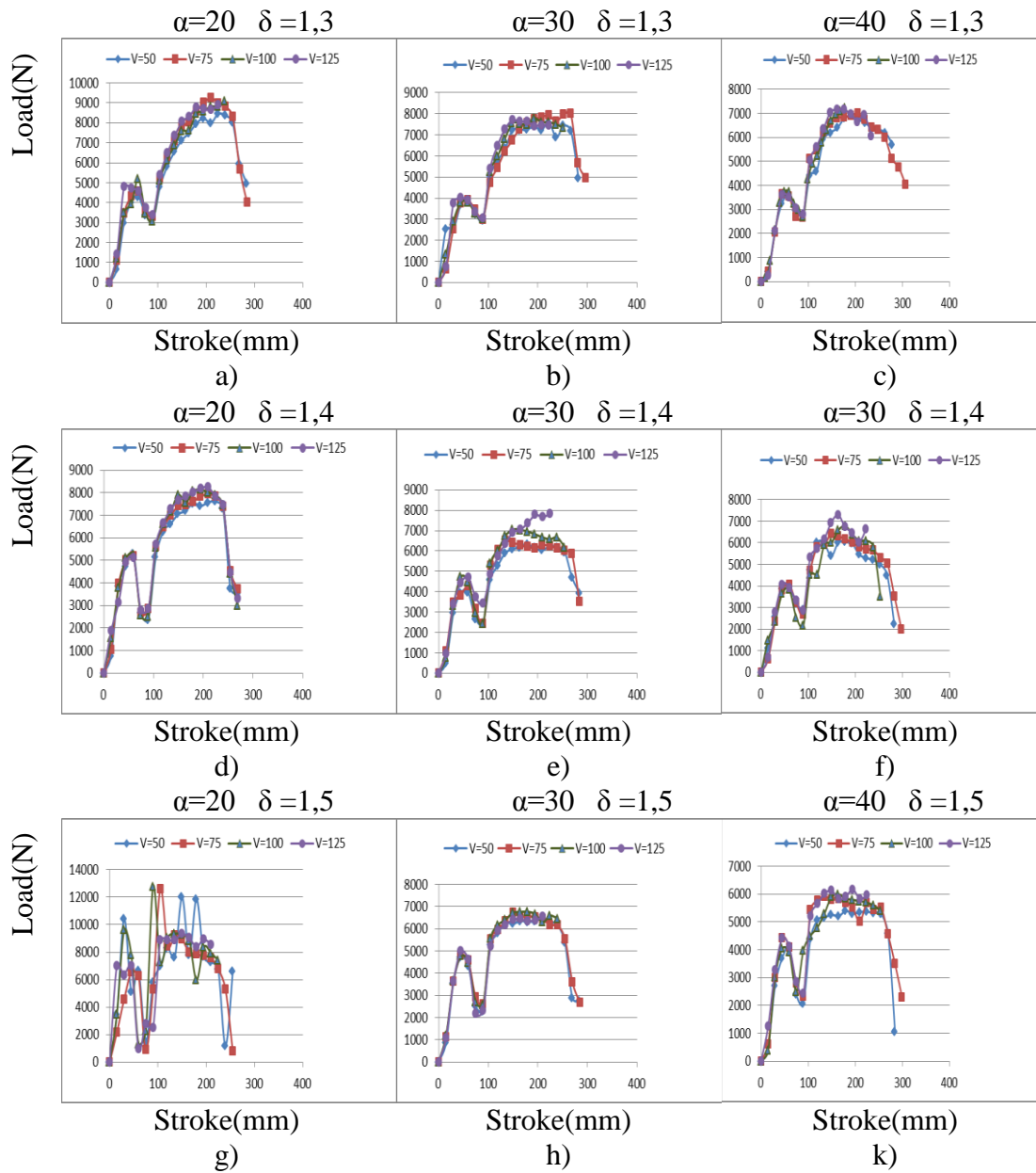
Following Figure demonstrate the variations of radial load graphs according to various stretching angle under $V=125$ mm/sn die velocity condition.



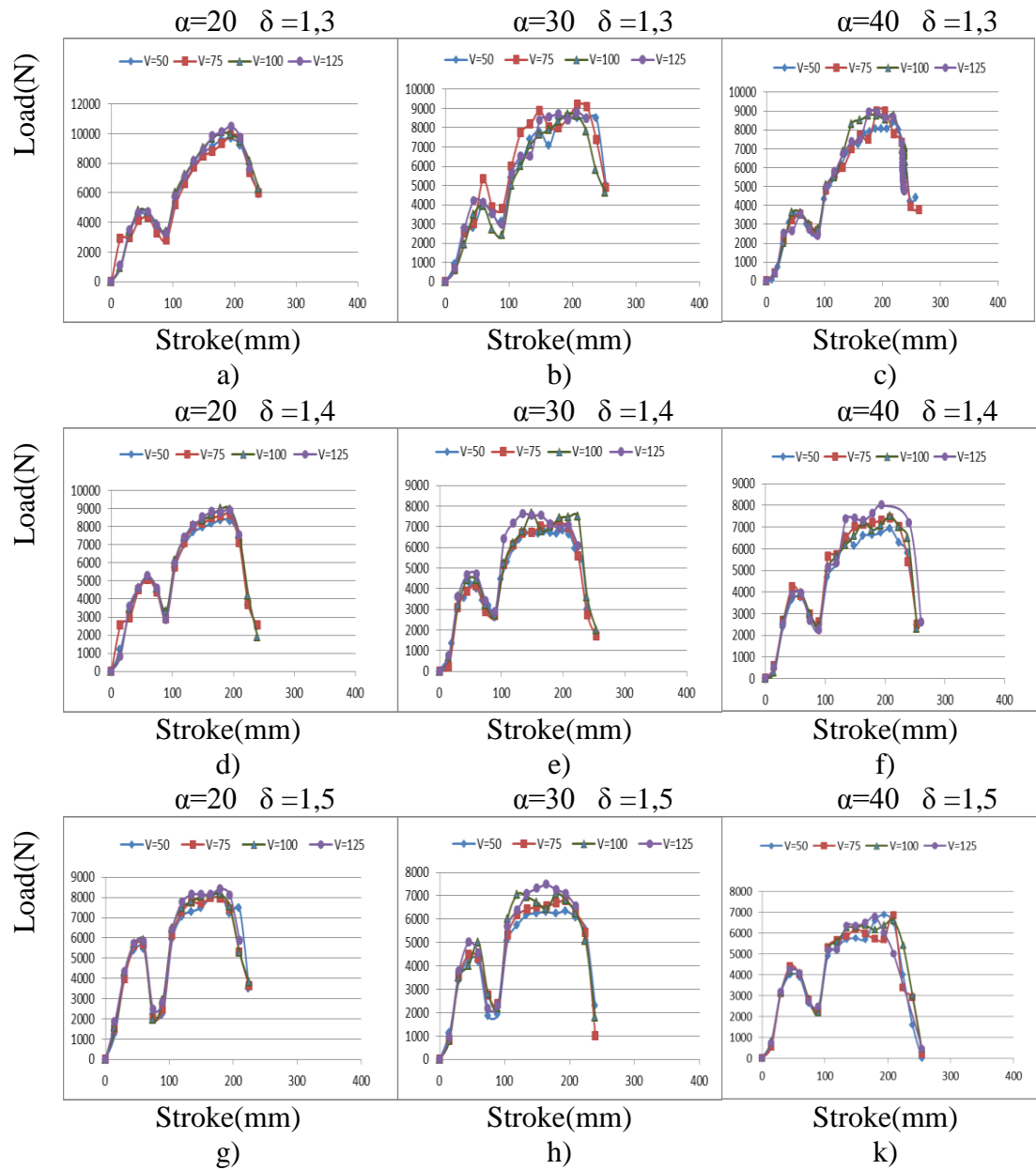
Following Figure demonstrate the variations of radial load graphs according to various die speed under $\beta = 4^\circ$ stretching angle condition.



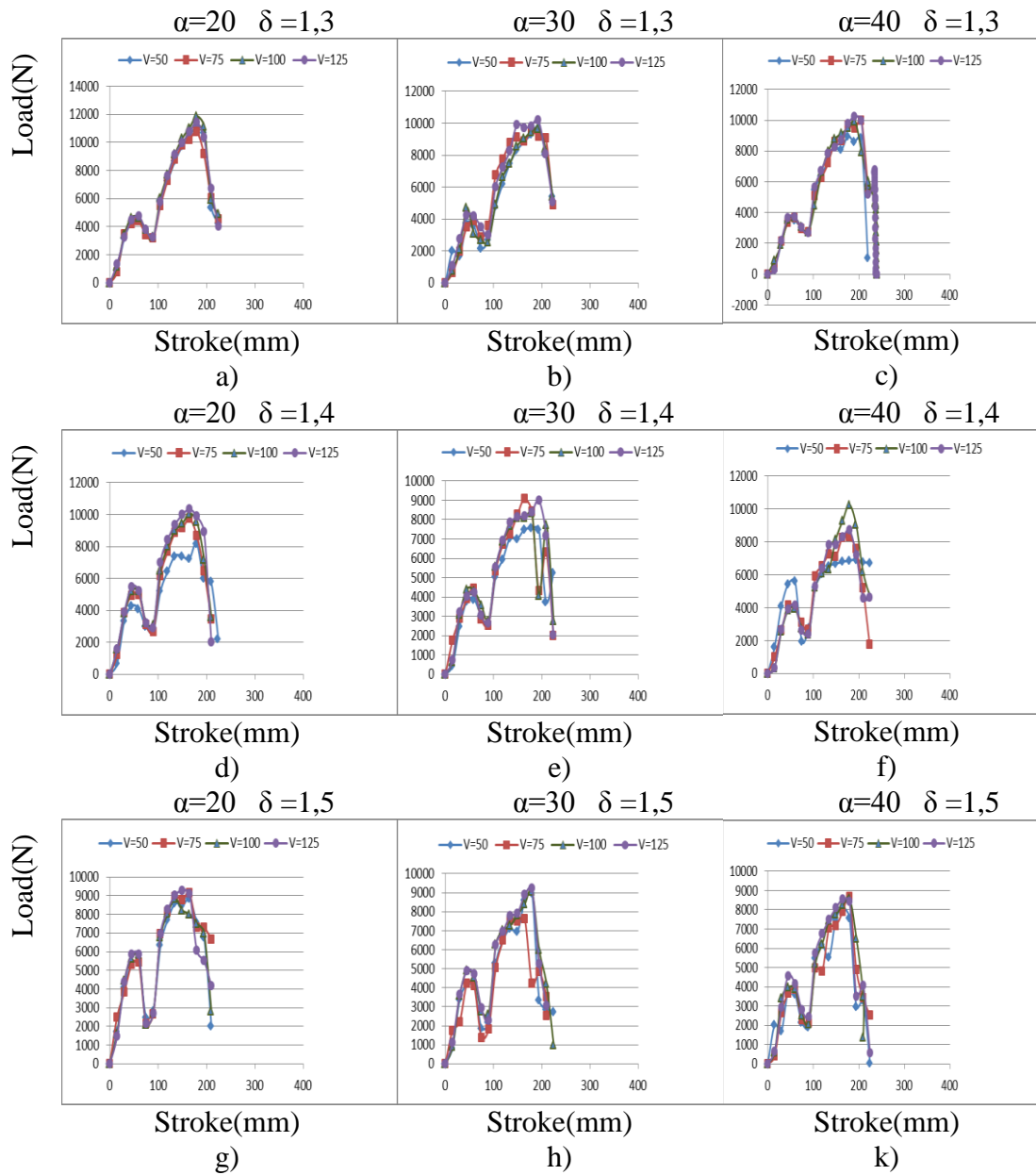
Following Figure demonstrate the variations of radial load graphs according to various die speed under $\beta = 6^\circ$ stretching angle condition.



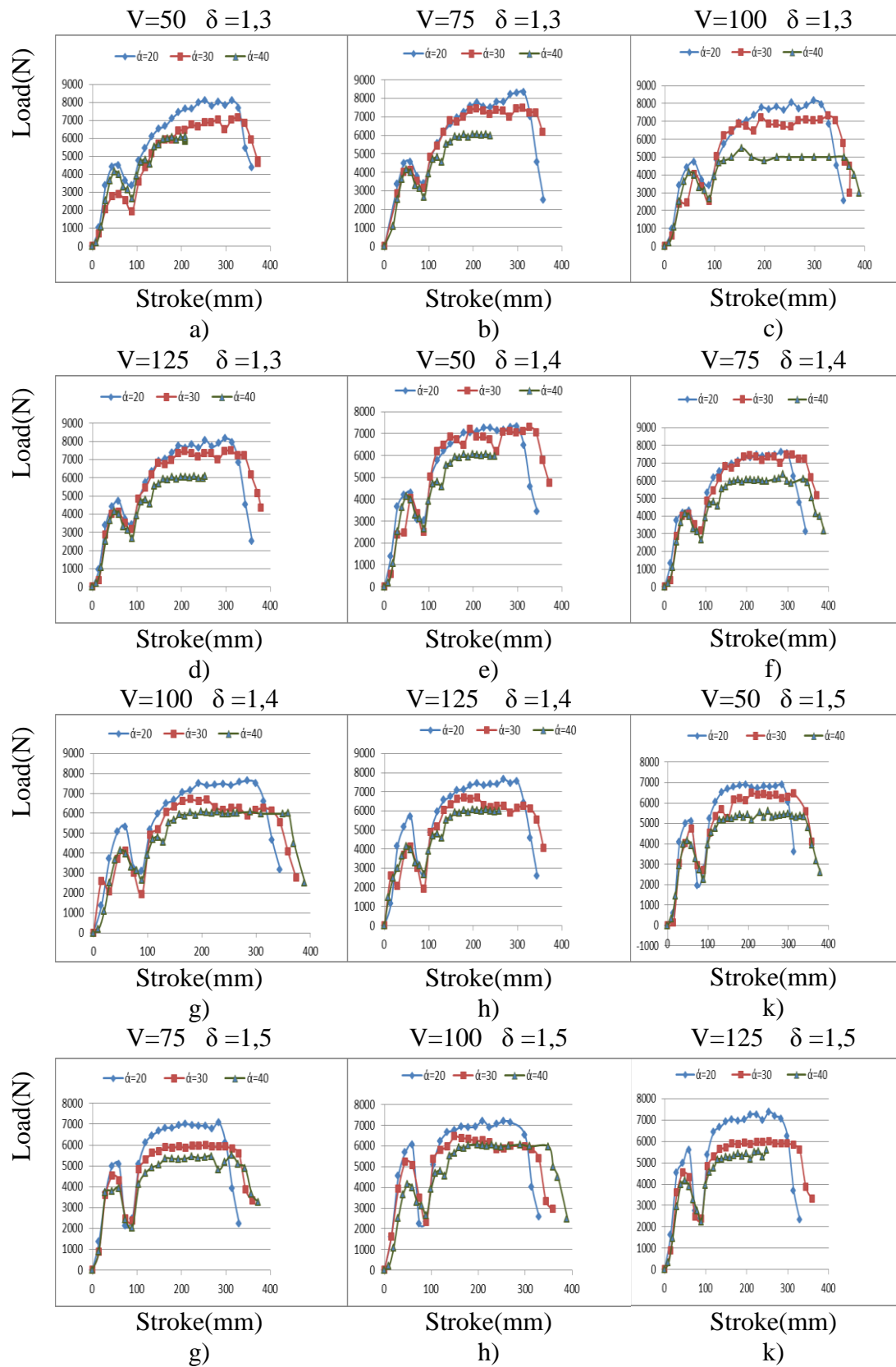
Following Figure demonstrate the variations of radial load graphs according to various die speed under $\beta = 8^\circ$ stretching angle condition.



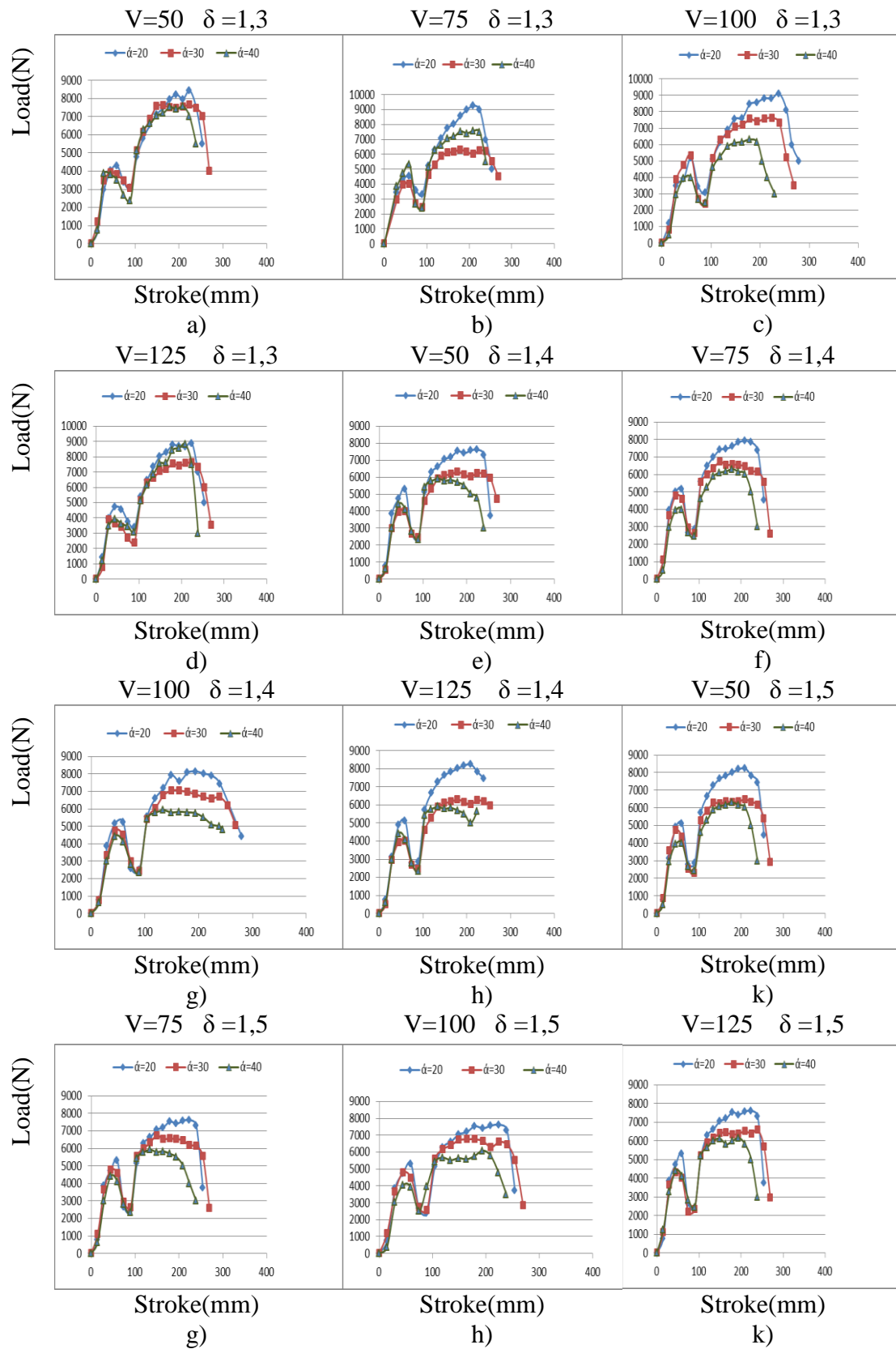
Following Figure demonstrate the variations of radial load graphs according to various die speed under $\beta = 10^\circ$ stretching angle condition.



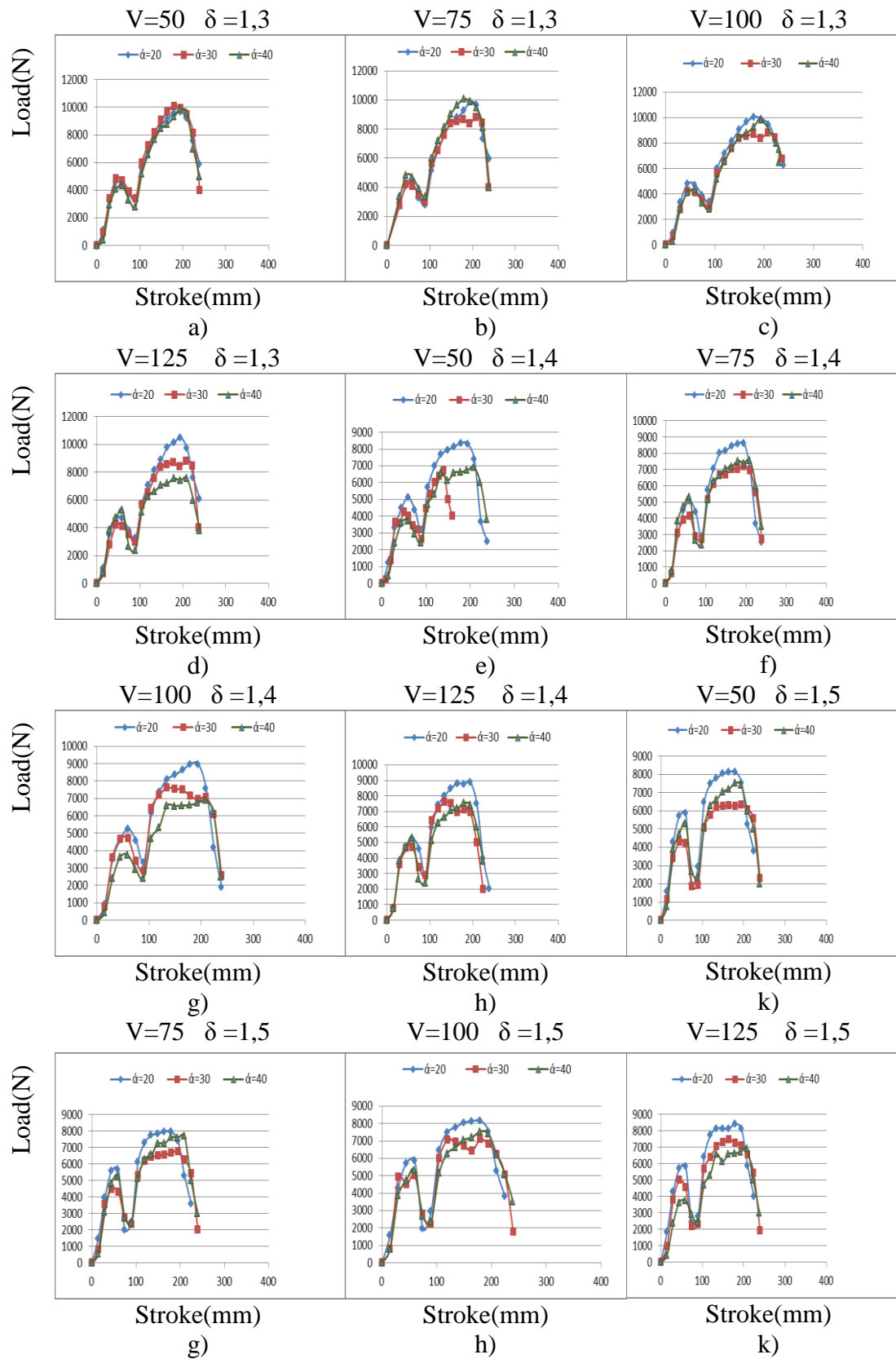
Following Figure demonstrate the variations of radial load graphs according to various forming angle under $\beta = 4^\circ$ stretching angle condition.



Following Figure demonstrate the variations of radial load graphs according to various forming angle under $\beta = 6^\circ$ stretching angle condition.



Following Figure demonstrate the variations of radial load graphs according to various forming angle under $\beta = 8^\circ$ stretching angle condition.



Following Figure demonstrate the variations of radial load graphs according to various forming angle under $\beta = 10^\circ$ stretching angle condition.

